UNIVERSITY OF SOUTHAMPTON

Department of Astronautics and Aeronautics

A STUDY OF PASSENGER AIRCRAFT AUTOMATIC LANDING SYSTEMS

By **Stephanie MISSUD**

Submitted for the degree of
Master of Philosophy

September 1996

This dissertation is concerned with a study for a variety of entry conditions and system disturbance of the dynamic performance of an automatic landing system for use with a large passenger aircraft which employed as its path-deviation sensor an airborne radio receiver suitable for the Instrument Landing System (ILS), the Microwave Landing System (MLS) or Global Positioning System (GPS).

A comprehensive simulation of the dynamics of the chosen aircraft (Boeing-747) was carried out to form the basis of the system simulation. Attitude control systems for both longitudinal and lateral motion were designed using two different control techniques, eigenvalue assignment and linear quadratic regulator theory. A speed control system was also designed to control the aircraft's speed during descent.

Vertical and azimuthal motions were essentially independent when the attitude control systems operated so that the research proceeded by designing a single coupling system to provide automatically horizontal and vertical control of the aircraft's path in which the path deviation sensor could be selected for ILS, MLS or GPS.

Results are shown which indicate that although ILS provides a satisfactory system it is restricted to straight approaches. MLS can provide as good dynamic performance, and for curved approaches. The GPS had a stationary error which this research has shown precludes its use for automatic landing, unless the system is complemented with a ground-based position error correcting station, in which case the new Differential Global Positioning System (DGPS) provides acceptable path deviation sensing to permit automatic landing.

A number of suggestions for further work are given.

PAGES

A/C :	Aircraft
AFCS :	Aircraft Flight Control System
c.g :	Centre of gravity
comm :	Command
DGPS :	Differential Global Positioning System
DH :	Decision Height
DoD :	Department of Defence
FANS :	Future Air Navigation Systems
G-P :	Glide-Path
GPS :	Global Positioning System
ICAO :	International Civil Aircraft Organization
ILS :	Instrument Landing System
MLS :	Microwave Landing system
ph :	Phugoid mode
ref :	Reference
RVR :	Runway Visual Range
RX :	Receiver
SAS :	Stability Augmentation System
sp :	Short period mode
TX :	Transmitter
UHF :	Ultra High Frequency
VHF :	Very High Frequency
VOR :	Very High Frequency Omnirange

Aircraft automatic landing systems are used when the weather conditions are so bad that visibility for a pilot is so impaired that it would not be possible to land his aircraft safely, even though not to do so implies, at worst, a diversion to another airport with better visibility, and all the inconvenience such a change of landing implies for passengers and airline alike, or, at least, another landing attempt at the same airport but in visibility which may be worse than the first attempt, with all the implications that such a situation has for aircraft safety.

In Europe, in particular, there is considerable economic benefit in equipping large passenger aircraft with automatic landing systems which will ensure that landing at the intended airport will take place no matter what is the visibility.

Aircraft instrument procedures currently use Very High Frequency Omnirange (VOR), Instrument Landing System (ILS) and Distance Measurement Equipment (DME) for approach and landing. The approaches are straight and the flight path angle is fixed at a value of about 3°. But, since the first automatic landing in 1965, the growth in air traffic has been so great that there is now being experienced at most large airports considerable difficulty in handling the present levels of traffic. An alternative solution, which permits a greater number of aircraft to use the existing runways, is to execute curved approaches using either the Microwave Landing System (MLS), which is a ground based system, or the Global Positioning System (GPS), which is a satellite navigation aid. Using GPS would avoid the expense of having to equip every airfield and maintaining and updating any ground equipment associated with MLS. However, since GPS is a system owned by the US DoD and its availability cannot be guaranteed, Europe cannot depend solely on this device for navigation information. Thus, MLS is still a viable system for widespread implementation.

The purpose of this research was to evaluate the dynamic performances of an automatic landing system using either ILS, MLS or GPS. This dissertation begins with a brief description of a 3-axes aircraft flight control system (AFCS) for use with a Boeing-747, which is representative of current long haul passenger aircraft. Information about the

ILS, MLS, and GPS follows, before the presentation of details of a simulation of the Boeing-747 on approach and then for the automatic landing system. System design, analysis and implementation have been carried out utilizing Matlab and the Control System Toolbox. The control systems incorporated the ideas of feedback and linear analysis. Since the longitudinal and lateral motions of the aircraft have been treated separately, a glide-path control system and a localiser control system were designed. All the tests were carried out for a number of different entry conditions and in presence of perturbations like atmospheric turbulence or sensor noise.

A particular feature of the research reported here was the design of a single automatic landing system, also capable of producing automatic approaches, suitable for use with the Boeing-747 but with the option of using as the path-deviation sensor a radio receiver operating with the ILS, or the MLS, or GPS. All the results presented here were based upon simulations of the Boeing-747 aircraft dynamics, its corresponding closed-loop attitude control systems, and the path-deviation-coupled automatic control system. ILS, MLS, and GPS were selected independently with appropriate entry conditions, capture logic, atmospheric disturbance and system errors.

1 Aircraft flight control system (AFCS)

Control is necessary for any flight. Without a stabilizing control, an aircraft after a disturbance, will not necessarily come back to its initial position ie there can exist a steady state error; if the aircraft does turn to the initial attitudes, it may do so only after too long a period. Conventionally, there are controls for pitch, roll and yaw, which affect motion about the transverse, the longitudinal and the normal axes. These controls are also used to minimise the effects of various disturbing factors. A flight control system will include actuators, sensors and controllers as well as the aircraft dynamics. A structure of such a system is shown in Figure 1.

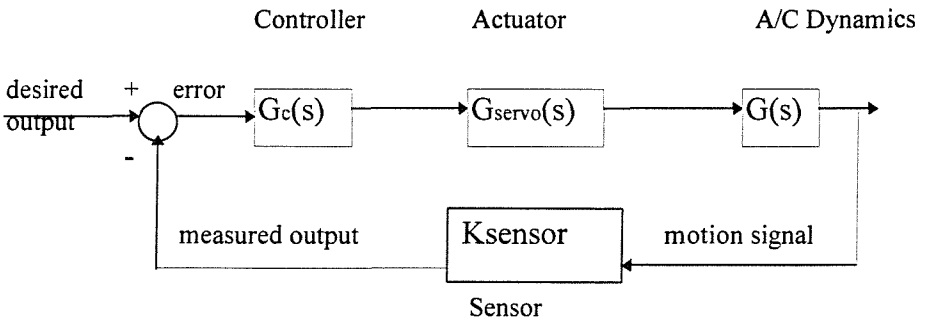

Figure 1.1

The actuators operate on the aircraft control surfaces (elevator, aileron, rudder), which are used for steering. In earlier days, only mechanical actuators were used : pitch and roll controls were activated by means of the yoke and to deflect the rudder the pilot moved his pedals in the cockpit. The yoke and pedals of the primary flying controls required the pilot to maintain a counterforce for steady manoeuvres. With large transport aircraft such as Boeing-747, it is impossible for a pilot to sustain the force required. Consequently, electrohydraulic actuators have been introduced. The command signals to these electrohydraulic actuators are electrical voltages supplied from the controller of an AFCS. It has been assumed in this work that the dynamic response of the actuator is instantaneous.

Therefore, the actuator dynamics have been represented by a simple transfer function :

$$\text{Gservo(s)} = \frac{\delta(s)}{\delta_c(s)} = K \qquad (1.1)$$

More specifically, Gservo(s) has been taken as 1°/V.[1]

Sensors provide measures of any changes in motion variables such as pitch angle, roll rate etc. Changes in motion usually occur either in response to a pilot's commands or to an encounter with some disturbance, or in response to both. The signals from these sensors are used as feedback signals for the AFCS. The sensors are frequently represented by their sensitivities, viz.

$$\frac{v_f}{y} = \text{Ksensor}, \qquad (1.2)$$

which is dimensional. In this project, the sensors have been considered as ideal;

i.e. $|\text{Ksensor}| = 1$. (1.3)[2]

An AFCS compares the commanded (or desired) motion with the measured motion and, if there is any difference, generates in accordance with the required control law, the signal to the actuator to produce the appropriate control surface deflections to bring the measured motion into correspondence with the commanded value (Draper, 1981).

[1] An exception is made for the engine dynamics, which are part of the speed control system (see chapter 4).
[2] An exception has been made for the Global Positioning System (GPS) receiver because of its inaccuracy.

2.1 Presentation

An automatic landing system is used to cause an aircraft to descend to a minimum height without any human intervention and in low-visibility. A classification for such landings exists and is detailed in Table 2.1 :

	DH	RVR
Category I	60 m	> 800 m
Category II	30 m	> 400 m
Category III		
a	< 30 m	> 200 m
b	< 30 m	> 50 m
c	< 30 m	= 0 m

Table 2.1

The automatic approaches are prohibited unless horizontal visibility, called " runway visual range " (RVR) exceeds a published threshold. The crew must execute a missed approach if the runway lights are not visible when the descent reaches a published " decision height " (DH). In the case of Category III aircraft, a missed-approach is not allowed below the DH. Therefore, the automatic landing system and all the equipment on the ground has to be of the very highest reliability.

An automatic landing system comprises a number of different stages (McLean, 1990), which are summarized in Figure 2.1 a :

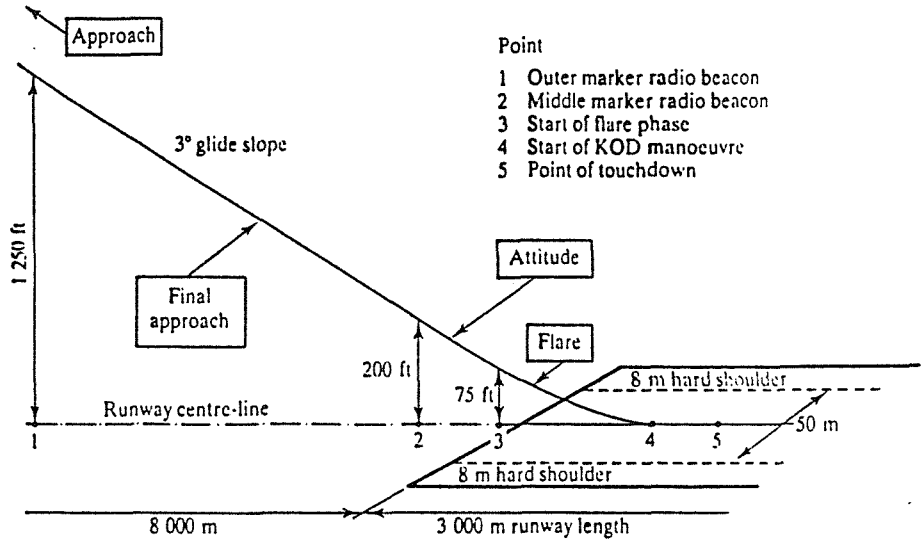

Figure 2.1 a

- During the approach, the aircraft is guided along the glide path by a glide-path-coupled controller and is steered onto the runway centre-line by means of a localizer-coupled control system.
- The flare manoeuvre is initiated once the aircraft has descended to about 50 ft altitude. The trajectory represents the path of the aircraft's wheels and has normally an exponential shape (see Figure 2.1 b).

The equation which governs this trajectory is :

$$h = h_o.e^{-t/T} \qquad (2.1)$$

where h_o is the flare entry height and T is the time constant of the exponential flare.

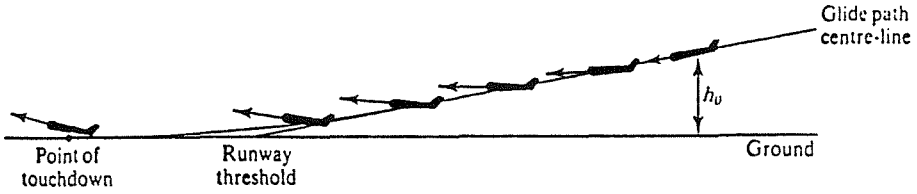

Figure 2.1 b

- The last stage of the flight is at touchdown when a command signal is applied to the elevator to lower the aircraft's nose to bring the nose wheel into contact with the runway. At this point, too, if any drift has built up in the lateral path, this is removed by the pilot executing a kick-off drift manoeuvre.

In this project, the Instrument Landing System (ILS), the Microwave Landing System (MLS), and the Global Positioning System (GPS) are discussed. ILS equipment is installed at every major airport and most commercial aircraft are equipped with airborne equipment which can receive the transmitted information. MLS is more accurate than the present ILS and has been recommended as its successor. Although there is no technical problem in replacing ILS with MLS, setting-up is quite slow for a number of reasons explained later in this chapter. GPS navigation has been recognised by the entire ICAO membership as the future air navigation system. It greatly improves navigation precision and covers the entire world. But, because it remains under US DoD control, its development for commercial aircraft in Europe remains uncertain, although its use as a world-wide area navigation system is most probable.

2.2 Instrument Landing System

The Instrument Landing System (ILS) has been the standard landing aid since 1948. It is only used with runways of length greater than 1800 m and is categorized as Category II or III. The approach trajectory is linear with a glide path angle about 3°. Its height above the runway threshold will be 15 m and the touchdown point will be 300 m from the threshold. This ideal trajectory is at the intersection of two planes (Alari, 1987) and is illustrated by Figure 2.2 :

- the localiser (LOC) defines a vertical plane (plane V). It provides information about whether an aircraft is to the left or to the right of the runway centre-line.
- the glide path transmitter (GLIDE) defines a slanting plane (plane G) and provides information about whether an aircraft is flying above or below the glide path.

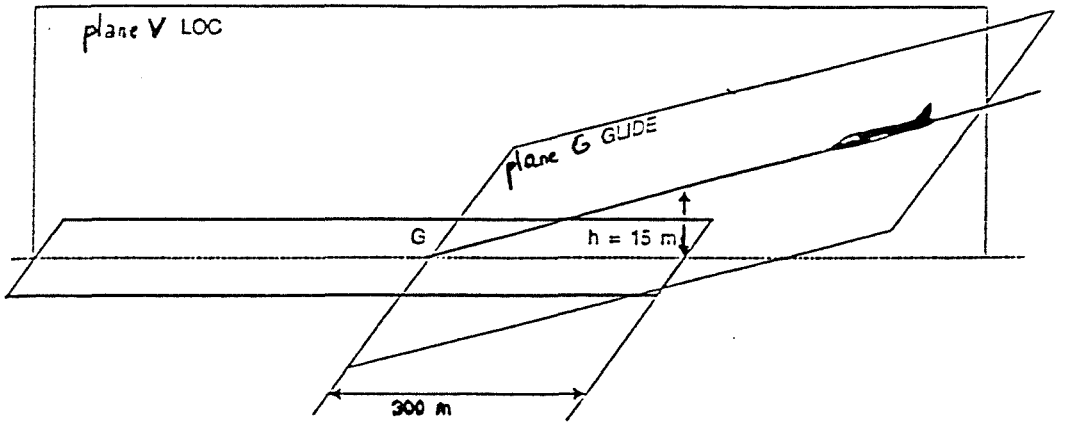

Figure 2.2

The system also provides distance information referenced to the runway threshold. Three marker beacons are located at nominal locations (see Figure 2.3) :

- 7200 m (outer marker)
- 1050 m (middle marker)
- when height is 30 m (inner marker).

The marker beacons operate at a frequency of 75 MHz; the modulation frequencies for the outer, middle and inner markers are 400, 1300 and 3000 Hz respectively.
By passing over the marker beacons, the marker receiver produces audio signals (MORSE) and displays visual signals (colours) in the aircraft cockpit (Combes, 1993).

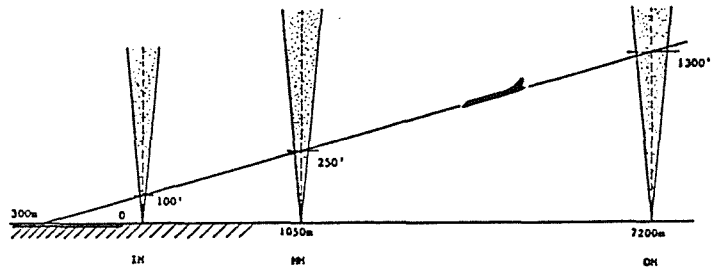

Figure 2.3

The transmitters LOC and GLIDE operate in frequency bands of 40 channels as follows :
- LOC : 108-112 MHz (VHF)
- GLIDE : 329-335 MHz (UHF)

The ground transmitter (VHF or UHF) transmits amplitude modulated signal at frequencies of 150 and 90 Hz (see Figure 2.4). The difference between the modulated signals (DDM) is proportional to the angular deviation (α or θ). If the amplitude modulated signal are called a and b, with $a < b$ respectively, and if m (equal to 0.4 for ILS transmitters) is the depth of modulation,
then :

$$ddm = m*(a - b) / (a+b) = 0.4* (a-b) / (a+b) \qquad (2.2)$$

On-board, this difference can be measured and used as a display signal.

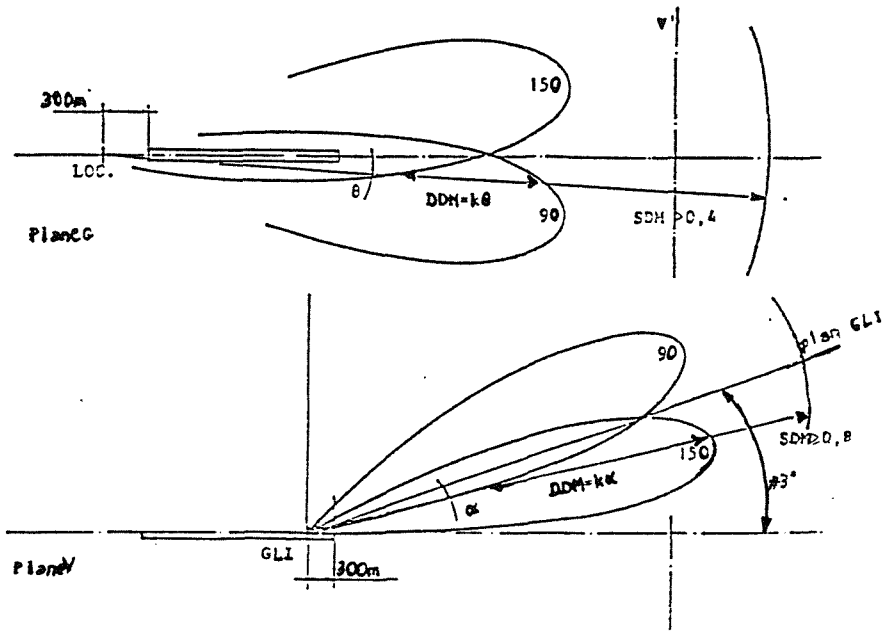

Figure 2.4

ILS has a coverage illustrated in Figure 2.5 :

In the lateral plane, the following hold :

- for the localiser, the coverage is ± 10° up to a range of 25 nm and ± 35° up to a range of 17 nm.
- for the glide : ± 8° up to a range of 10 nm.

For the vertical plane, the parameters are :

- for the localiser, ILS covers from 0 to 7°.
- for the glide, the coverage is from 0.45γ to 1.75γ (γ : glide path angle).

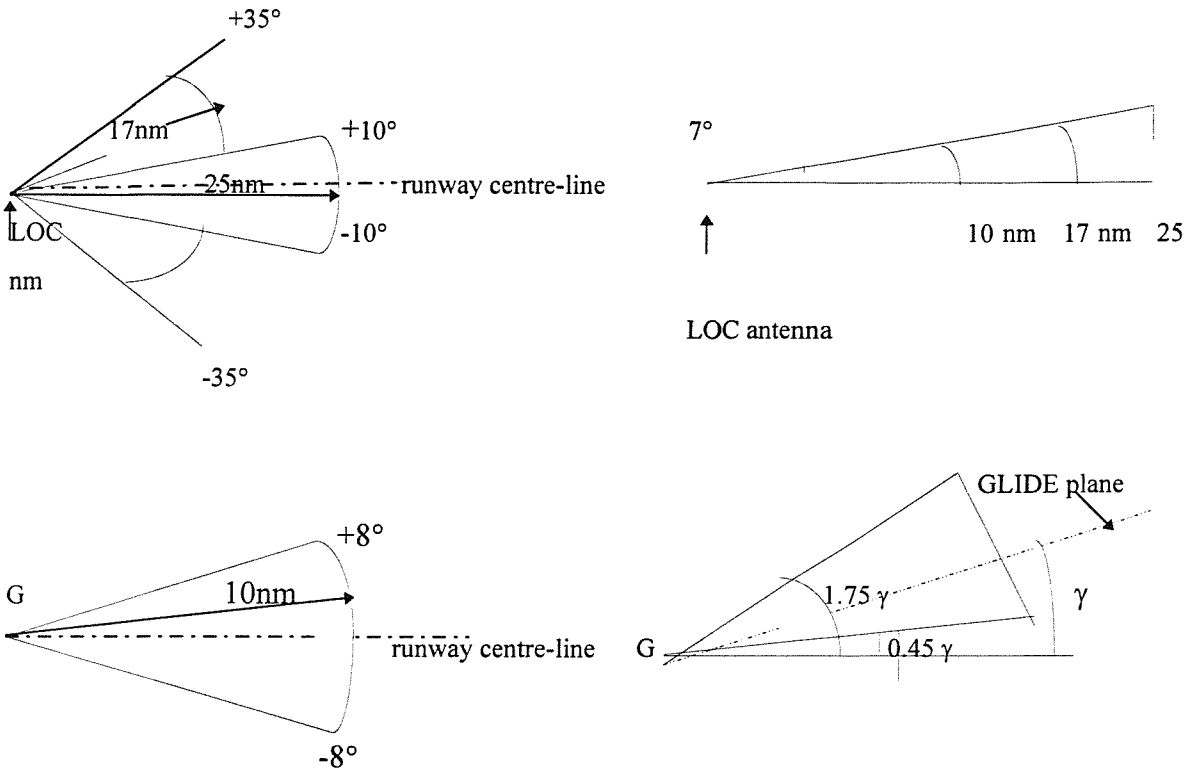

G is at the intersection between the ideal trajectory and the ground.

Figure 2.5

The ILS system has a number of limitations at present but it is not now possible to improve it any further. These limitations include :

- single aircraft approach;
- restricted coverage; beam capture problems.
- large antennas; implementation problems.
- high sensitivity to unwanted reflections and interference.
- VHF band is overcrowded at present, with no possibility of adding new channels.

2.3 Microwave Landing System

With this system (CAA, 1988), several simultaneous approach paths are possible. Segmented and curved approaches with various glide path angles are available. The aircraft's position is accurately known as a consequence of the permanent distance information given by the DME (Distance Measurement Equipment) or DME/P system (P stands for precision).

There are five ground stations (see Figure 2.6) :
- a front azimuth station (AZ) at the far end of the runway and located on the centre-line,
- a back azimuth station (BK AZ) located at the runway threshold,
- an elevation station (EL) located at 300 m from the runway threshold and to the left of the runway,
- a station for the flare manoeuvre (FL) at 1000 m from the runway threshold,
- and a DME or DME/P station.

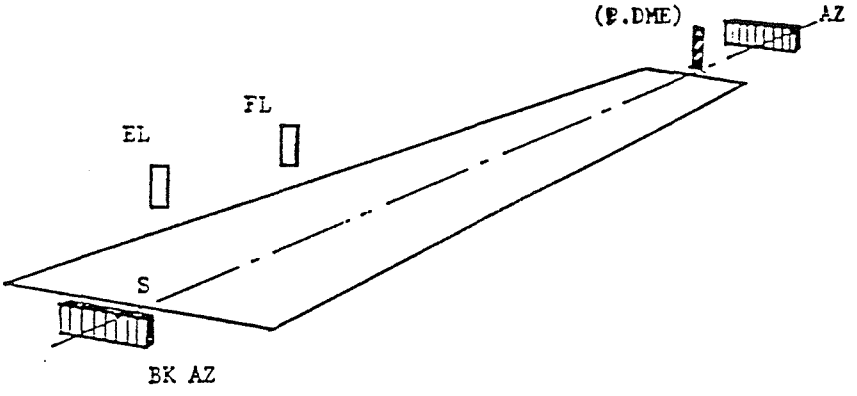

Figure 2.6

The first four stations take it in turns to operate at a frequency of about 5GHz (C-band or SHF) on 200 channels. A whole cycle lasts 64 ms (see Figure 2.7).

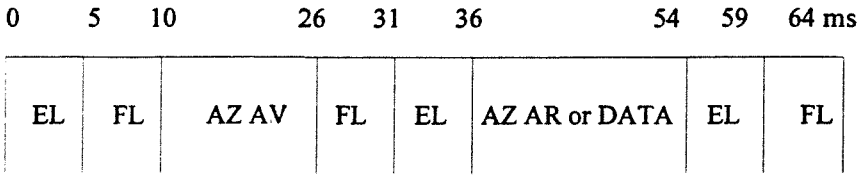

Figure 2.7

The MLS uses a technique called Time Reference Scanning Beam (TRSB), the principle of which is explained in the following section (Kelly, 1976) and is illustrated in Figure 2.8 (which is the special case of the AZ station).

Each transmitter (AZ and EL) produces a narrow beam (1°-3°), which is rapidly scanned to and fro or up and down across the coverage region. The lateral and vertical position of the aircraft within the sector is determined by the time difference between the beams crossing the aircraft's antennas.

On board, the signals are received on a single UHF receiver, decoded and sent either directly to a ADI (Attitude Director Indictor) or to a navigation computer.

Front AZ station :

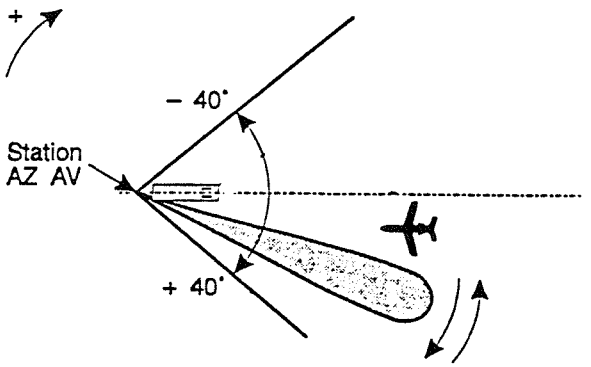

On-board :

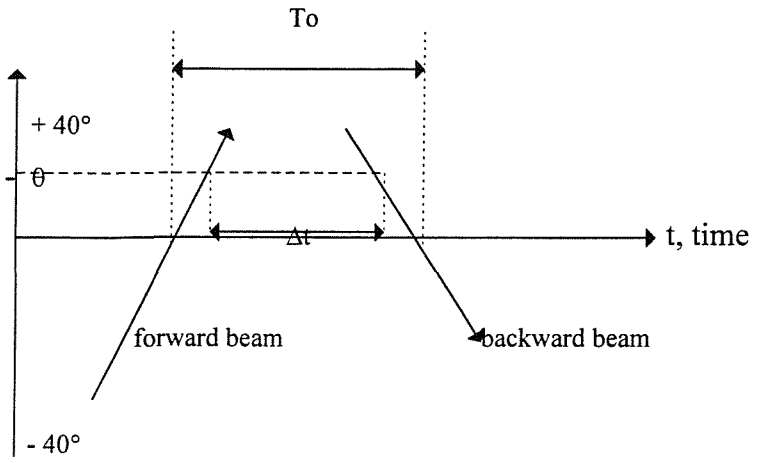

Δt is the time difference between the reception of the forward and backward beams.

$\theta = k.(To - \Delta t)$ (2.3)

where k is the angular velocity of the beam.

Figure 2.8

DME measures the slanting range R between the plane and the ground. It is used in conjunction with VOR (Kayton and Freid, 1969), which provides bearing (θ) information[3]. The DME operates in the frequency band 960-1215 MHz (UHF, L-band) and the VOR within 108-135 MHz (VHF).

The principle is the same as for a secondary radar but in the reverse direction. The ground DME station responds upon receipt of a signal from the airborne transmitter. On detecting this signal, the station replies using a pulsed transmission, coded in MORSE, with a delay of 50 μs. The onboard receiver measures the time difference between the to and from signals and computes the range R viz.

$$R = \frac{c.t}{2} \quad (2.4)$$

[3] This system is also called a rho - theta navigation system, where rho is the range (equivalent to R).

There are 2 levels of accuracy :

- ± 0.2 nm for the DME
- ± 0.02 nm for the DME/P.

The DME is rarely affected by atmospheric perturbations. The only problem comes from its capacity, which is limited to one hundred aircraft.

Figure 2.9 gives details of the MLS coverage :

- ± 40° for the front AZ.
- ± 20° for the back AZ.
- from 1 to 7.5° for the front EL.
- from 1 to 20° for the back EL.

At the front of the runway threshold, the length is 20 nm and the height is 20 000 ft. For the back area, the values are divided by four.

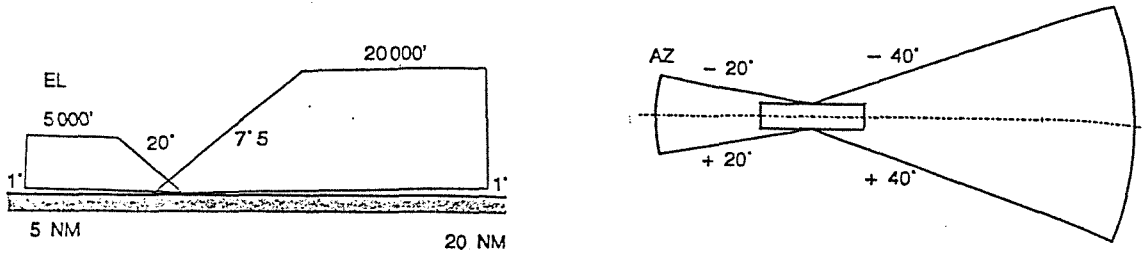

Figure 2.9

Different MLS operational procedures are used :

- The basic procedure follows the same procedure as ILS but, as soon as the aircraft is in the coverage volume, proportional instrument guidance and continuous distance information are used.
- In the segmented procedure, guidance is provided via predetermined points (waypoints). Segmented approaches are quite useful in areas where terrain, environment or obstacles reduce capacity and flexibility.
- The curved procedures are similar to the segmented ones, but they require higher tracking accuracy during turns, to provide greater navigation accuracy.

With segmented and curved procedures, the operational utilisation of the airspace is increased, with the approach track becoming shorter, and the pilot workload reducing.

Compared with the installation costs for ILS GLIDE and LOC transmitters, setting-up of the MLS ground stations is cheaper. But on-board the aircraft, the situation is reversed : because there are many ground stations, more antennas are required in the aeroplane. Furthermore, since multiple approaches are possible, it is no longer a single approach which has to be visualized but an air traffic lane.

Hence, the setting-up of MLS is quite slow : besides the reorganization required, compatibility between ILS and MLS must exist for the duration of any transition period (since ILS will remain the primary ICAO landing aid system until January 1998).

2.4 Global Positioning System (GPS)

This system, based upon artificial satellite positions, is able to locate a mobile or fixed station. It has been developed by the DoD of the USA for military purposes. It comprises three sub-systems : the space segment, the user segment and the ground control segment (Carel, 1993).

Space segment

This segment comprises 18 satellites plus 3 spare satellites and has the following characteristics (see Figure 2.10) :

- 6 quasi-circular orbits
- period of a satellite : T = 11h57'58''
- altitude : h = 20180 km
- orbits have an inclination of 55° (reference is equator)
- 120° longitude angle between each satellite
- anywhere in the world, 5 satellites can be used simultaneously (11 is a maximum).
- each satellite has a caesium clock synchronised to the international atomic time.
- life of each satellite is 7.5 years.

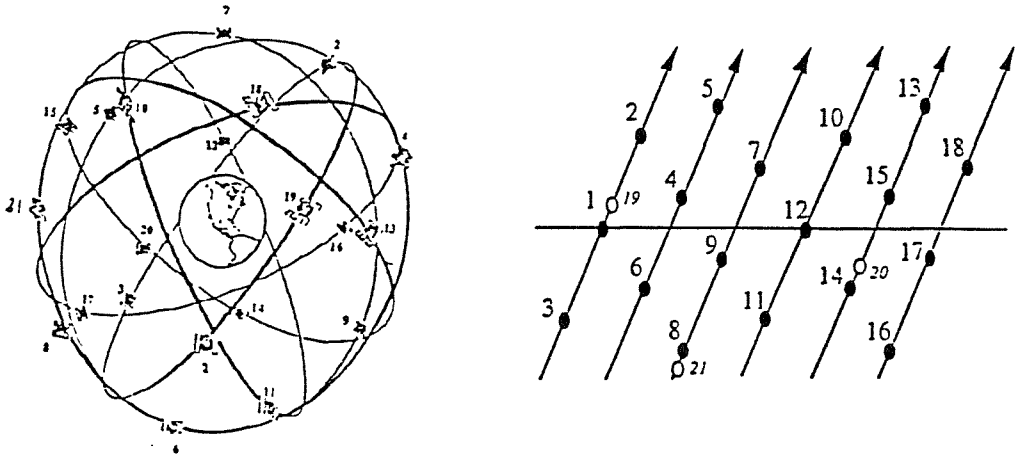

Figure 2.10

The distribution of the satellites in the 6 orbital planes is shown in Table 2.2.

Orbital Plane	Satellite Number	Longitude	Latitude
1	1	0	0
1	2	0	120
1	3	0	240
2	4	60	40
2	5	60	160
2	6	60	280
3	7	120	80
3	8	120	200
3	9	120	320
4	10	180	120
4	11	180	240
4	12	180	360
5	13	240	160
5	14	240	280
5	15	240	40
6	16	300	200
6	17	300	320
6	18	300	80
1	spare 1	0	30
5	spare 2	120	170
3	spare 3	240	310

Table 2.2

Each satellite produces its own code from the following classes :

- code C/A (Coarse Acquisition) on a frequency L1 = 1575.42 MHz.

1023 bytes are generated in 1 ms. The precision is 175 m to 0.95 probability.

- code P (Precision -for military services only-) on a frequency L2 = 1227.60 MHz.

10.23 Mbytes are generated in 1 s. The precision is 37 m to 0.95 probability.

These codes allow the identification of each satellite and the measurement of the propagation time, Δt_i as shown in Figure 2.11.

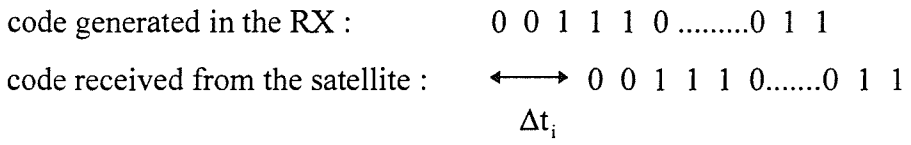

Figure 2.11

User segment

This segment relates to the vehicle[4], the location of which is to be found in four dimensions : latitude, longitude, altitude and universal time. On board a civil vehicle, there are :

- a computer to process the information;
- a UHF receptor (L-band) which operates at 1575.42 MHz.
- a quartz clock, which is not synchronised to the universal time. The clock error induced is one of the unknowns of the localisation problem.

Four satellites are required to solve the problem. Each of them gives a pseudo-range, different from the true range, because of the RX clock bias : as it is a quartz clock, it is not as accurate as the caesium atomic clock used in the ground segment.

The determination of the pseudo-ranges is based upon the propagation time of an electromagnetic wave (cf equation (2.4)).

[4] Among the possible users there are : the airplane, the helicopter, the ship, the human ...

The coordinates x,y,z (in an earth reference axis system) representing the position of the aircraft can be computed by means of the following system :

$$(x - X_i)^2 + (y - Y_i)^2 + (z - Z_i)^2 = (d_i - c.E_L)^2 = D_i^2 \qquad (2.5)$$

where

E_L denotes the receiver clock bias;
D_i is the true range;
$d_i$denotes the pseudo – range given by $\Delta t_i * c$ or $D_i + c.E_L$;
X_i, Y_i, Z_i represents the satellites' coordinates (from the ephemerides)
c is the speed of the light.

There are also secondary terms errors, including for example, the ionospheric delay[5] (Kingsley and Quegan, 1992), but because such terms are very small, they are normally ignored.

Ground control segment

This segment consists of 5 stations (see Figure 2.12) :

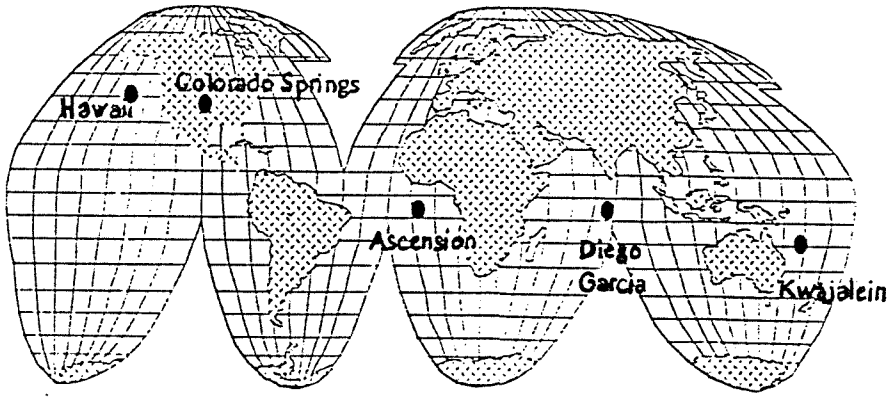

Figure 2.12

[5] The effect of the ionosphere (from 60 km to 1000 km) on radio waves passing through it is to cause attenuation, refraction and a rotation of the plane of polarization known as Faraday roation.

- a Master Control Station (MCS) in Colorado Springs.
- 4 others in Hawaii, Ascension, Diego Garcia and Kwajalein. These stations receive messages from the satellites and transmit the information to the MCS, which computes the orbit of each satellite, its position on its orbit and the corrections necessary to syncronise their clocks. The MCS sends these results to the user segment in order to enable the system of four equations to be solved.

Because DoD of the USA does not want civil users to have too good an accuracy, it adds some errors. Without any Selective Availability (SA), the accuracy at the frequency 1575.42 MHz could be about 30 m. An example of SA can be the modification of the satellites'coordinates.

Techniques have been implemented to counteract SA. Among them, there is the DGPS (Differential Global Positioning System). The idea is to use another receiver, whose position is known. This receiver computes the satellites'coordinates. The results from the stations and the receiver are compared and the error is transmitted to the user segment.
One example is the DGPS developed by Honeywell and Pelorus (Canada). Three ground receivers collect the signal from at least 4 satellites and a ground station computes the corresponding errors, which are transmitted to the aeroplane (Daoust, 1996).

Because of its complete world coverage and its high accuracy, this system is very attractive for use in aircraft operations. But the system is not without its disadvantages :
- during 15 min or 30 min, holes in the coverage can occur;
- a satellite may not be operational and the user may be unaware of the fact;
- interference with other transmitters;

- the operation and maintenance of the GPS is undertaken solely in the USA. Therefore, without any notice the system could be denied at any time to all civilian users by the US defence authorities.

To compensate for these problems, ICAO advises that GPS be coupled with another existing area navigation system such as OMEGA or VOR/DME, although these navaids are scheduled to be phased out in the long term.
A project to improve the space segment, is being established : a geostationnary satellite in connection with some ground stations will check the state of the satellites. GPS will gain integrity and reliability thereby (Carel, 1993).

3.1 Aircraft dynamics and stability

To implement the automatic landing systems, a mathematical model has been built based on differential equations, which describe the motion of the Boeing-747 on approach. The equations have been linearized, which allows Laplace transforms to be used (Dorf and Bishop, 1995). Because the topic mainly deals with flight control, the equations of motion have been based on the aircraft stability axes, which are a special case of body-fixed axes (See Figure 3.1).

U, V, W are the forward, side and vertical velocities

L, M, N are roll, pitch and yaw moments

P, Q, R are the angular velocities, roll, pitch and yaw.

ϕ, θ, ψ are roll, pitch and yaw angles.

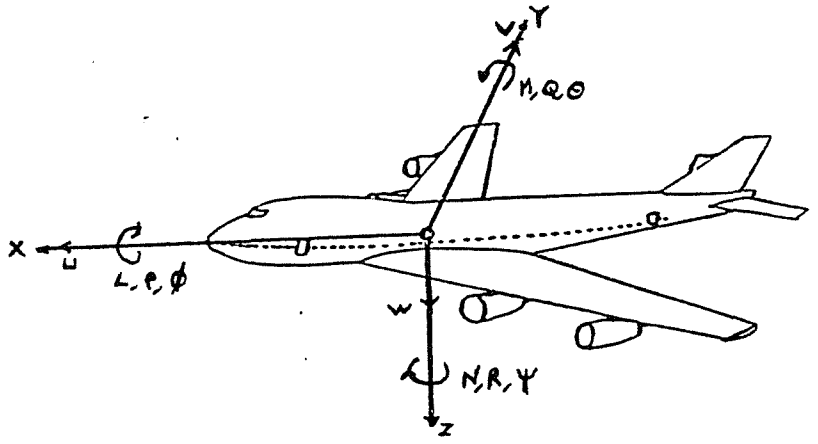

Figure 3.1

The aircraft dynamics are represented by a state variable model and not by a transfer function for several reasons :

- the aircraft motion is multivariable;
- the initial conditions cannot be assumed to be zero;

- a transfer function does not include any information concerning the internal structure of the dynamic system it represents;
- state variable models lend themselves to easier computer simulation.

The system is totally defined by the knowledge of its input vector, **u**, its state vector, **x**, and its output vector, **y** (see Figure 3.2).

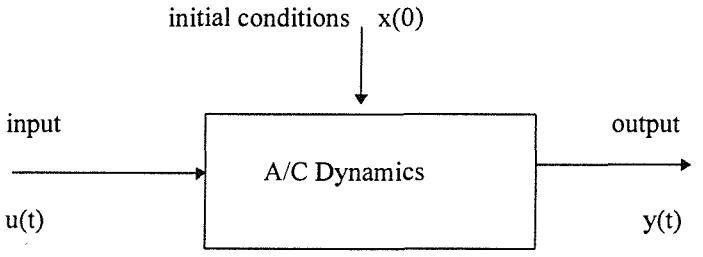

Figure 3.2

The rate of change of the state vector of the system relates to the state vector of the system and the input vector, and is represented by the following equation, called a "state equation" [6]:

$$\dot{\mathbf{x}} = A\mathbf{x} + B\mathbf{u} \qquad (3.1)$$

where

- A is a square matrix of order n*n;
- B is a matrix of order n*m;
- **x** is the state vector of dimension n, consisting of the state variables, which are chosen so that they fully characterise the system.
- **u** is the control vector of dimension m, consisting of the control input signals.

The A matrix comprises the stability derivatives, gravity and the forward speed.

[6] Boldfaced lowercase letters denote vector quantities.

The output of the system is identified in terms of the state variables and the control input signals. The corresponding equation is called "output equation" :

$$\mathbf{y} = C\mathbf{x} + D\mathbf{u} \tag{3.2}$$

where

- **y** is the output vector of dimension p ;
- C is the output matrix of order p*n;
- D is the direct matrix of order p*m.

Disturbances like atmospheric turbulence are taken into account by adding a term to the right hand side of the state equation thus (McLean, 1990) :

$$\dot{\mathbf{x}} = A\mathbf{x} + B\mathbf{u} + E\mathbf{d} \tag{3.3}$$

where

d represents the disturbance vector of dimension l;

E is a matrix of order n*l.

In order to incorporate noise effects on sensors, another term can be added to the output equation :

$$\mathbf{y} = C\mathbf{x} + D\mathbf{u} + F.\xi \tag{3.4}$$

where

ξ denotes the noise vector of dimension h;

F is a matrix of order p*h.

In this research, the output equation depended solely upon the state vector, viz.

$$D = 0. \tag{3.5}$$

The system relationships are represented by diagrammatic means. A software package called Simulink has been used in conjunction with Matlab (mathematical tool box) for control system design and analysis.

Since small perturbations were assumed, the longitudinal and lateral motions could be treated separately. In both cases, a state variable model was constructed. Results relating to

aircraft's dynamic stability are also presented. Finally, the last part of this chapter deals with the response of the uncontrolled Boeing-747 to a step input.

Information about the dynamic stability of the aircraft can be obtained by considering the eigenvalues of the A matrix. The function, EIG, in Matlab computes these eigenvalues by solving the equation :

$$|\lambda I - A| = 0 \tag{3.6}$$

where I is a square identity matrix.

The aircraft is said to be dynamically stable if all its eigenvalues λ_i have negative real parts.

3.1.a Longitudinal motion

The longitudinal motion was assumed to include forward, downward and pitch motions. Hence, the following state variables were considered :

- u, which denotes the change in forward velocity [$m.s^{-1}$];
- w, which denotes the change in vertical velocity [$m.s^{-1}$];
- q, which denotes the change in pitch rate [$deg.s^{-1}$];
- θ, which denotes the change in pitch angle [deg].

The state vector **x** can be written as follow :

$$\mathbf{x} = \begin{bmatrix} u \\ w \\ q \\ \theta \end{bmatrix} \tag{3.7}$$

Since the control surfaces being considered were the elevator and the engine thrust, the control vector **u** is :

$$\mathbf{u} = \begin{bmatrix} \delta_E \\ \delta_{TH} \end{bmatrix}. \tag{3.8}$$

The sign convention adopted for the various control deflections is illustrated in Figure 3.3.

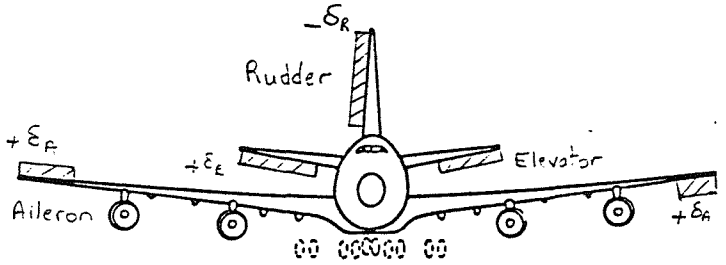

Figure 3.3

The equations of longitudinal motion can be represented by :

$$\dot{u} = X_u u + X_w w - g\theta + X_{\delta_E}\delta_E + X_{\delta_{TH}}\delta_{TH} \quad (3.9)$$

$$\dot{w} = Z_u u + Z_w w + U_o q + Z_{\delta_E}\delta_E + Z_{\delta_{TH}}\delta_{TH} \quad (3.10)$$

$$\dot{q} = \tilde{M}_u u + \tilde{M}_w w + \tilde{M}_q q + \tilde{M}_{\delta_E}\delta_E + \tilde{M}_{\delta_{TH}}\delta_{TH} \quad (3.11)$$

$$\dot{\theta} = q \quad (3.12)$$

where

$$\tilde{M}_u = (M_u + M_{\dot{w}} Z_u) \quad (3.13)$$

$$\tilde{M}_w = (M_w + M_{\dot{w}} Z_w) \quad (3.14)$$

$$\tilde{M}_q = (M_q + U_o M_{\dot{w}}) \quad (3.15)$$

$$\tilde{M}_{\delta_E} = (M_{\delta_E} + M_{\dot{w}} Z_{\delta_E}) \quad (3.16)$$

$$\tilde{M}_{\delta_{TH}} = (M_{\delta_{TH}} + M_{\dot{w}} Z_{\delta_{TH}})$$

The state coefficient matrix A is given by[7] :

$$A_1 = \begin{bmatrix} X_u & X_w & 0 & -g \\ Z_u & Z_w & U_o & 0 \\ \tilde{M}_u & \tilde{M}_w & \tilde{M}_q & 0 \\ 0 & 0 & 1 & 0 \end{bmatrix} = \begin{bmatrix} -.0209 & .122 & 0 & -32.2 \\ -.202 & -.512 & 221 & 0 \\ .001 & -.0018 & -.357 & 0 \\ 0 & 0 & 1 & 0 \end{bmatrix} \quad (3.18)$$

and the driving matrix B is given by :

$$B_1 = \begin{bmatrix} X_{\delta_E} & X_{\delta_{TH}} \\ Z_{\delta_E} & Z_{\delta_{TH}} \\ \tilde{M}_{\delta_E} & \tilde{M}_{\delta_{TH}} \\ 0 & 0 \end{bmatrix} = \begin{bmatrix} .959 & .000057 \\ -6.42 & -.00000249 \\ -.378 & .00000031 \\ 0 & 0 \end{bmatrix} \quad (3.19)$$

Table 3.1 summarizes some of the results related to the longitudinal dynamic stability :

Mode	Eigenvalue	Natural Frequency rad/s	Damping ratio	Period s	Settling Time s
Short period	-.4439±j.6286	.769	.577	1.3	-
Phugoid	-.0011±j.1507	.151	.0073	41.610	4536

Table 3.1

Figure 3.4 shows the pitch attitude and pitch rate responses to an unit step elevator input with two time scales (60 and 6000 s). The corresponding open-loop block diagram is also given.

Note that the settling time for both θ and q corresponds to too long a period and that after the transient response has decayed, a steady-state error exists.

[7] The numerical values are specific to the Boeing-747, on approach.

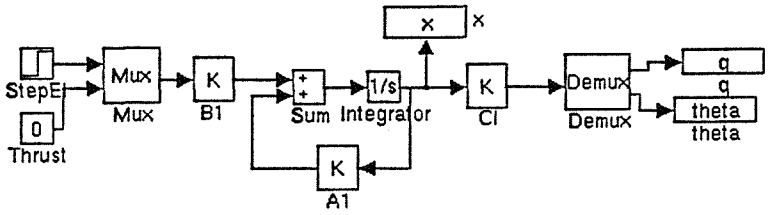
x
x
StepE
0
Thrust
Mux
Mux
K
B1
Sum
1/s
Integrator
K
C1
Demux
Demux
q
q
theta
theta
K
A1

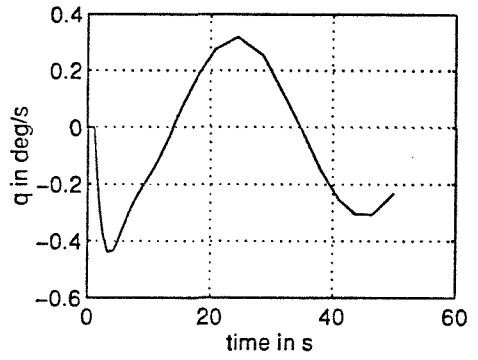
q in deg/s
time in s

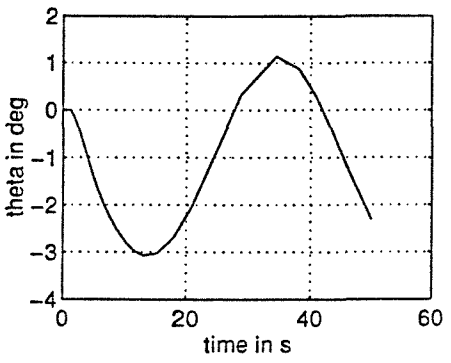
theta in deg
time in s

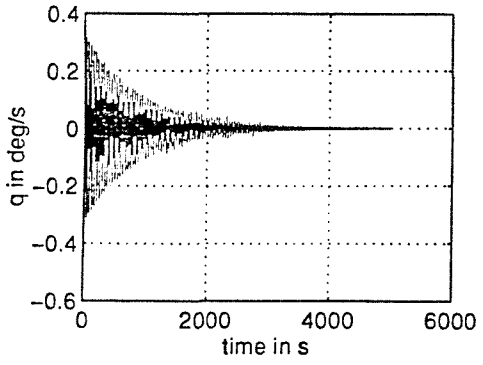
q in deg/s
time in s

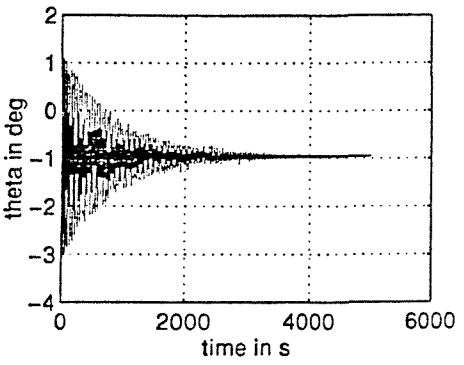
theta in deg
time in s

Figure 3.4

3.1.b Lateral motion

Lateral motion involves sideslip, roll and yaw motions, which correspond to the following state variables :

- β, the change in sideslip [deg];
- p, the change in roll rate [$ft.s^{-1}$];
- r, the change in yaw rate [$ft.s^{-1}$];
- φ, the change in bank angle [deg].

Hence, the state vector x representing lateral motion can be expressed as :

$$\mathbf{x} = \begin{bmatrix} \beta \\ p \\ r \\ \varphi \end{bmatrix} \tag{3.20}$$

The ailerons and the rudders are the control surfaces involved in lateral motion, hence the control vector **u** may be written as :

$$\mathbf{u} = \begin{bmatrix} \delta_A \\ \delta_R \end{bmatrix} \tag{3.21}$$

The equations of motion are :

$$\dot{\beta} = Y_v\beta - r + \frac{g}{U_o}\phi + Y_{\delta_A}{}^*\delta_A + Y_{\delta_R}{}^*\delta_R \tag{3.22}$$

$$\dot{p} = L'_\beta\beta + L'_p p + L'_r r + L'_{\delta_A}\delta_A + L'_{\delta_R}\delta_R \tag{3.23}$$

$$\dot{r} = N'_\beta\beta + N'_p p + N'_r r + N'_{\delta_A}\delta_A + N'_{\delta_R}\delta_R \tag{3.24}$$

$$\dot{\phi} = p \tag{3.25}$$

$$\dot{\psi} = r \tag{3.26}$$

[8] This equation is rarely carried on, which is why the state coefficient matrix has only 4 rows.

The state coefficient matrix A can be expressed as :

$$A = \begin{bmatrix} Y_v & 0 & -1 & -g/U_o \\ L'_\beta & L'_p & L'_r & 0 \\ N'_\beta & N'_p & N'_r & 0 \\ 0 & 1 & 0 & 0 \end{bmatrix} = \begin{bmatrix} -.089 & 0 & -1 & .1457 \\ -1.39 & -.975 & .327 & 0 \\ .186 & -.166 & -.3 & 0 \\ 0 & 1 & 0 & 0 \end{bmatrix} \quad (3.27)$$

and the driving matrix B as :

$$B = \begin{bmatrix} 0 & Y^*_{d_R} \\ L'_{\delta_A} & L'_{\delta_R} \\ N'_{\delta_A} & N'_{\delta_R} \\ 0 & 0 \end{bmatrix} = \begin{bmatrix} 0 & .0148 \\ .227 & .0636 \\ .0264 & -.151 \\ 0 & 0 \end{bmatrix} \quad (3.28)$$

Table 3.2 summarizes some of the results related to lateral dynamic stability :

Mode	Eigenvalue	Natural Frequency rad/s	Damping Ratio	Period s	Settling Time s
Spiral convergence	-.0848	-	-	-	-
Rolling subsidence	-1.227	-	-	-	-
Dutch roll	-.0261± j.6877	.6884	.0379	9.127	192

Table 3.2

Figure 3.5 shows the roll rate and yaw rate responses to an unit step aileron command with two time scales (60 and 600 s). The corresponding open-loop block diagram is also shown.

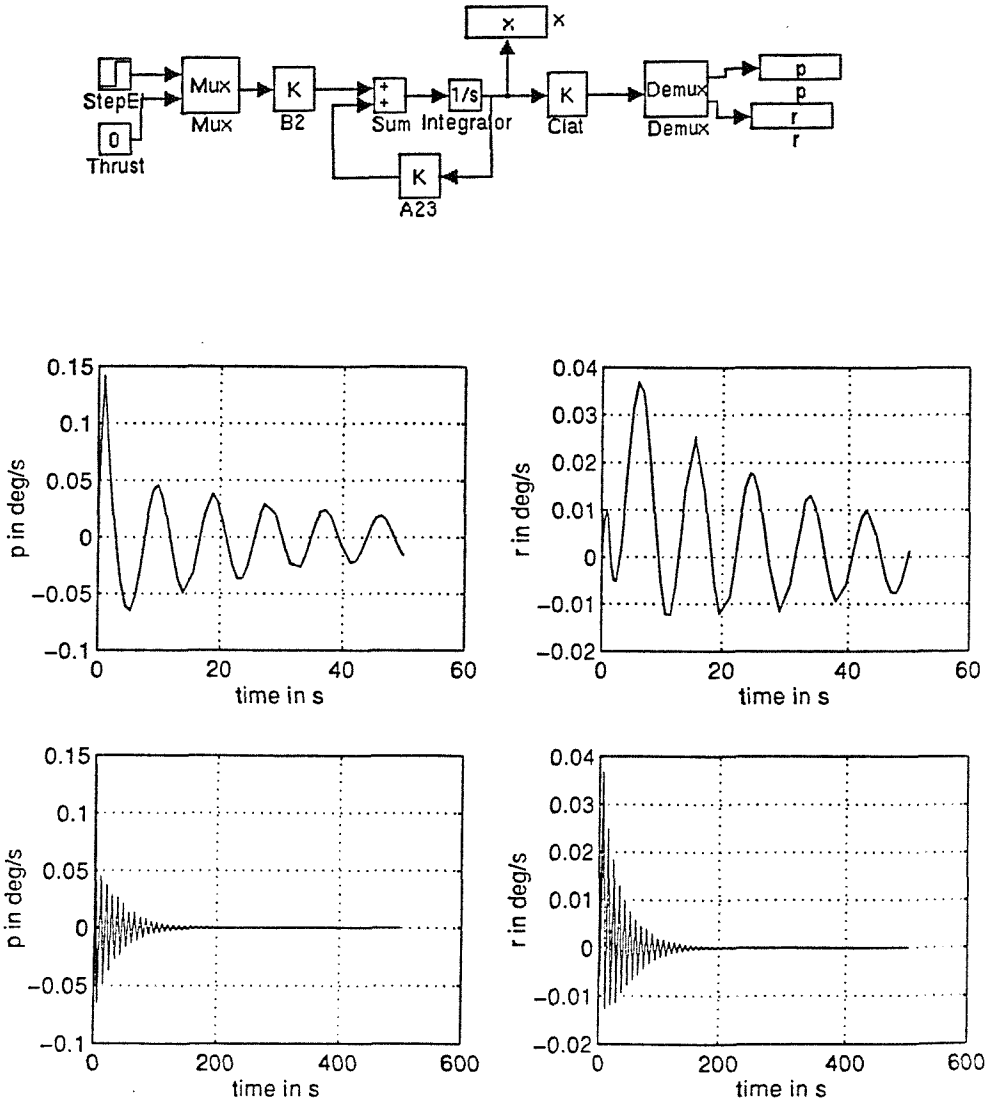
x
x
StepE
0
Thrust
Mux
Mux
K
B2
Sum
1/s
Integrator
K
Clat
Demux
Demux
p
p
r
r
K
A23
p in deg/s
time in s
r in deg/s
time in s
p in deg/s
time in s
r in deg/s
time in s

Figure 3.5

The responses for p and r are dominated by the rolling subsidence and the dutch roll modes and converge to zero after a settling-time about 200s. Here the usual UK definition of settling time has been used viz the time taken to settle within 1% of the final steady value. The usual approximation of 5 X the principal time constant applies.

Without any feedback control, the Boeing-747 is seen to be underdamped, particularly for the longitudinal motion. Therefore, the use of a Stability Augmentation System (SAS) is required.

3.2 SAS and attitude control

A Stability Augmentation System (SAS) should increase the dynamic stability of an aircraft (McRuer and Graham, 1981). Since the design of such a stabilizing control involves full state variable feedback, attitude control system is treated at the same time. This attitude control allows an aircraft to be placed and maintained in any required specified orientation in space.

3.2.a Longitudinal control

The method of eigenvalues assignment was chosen for the SAS design since it gives the designer an opportunity of precisely locating the eigenvalues of the closed-loop system in such a way that the dynamic response of the system is acceptable. The problem consists of finding a feedback matrix, K_C, to be used in the control law :

$$\mathbf{u} = K_C.\mathbf{x}, \tag{3.29}$$

such that the eigenvalues, λ_i, of the closed-loop system are placed at specified locations. Note that the closed-loop system is defined by :

$$\dot{\mathbf{x}} = (A + BK_C)\mathbf{x} \tag{3.30}$$

Therefore the eigenvalues, λ_i, are determined from the characteristic polynomial, $f(\lambda)$:

$$f(\lambda) = |\lambda I - A - B K_C| \tag{3.31}$$

To determine the feedback matrix a method involving " equating coefficients" was used : K_C was determined by equating the coefficients of the polynomial equation (3.31) with those of the desired polynomial, which was formed from the specified eigenvalues.

In the particular case of this research, the following situation obtained :

- open-loop eigenvalues :

  $-.4439 \pm j.6286$

  $-.0011 \pm j.1507$

- desired closed-loop eigenvalues :

-.5 ± j .4

-10 ± j 7.071

which yielded to the feedback matrix, K_c:

$$Kc = \begin{bmatrix} -.1983279 & -1.144660 & -30.86533 & -114.8368 \\ 16497.426 & -235.6975 & 1108199.4 & 12809960.3 \end{bmatrix} \quad (3.32)$$

The high values of feedback gains reflect the fact that one of the inputs to the aircraft dynamics is engine thrust. These "gains" are much smaller when engine gain is factored out.

The feedback matrix Kc was found by using the Matlab function PLACE :

Kc = PLACE(A,B,P)

where

P = [-5+J*.4; -5-J*.4; -10+J*7.071; -10-J*7.071] (3.33)

and J = SQRT(-1). (3.34)

Table 3.3 presents the resulting longitudinal dynamic stability information :

Mode	Eigenvalue	Natural Frequency rad/s	Damping ratio	Period s	Settling Time s
Phugoid	-.5±j.4	.64	.78	9.817	-
Short period	-10±j7.071	12.22	.818	.514	.50

Table 3.3

Figure 3.6 shows the closed-loop responses which resulted when an unit step command input was applied.

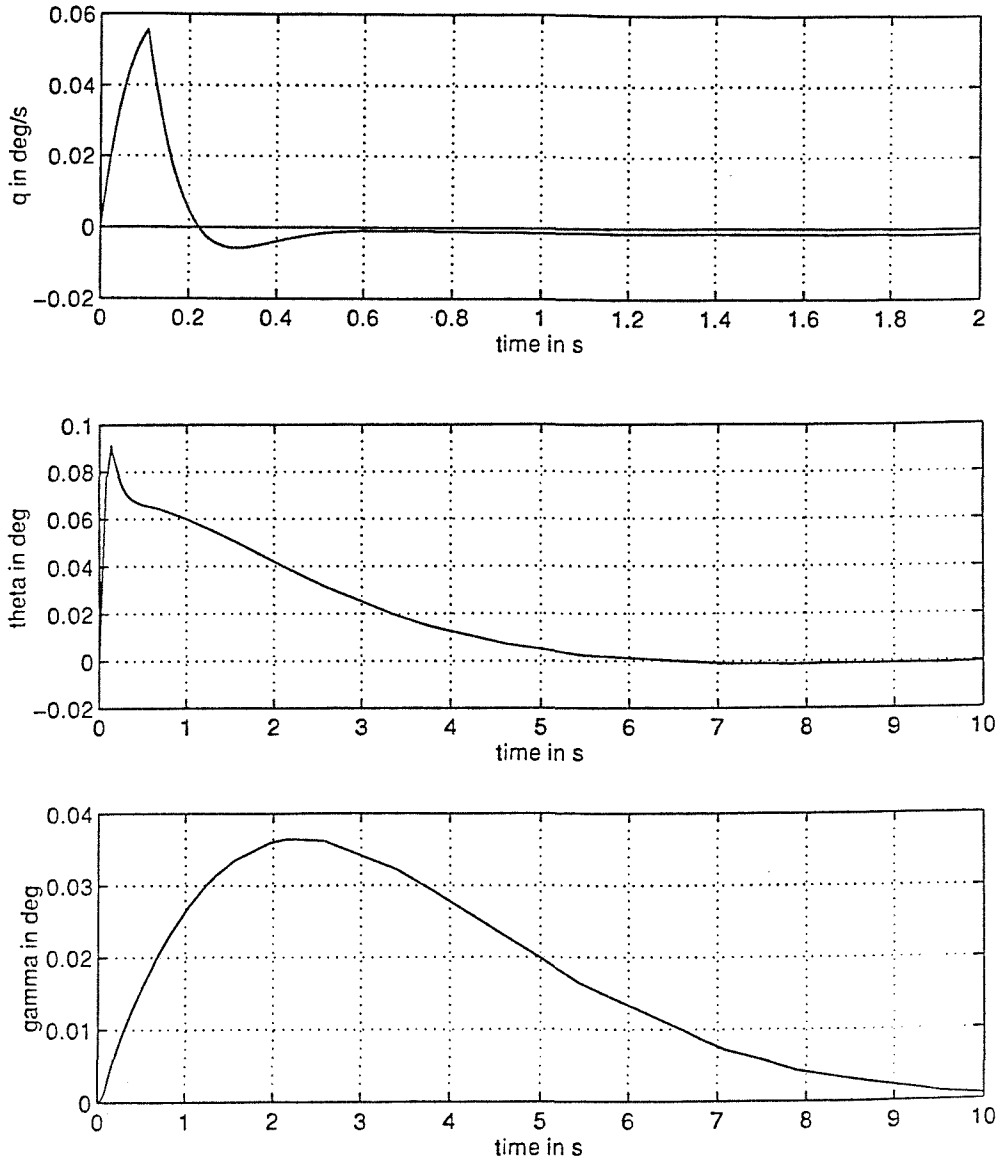
q in deg/s
0.06
0.04
0.02
0
-0.02
0
0.2
0.4
0.6
0.8
1
1.2
1.4
1.6
1.8
2
time in s
theta in deg
0.1
0.08
0.06
0.04
0.02
0
-0.02
0
1
2
3
4
5
6
7
8
9
10
time in s
gamma in deg
0.04
0.03
0.02
0.01
0
0
1
2
3
4
5
6
7
8
9
10
time in s

Figure 3.6

Notice that the flight path angle, γ, of the aircraft is obtained from the kinematic relationship :

$$\frac{\gamma(s)}{\theta(s)} = \frac{1}{1+sT_A} \tag{3.35}$$

where

$$\gamma = \theta - \alpha; \tag{3.36}$$

$$\alpha = w/Uo; \tag{3.37}$$

$T_A = -Z_W^{-1}$ is the aircraft time constant and equals to -0.512. (3.38)

The corresponding block diagram is given in Figure 3.7 :

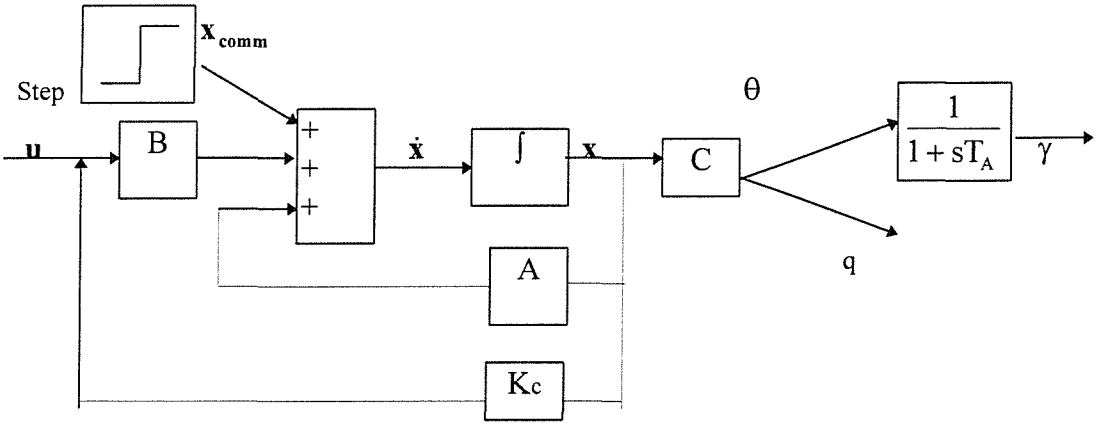

Figure 3.7

The results correspond now to acceptable flying qualities; ie well-damped pitch attitude θ with flight path angle, γ, returning to zero after being disturbed.

3.2.b Lateral control

The lateral SAS was designed using the modern theory of optimal control, because the design is unique and meets exactly a specified performance criterion. Eigenvalue assignment could also have been used, but there is less assurance in assigned eigenvalues providing required dynamic response with lateral motion, in which the modes of motion are coupled. An optimal control system is a system whose parameters are adjusted so that a performance index, J, has a minimum value. The performance index is of the form :

$$J = \frac{1}{2}\int_0^\infty (\mathbf{x}^T.Q.\mathbf{x} + \mathbf{u}^T.G.\mathbf{u})dt \qquad (3.39)$$ [9]

This problem is referred to in the literature as the "linear quadratic problem" which requires for its solution the determination of an optimal control, **u**, which will minimize the index , J, and which will control the aircraft whose dynamics are described by the state equation (3.1), ie.

$\dot{\mathbf{x}} = A\mathbf{x} + B\mathbf{u}$

Q and G are weighting matrices of order n*n and m*m, respectively, which have to be chosen by the designer.

The theory of the LQP shows that minimizing the index J with respect to the control function **u**, is equivalent to solving an algebraic Riccati equation (ARE) viz.

$$0 = P.A + A^T.P - P.B.G^{-1}.B^T.P + Q \qquad (3.40)$$

Solving equation (3.40) provides the linear optimal control law :

$$\mathbf{u} = -G^{-1}.B^T.P.\mathbf{x} = K_C.\mathbf{x} \qquad (3.41)$$

[9] T denotes the transpose of a matrix.

where

K_c is the feedback gain matrix.

The feedback matrix, K_c, used in the lateral control law was computed using the Matlab function, LQR ie.

$K_C = LQR(A, B, Q, G)$

where

$Q = diag\ \{ .1\ 10.0\ 5.0\ 2.0\}$ (3.42)

$G = diag\ \{.1\ 5.0\}$ (3.43)

It was determined that :

$$Kc = \begin{bmatrix} -4.182 & 8.303 & 1.591 & 4.366 \\ .094 & .076 & -.485 & .037 \end{bmatrix} \quad (3.44)$$

The resulting closed-loop system is characterised by the parameters quoted in Table 3.4 :

Mode	Eigenvalue	Natural Frequency rad/s	Damping Ratio	Period s	Settling Time s
Spiral convergence	-.0848	-	-	-	-
Rolling subsidence	-1.227	-	-	-	-
Dutch roll	-.0261± j.6877	.6884	.0379	9.127	192

Table 3.4

Figure 3.8 gives the corresponding block diagram :

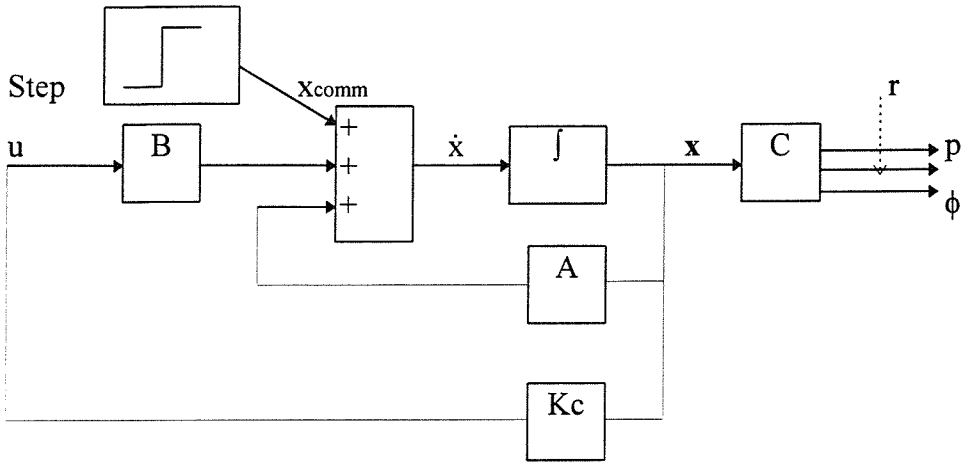

Figure 3.8

Figure 3.9 shows the closed-loop responses for roll rate, yaw rate and bank angle, which were obtained for an unit step command input.

The results are dynamically satisfactory; ie not too oscillatory with zero steady-state error.

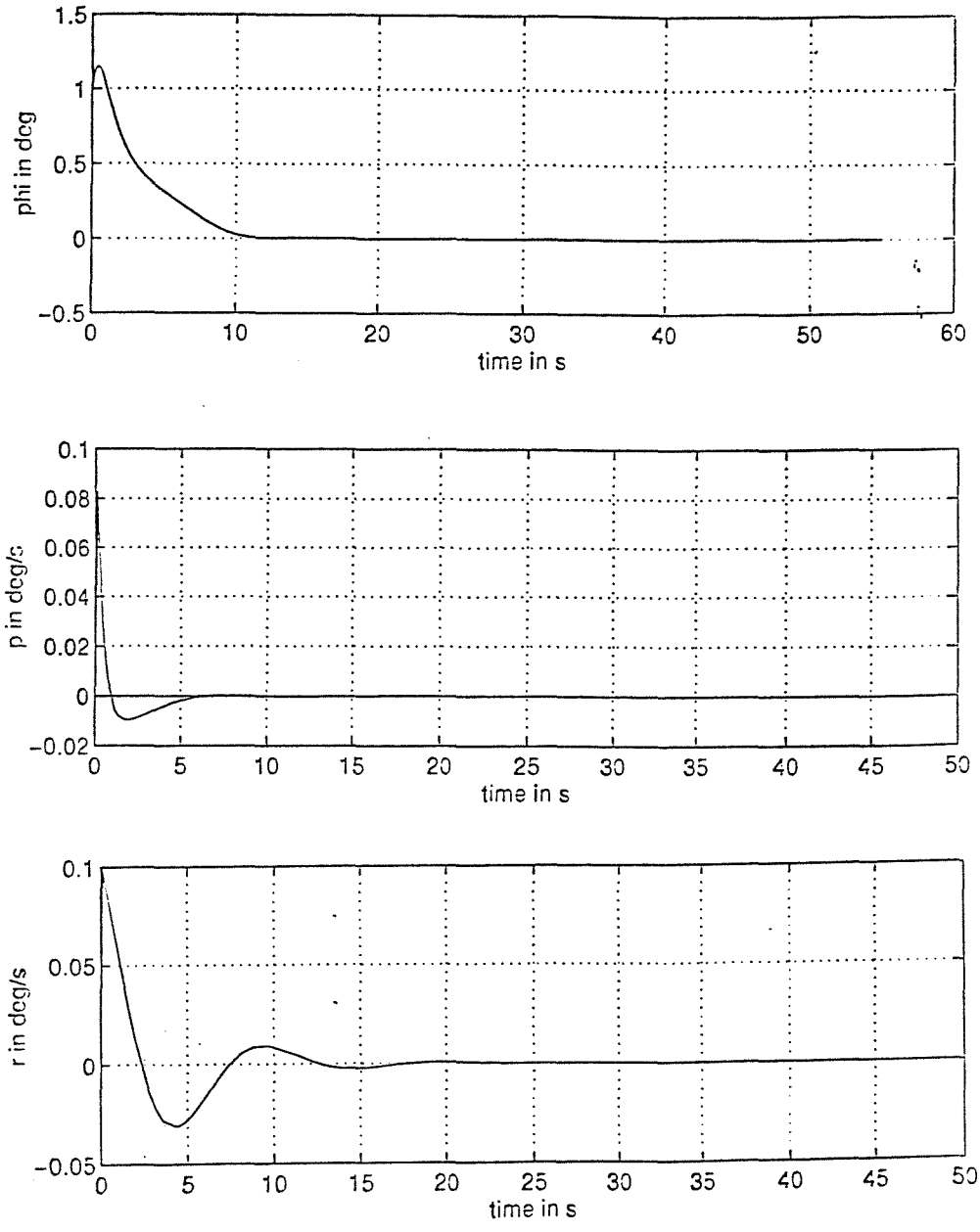

Figure 3.9

But, the yaw damper, just described, tends to oppose any change in yaw rate even when it has been commanded. Therefore, to avoid such opposition, another feedback signal only acting on the rudder has been added. This feedback signal consists of two elements :

- a proportional controller, with a gain of value 2.0.
- a wash-out filter, whose transfer function is given by :

$$\frac{s}{s+1/T_{wo}} \tag{3.45}$$

where

$$T_{wo} = 0.15. \tag{3.46}$$

This value of wash out time constant was chosen as a compromise between good d.c. rejection and minimal impairment of system transient response.

Figure 3.10 shows the block diagram, which incorporates the wash-out filter :

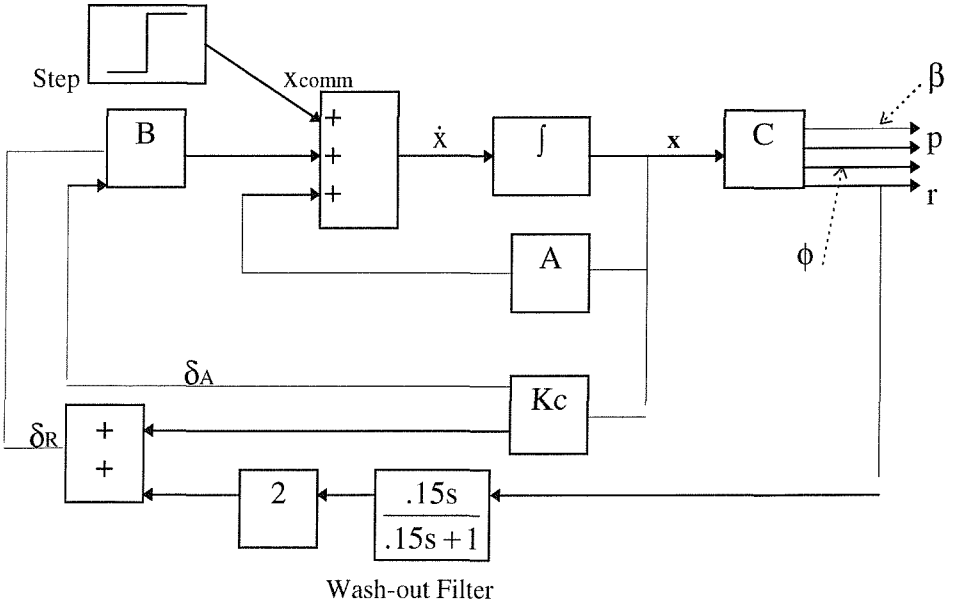

Figure 3.10

Figure 3.11 shows the responses for the sideslip, the roll and yaw rates and the bank angle. The results converge quickly to a zero value.

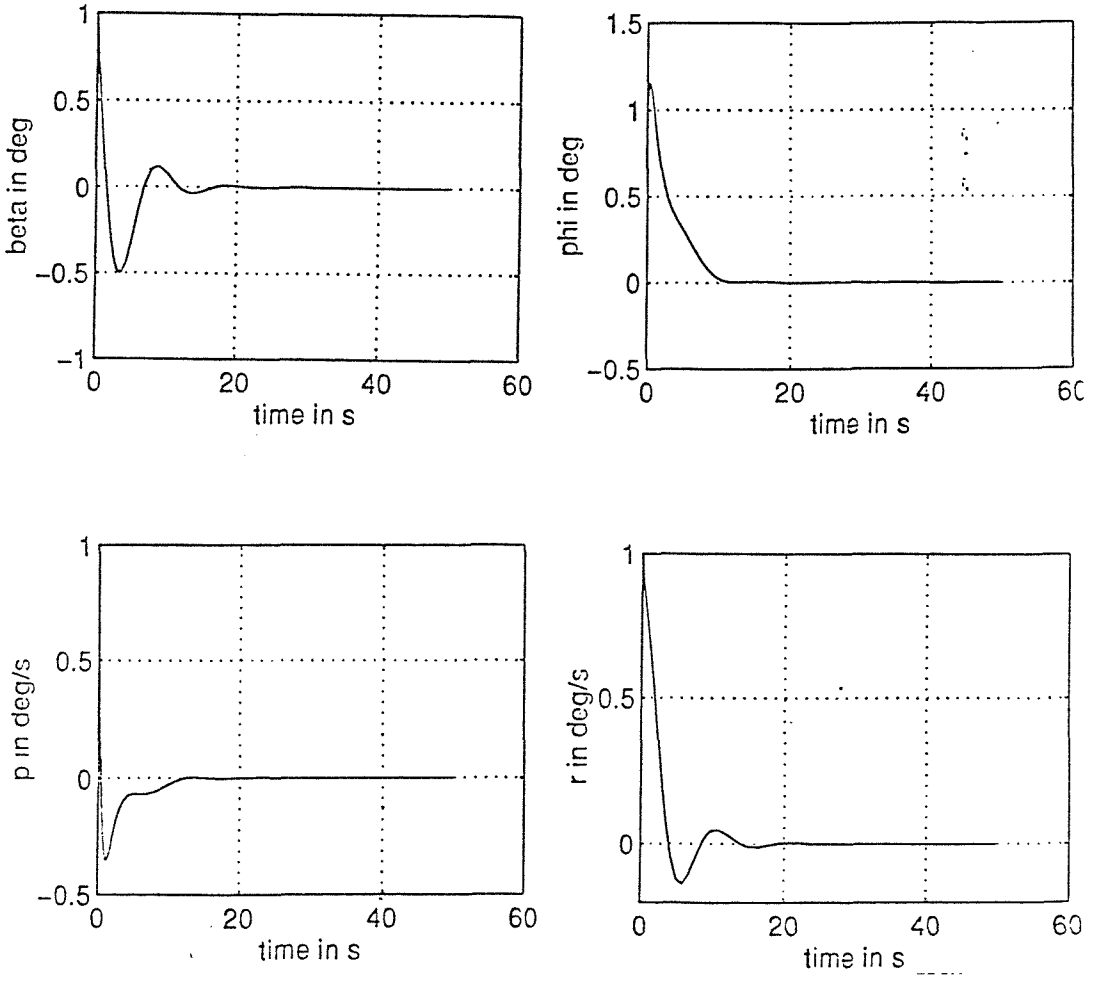
beta in deg
time in s
phi in deg
time in s
p in deg/s
time in s
r in deg/s
time in s

Figure 3.11

The flight path control system permits the control of translation in either the normal or lateral direction. Because there are no special control surfaces to control the translational motion, the production of a lateral or normal displacement requires the indirect use of attitude control systems. Consequently, flight path control systems form outer loops around the attitude control systems.

Results for flight path control systems using ILS, MLS and DGPS to serve such translational displacements are given in this chapter for several different entry conditions and a number of atmospheric conditions.

4.1 Glide-Path-Coupled control system

Such a system is designed to closely control an aircraft's deviation above or below some desired glide path.

4.1.a Generalities

The output signal from a glide path receiver in the aircraft is used as a guidance command to the attitude control system. The aircraft's flight path angle, γ, translates into a linear displacement, d, from the desired glide path, viz.

$$d(t) = \frac{Uo}{57.3} * \int(\gamma + \gamma_{ref})dt \qquad (4.1)$$ [10]

where

γ_{ref} is the reference flight path angle which, if flown by the aircraft, would result in the aircraft descending along the glide path.

[10] The division by 57.3 transforms (γ+γref) from degrees to radians.

The signal measured by the glide path receiver is the angular deviation, Γ, or glide path error.

Γ is expressed in radians and is defined as :

$$\Gamma(t) = \frac{57.3}{R(t)} * d(t) \qquad (4.2)^{11}$$

where

- R(t) is the slant range in metres given by :

$$R(t) = Ro - Uo*t \qquad (4.3)$$

- Uo = 67 m/s; (4.4)

- Ro = 9000 m; (4.5)

- t is the time expressed in seconds.

For small values of R the closed-loop system becomes unstable ($\frac{57.3}{R} \rightarrow \infty$). Hence, the range must always exceed a critical minimum value, which was chosen in this work to be 200 m.

Notice that if $\gamma = \gamma_{ref}$ then $\Gamma = 0$.

The situation is represented in Figure 4.1 :

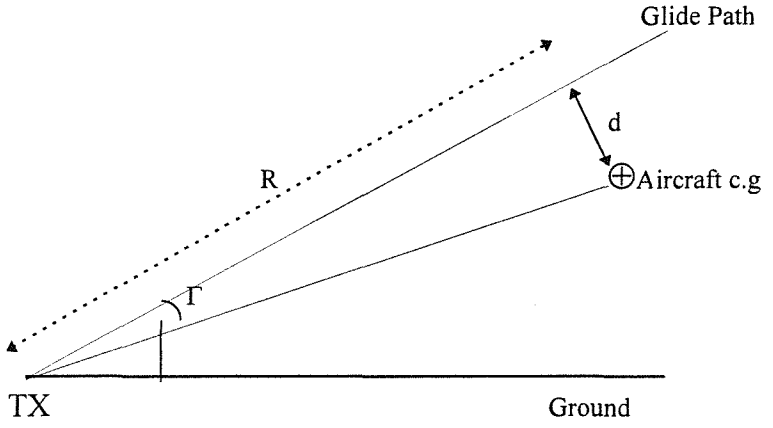

Figure 4.1

[11] The multiplication by 57.3 transforms Γ from radians to degrees.

The transfer function, Gc(s), of the glide-path-coupled controller has two terms :

- a proportional plus integral term equal to :

$$(-6 - \frac{.1}{s})$$

- a phase advance term, which is introduced to provide additional stabilization. This term was designed to be :

$$\left(\frac{.4s+1}{.04s+1}\right)$$

The controller transfer function, Gc(s), used therefore was given by :

$$Gc(s) = -\left(6+\frac{.1}{s}\right)\left(\frac{.4s+1}{.04s+1}\right) \qquad (4.6)$$

The design of this conventional controller was based on complex frequency domain techniques and was arranged to provide good transient response with zero steady-state error.

Figure 4.2 shows the corresponding block diagram of the glide-path coupled system.

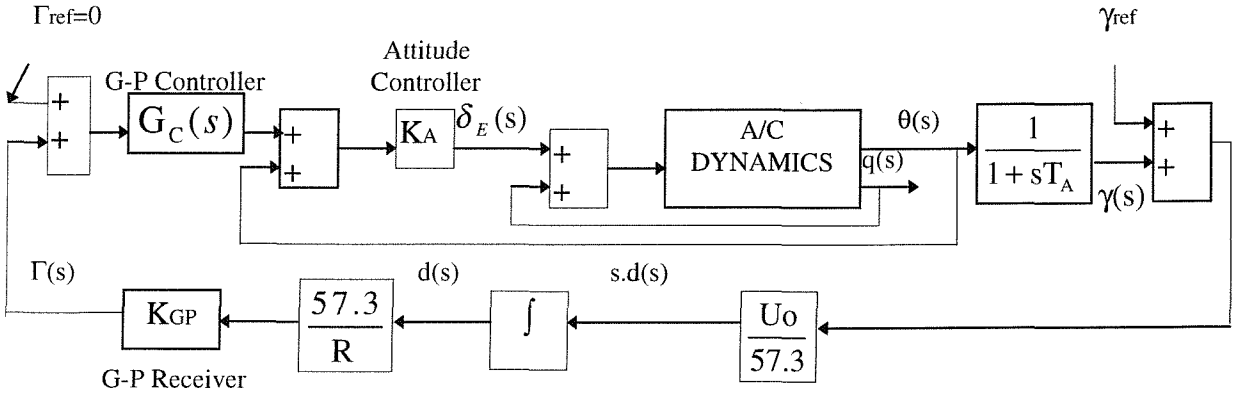

Figure 4.2

So far, the speed of the aircraft had been assumed to be constant and equal to 67 m/s. In practice, however, the aircraft speed will change with time, from the value, U_0, at the start of the approach to a lower value, U_1, at the end of the approach phase.

In this research work :

- $U_0 = 67$ m/s (4.7)

- $U_1 = 52$ m/s (4.8)

The time of the interval between the beginning and the end of the approach was taken as 100 s, which represents a practical value.

Hence, the change in reference speed ,u_{ref}, was defined as :

$$u_{ref}(t) = -.33t + 67.0 \quad (4.9)$$

In order that the change in aircraft speed would correspond with the appropriate speed schedule, $u_{ref}(t)$, an aircraft speed control system was added to the glide-path coupled control system.

The speed of the aircraft was controlled by changing the thrust, δ_{TH}, of the engines. The transfer function representing the engine dynamics, $G_E(s)$, was assumed to be linear and was approximated as follows :

$$G_E(s) = \frac{K_E}{1 + sT_E} \quad (4.10)$$

where

- $T_E = 1$s (4.11)

- $K_E = 35000$ N/rad (4.12)

K_E was determinated in the following way :

The excess thrust of an aircraft is given by :

$$T_{EXCESS} = T_{MAX} - \frac{W}{L/D} \quad (4.13)$$

where

- T_{MAX} denotes the maximum thrust from the engines. For the Boeing-747, T_{MAX} approximately equals 800 000 N;
- W denotes the landing weight, which was equal to 2 450 000 N;
- L/D is the Lift/Drag ratio. On approach, this ratio was quoted as 8.9.

Hence :

$T_{EXCESS} = 525\ 000$ N. (4.14)

The maximum throttle deflection, θ_{max}, was assumed to be 1.5 rad and the control authority, η, was restricted to 10 %., For this authority figure, the engine gain was given by :

$$K_E = \eta * \frac{T_{EXCESS}}{\theta_{max}}, \text{ ie.} \quad (4.15)$$

$$K_E = 35000 N.rad^{-1} \quad (4.16)$$

The transfer function, G'_C, of the speed controller was defined as :

$$G'_C(s) = K_{C_1} * (1 + \frac{K_{C_2}}{s}) \quad (4.17)$$

where the controller gains were designed to be :

- $K_{C_1} = 25$ (4.18)

- and $K_{C_2} = 0.1$ (4.19)

The design was based on complex frequency methods and was arranged to provide acceptable transient response - minimal overshoot, no oscillation, rapid rise time and short settling time.

Notice that the speed control law involved an integral term thereby which eliminated any steady-state error.

The feedback was based upon sensed airspeed and sensed acceleration. A block diagram of the speed control system is shown in Figure 4.3.

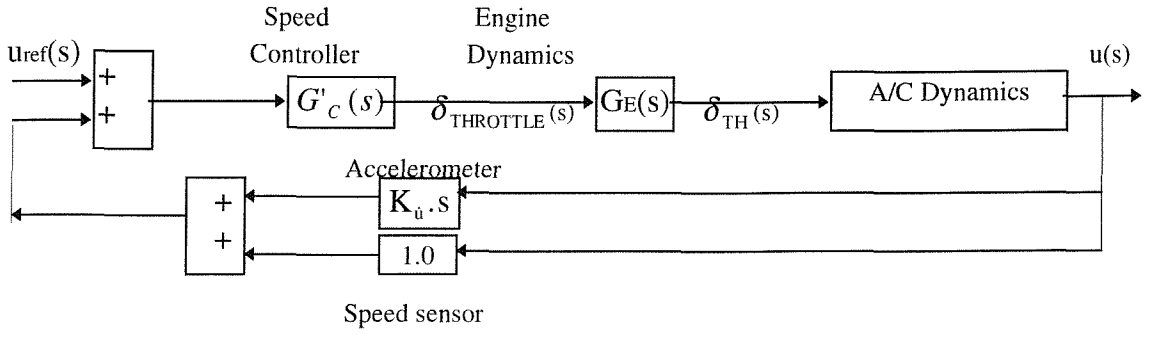

Figure 4.3

4.1.b Use of the ILS

The dynamics of the ILS glide-path receiver were considered to be instantaneous even though it contains filters for the 90 Hz and 150 Hz modulation components of the glide path signal. The receiver transfer function was represented by its sensitivity, K_{GP}, viz :

$$K_{GP} = 1 \text{ V/°} \qquad (4.20)$$

The reference flight path angle was 3°.

4.1.b.(i) Responses for different entry conditions

The system responses for the initial values of pitch attitude, θ, flight path angle, γ, displacement, d, are shown in Figures 4.4 to 4.9 for the approach entry conditions given in table 4.1.

FIGURE	γ (0) Degrees	θ(0) Degrees	d(0) Metres
4.4	- 3.0	-3.0	0
4.5	-2.0	-2.0	0
4.6	-3.0	-3.0	- 50
4.7	- 3.0	-3.0	+ 50
4.8	0	0	- 50
4.9	0	0	+ 50

Table 4.1

In every case, the glide path angle, γ, converged to a value equal to or very close to the desired value, -3°. It can be seen from the figures that the responses for θ, d and Γ often approach a value, which was not exactly zero although very close. Irregardless of these

steady-state errors, the dynamic responses with the glide-path coupled control system were all satisfactory, and corresponded to acceptable performance for the closed-loop system. It should be noted, that the aircraft had to produce very large changes in flight path angle for the extreme "incorrect" entry conditions being applied (See Figures 4.8 and 4.9).

In the following figures Lambda denotes the beam error, Γ

Figures 4.5 - 4.9
4.11 - 4.22
4.24 - 4.31
4.34
4.36 - 4.42
4.44 - 4.52

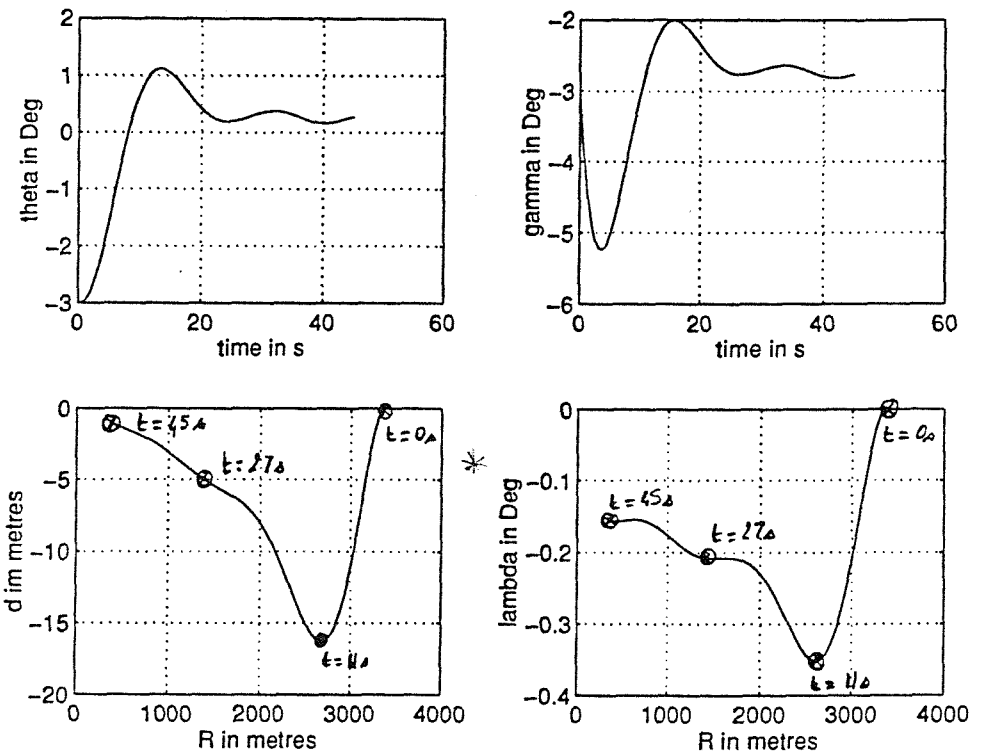

$\gamma(0) = -3.0°$

$\theta(0) = -3.0°$

$d(0) = 0.0$ m

Figure 4.4

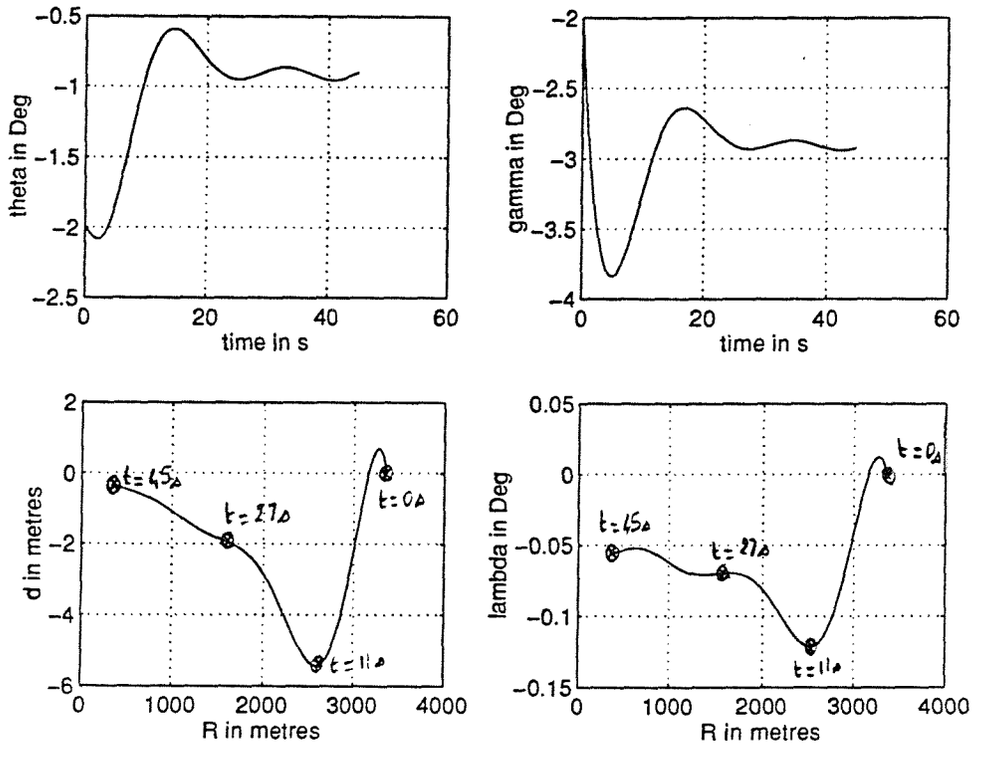

$\gamma(0) = -2.0°$

$\theta(0) = -2.0°$

$d(0) = 0.0$ m

Figure 4.5

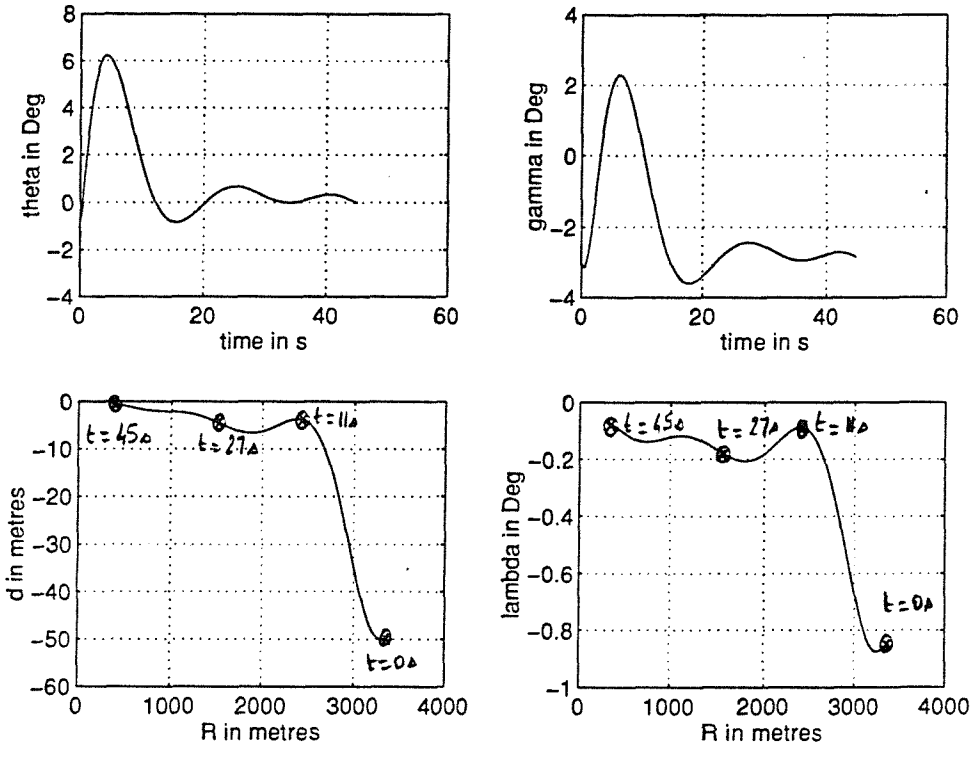

$\gamma(0) = -3.0°$

$\theta(0) = -3.0°$

$d(0) = -50.0$ m

Figure 4.6

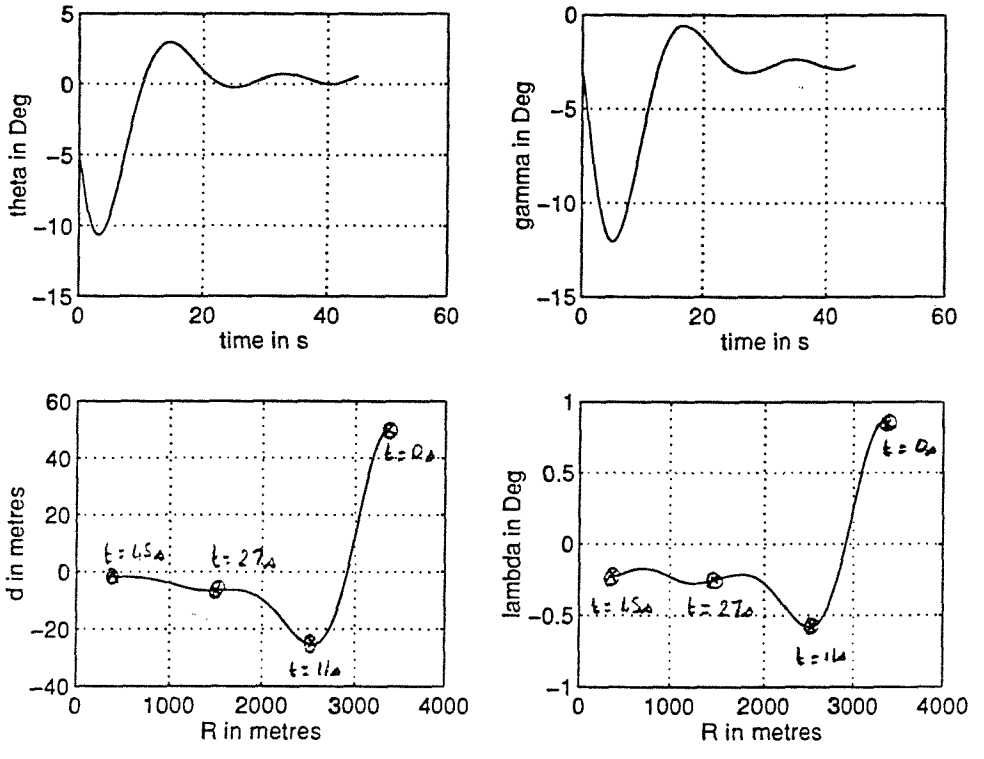

$\gamma(0) = -3.0°$

$\theta(0) = -3.0°$

$d(0) = +50.0$ m

Figure 4.7

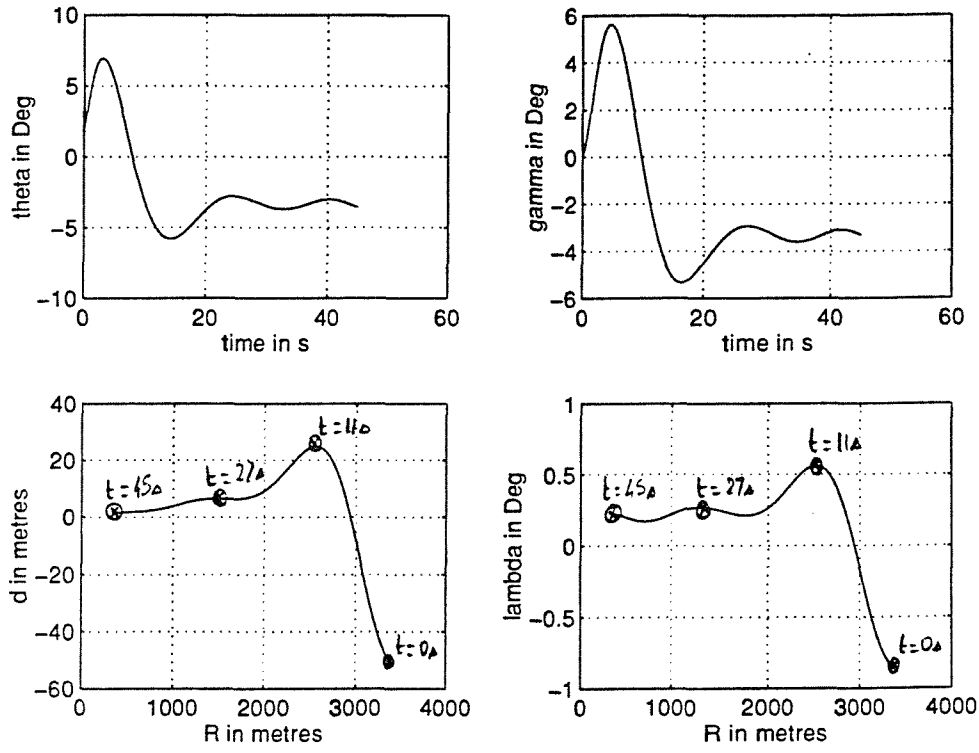

$\gamma(0) = 0°$

$\theta(0) = 0°$

$d(0) = -50.0$ m

Figure 4.8

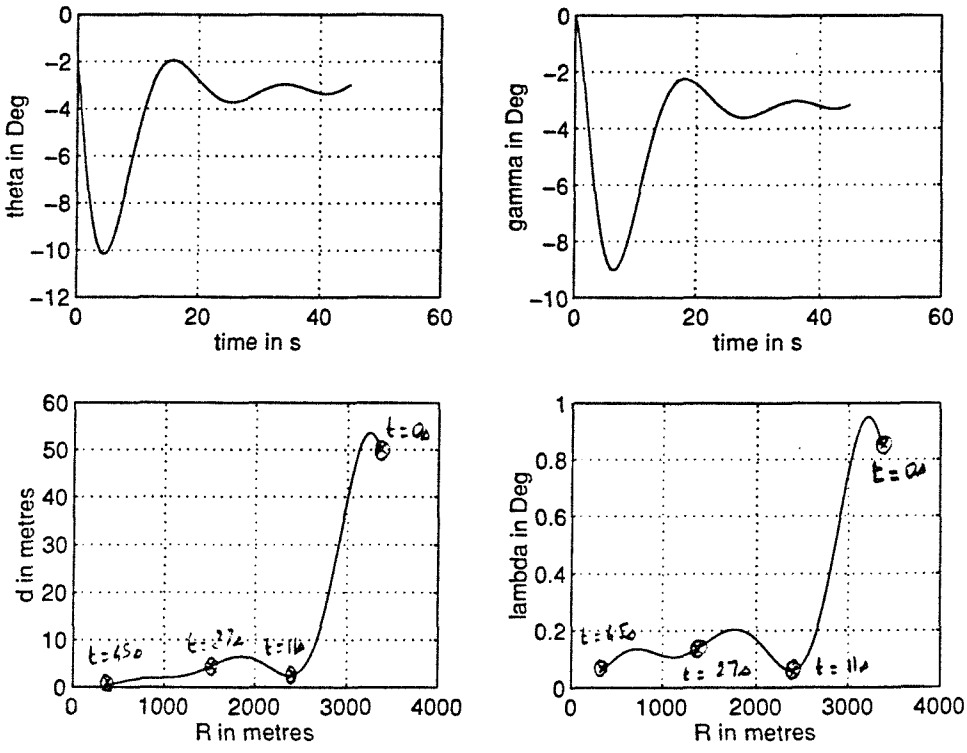

$\gamma(0) = 0°$

$\theta(0) = 0°$

$d(0) = +50.0$ m

Figure 4.9

4.1.b.(ii) Responses for different atmospheric conditions

This section describes the performances of the ILS glide-path coupled control system in the presence of air turbulence, which is considered to be continuous. Since air turbulence is a random process, atmospheric turbulence must be defined in a statistical manner, via the power spectral density (PSD), $\phi(\omega)$.

There are two particular analytical representations for the PSD function in AFCS studies (Chalk et al., 1969) :

- that based on a spectrum proposed by Von Karman.
- and an alternative PSD function proposed by Dryden.

In this research, the Dryden PSD representation, which is a practical improvement on the Von Karman model, was chosen. It had the following parameters :

- U_0, the equilibrium speed of the aircraft, at the start of the coupled descent, was chosen to be 221 ft/s;
- σ_ω, the overall root mean squared gust velocity was chosen to be 6 ft/s;
- L_ω, the turbulence scale length is defined by :

$$L_\omega = 145 * h_{cg}^{\frac{1}{3}} \qquad (4.21)$$

where :

- h_{cg} is the height of the aircraft encountering the turbulence. For the nominal approach :

$$h_{cg} = 942 \text{ ft.} \qquad (4.22)$$

$$\text{ie, } L_\omega = 1421.4 \text{ ft.} \qquad (4.23)$$

A white noise source is chosen with a PSD function, $\phi_N(\omega)$, of :

$$\phi_N(\omega) = 1.0, \qquad (4.24)$$

to provide the input signal to a linear filter, $G_i(s)$.

The filter is defined by :

$$G_i(s) = \sqrt{K_\omega} * \frac{s + \beta_\omega}{(s + \lambda_\omega)^2} \qquad (4.25)$$

where :

$$- K_\omega = \frac{3.\sigma_\omega^{\,2}}{L_\omega . \pi . U_0} \qquad (4.26)$$

$$- \beta_\omega = \frac{U_0}{\sqrt{3}.L_\omega} \qquad (4.27)$$

$$- \lambda_\omega = \frac{U_0}{L_\omega} \qquad (4.28)$$

A block diagram showing how such a turbulence signal is given as figure 4.10.

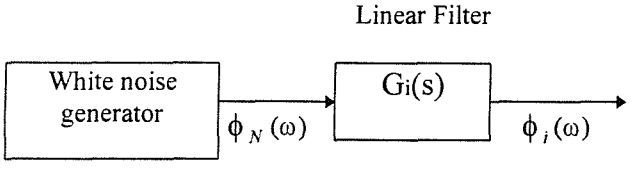

Figure 4.10

The results for θ, γ, d and Γ in the presence of atmospheric disturbances and for the entry conditions indicated in Table 4.2 are shown in Figures 4.11 to 4.16.

Even in the presence of air turbulence, the automatic landing system still provides good performance. Note the final values of longitudinal displacement, pitch attitude and flight path angle. Once again the large variations in pitch attitude and flight path angle which occur as a result of "incorrect" entry conditions should again be noted (See Figures 4.15 and 4.16).

FIGURE	γ (0) Degrees	θ(0) Degrees	d(0) Metres
4.11	- 3.0	-3.0	0
4.12	-2.0	-2.0	0
4.13	-3.0	-3.0	- 50
4.14	- 3.0	-3.0	+ 50
4.15	0	0	- 50
4.16	0	0	+ 50

Table 4.2

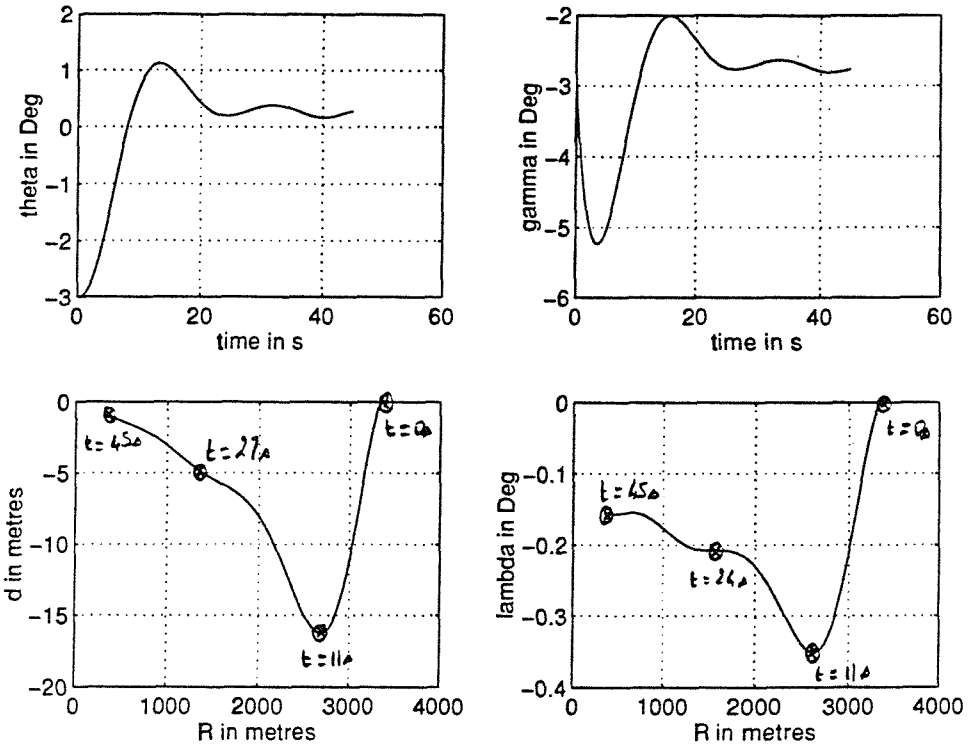

$\gamma(0) = -3.0°$

$\theta(0) = -3.0°$

$d(0) = 0$ m

Figure 4.11

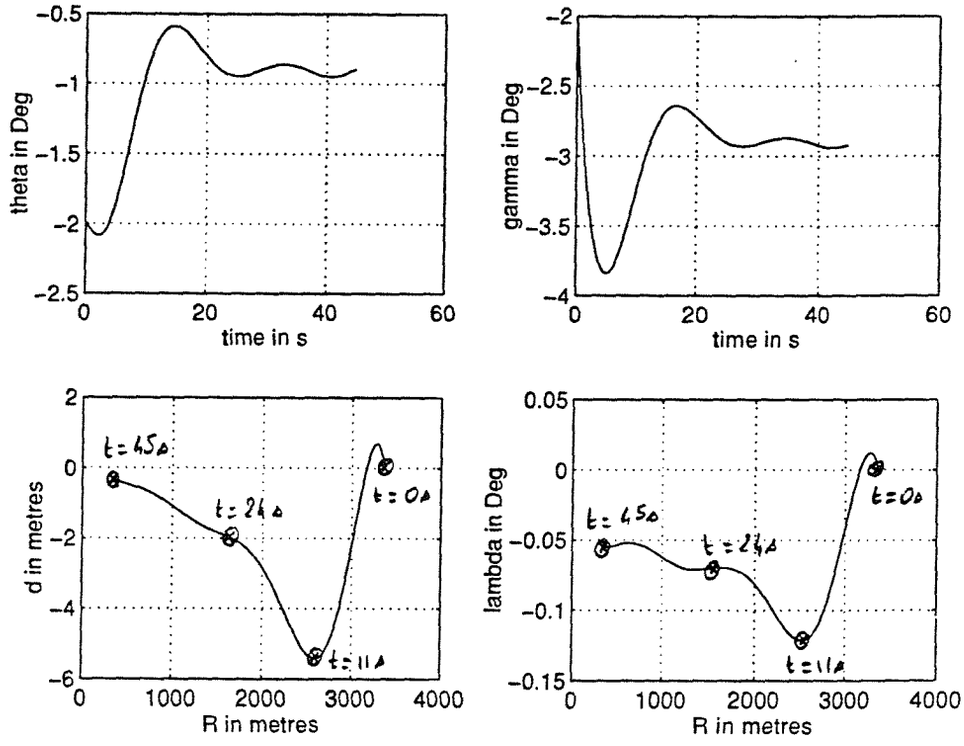

$\gamma(0) = -2.0°$

$\theta(0) = -2.0°$

$d(0) = 0$ m

Figure 4.12

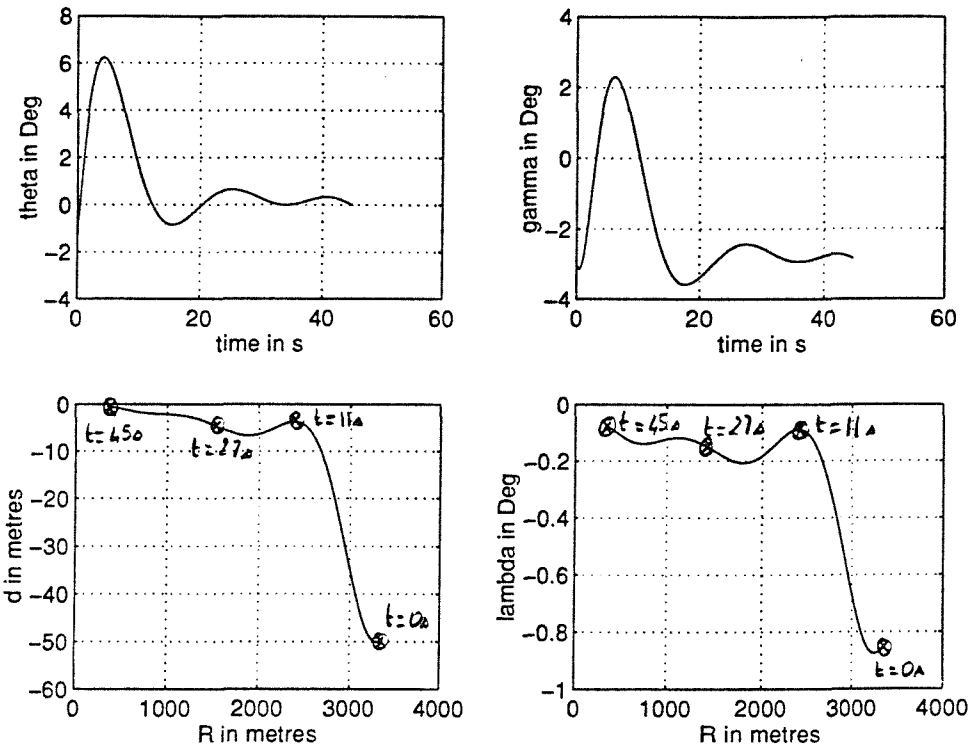

$\gamma(0) = -3.0°$

$\theta(0) = -3.0°$

$d(0) = -50$ m

Figure 4.13

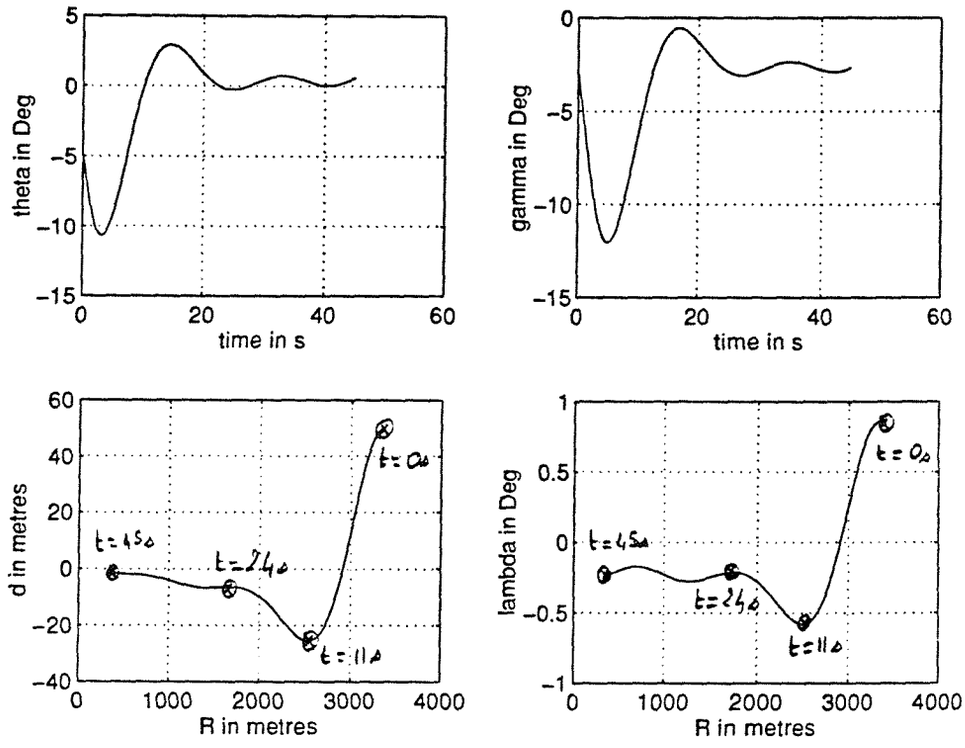

$\gamma(0) = -3.0°$

$\theta(0) = -3.0°$

$d(0) = +50$ m

Figure 4.14

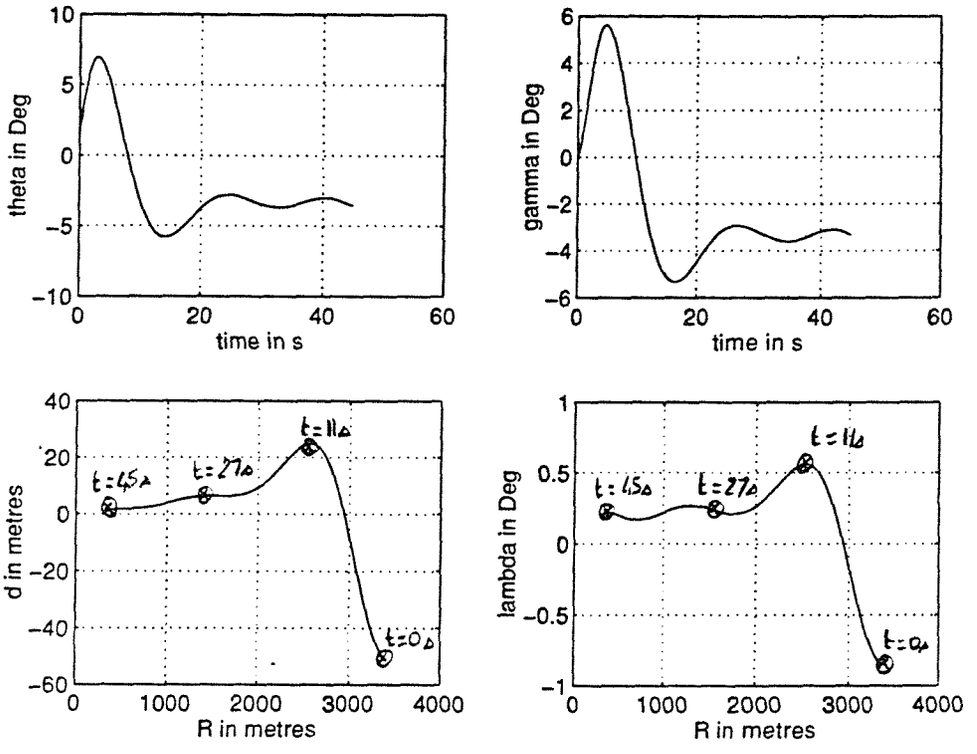

$\gamma(0) = 0°$

$\theta(0) = 0°$

$d(0) = -50$ m

Figure 4.15

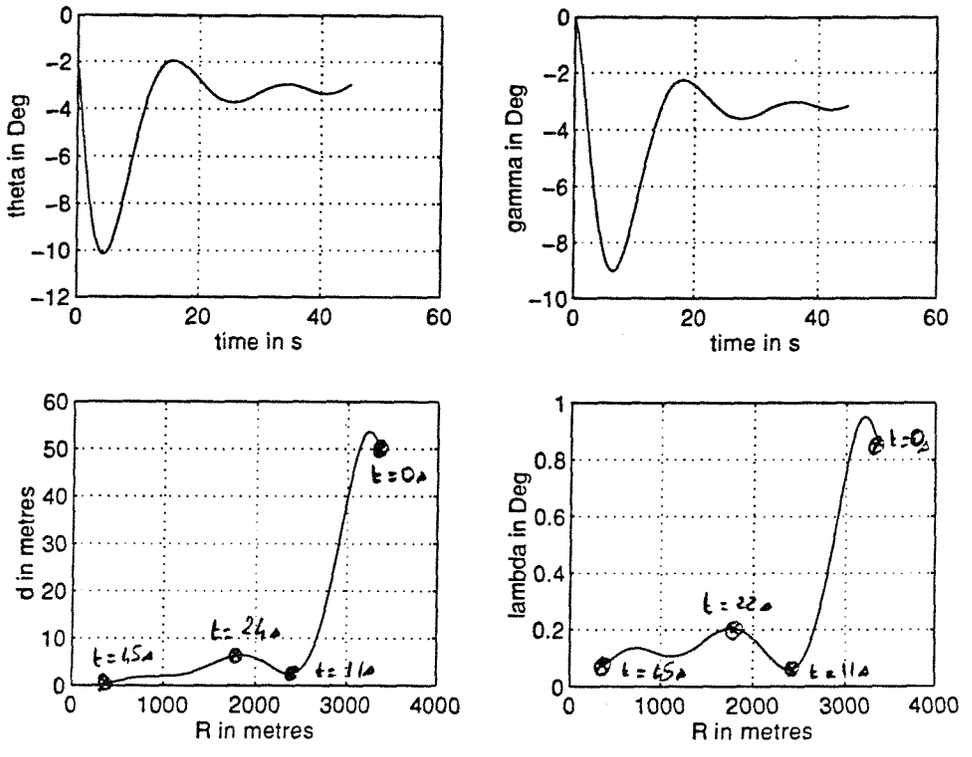

$\gamma(0) = 0°$

$\theta(0) = 0°$

$d(0) = +50$ m

Figure 4.16

4.1.c Use of the MLS

As with the ILS, the dynamics of the MLS glide-path receiver were considered to be instantaneous. The receiver transfer function was simply represented by its sensitivity, K_{GP}, viz.

$$K_{GP} = 1V/° \qquad (4.29)$$

The reference flight path angle was 6°, which is the nominal value for MLS approaches.

4.1.c.(i) Responses for different entry conditions

The system responses for initial values of pitch attitude, θ, flight path angle, γ, and path displacement ,d, are shown in Figures 4.17 to 4.22 for the approach conditions quoted in Table 4.3.

FIGURE	γ(0) Degrees	θ(0) Degrees	d(0) Metres
4.17	-2	-3	-50
4.18	-2	-3	+50
4.19	-6	-3	+50
4.20	-6	-3	-50
4.21	-4	-3	+50
4.22	-4	-3	-50

Table 4.3

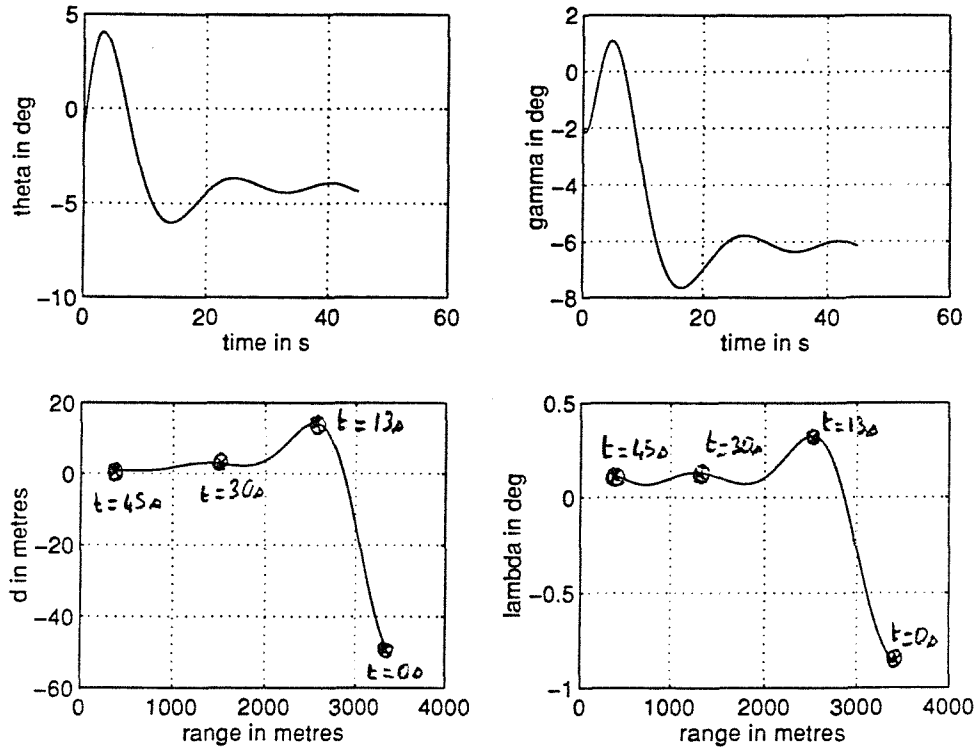

$\theta(0) = -3°$

$\gamma(0) = -2°$

$d(0) = -50$ m

Figure 4.17

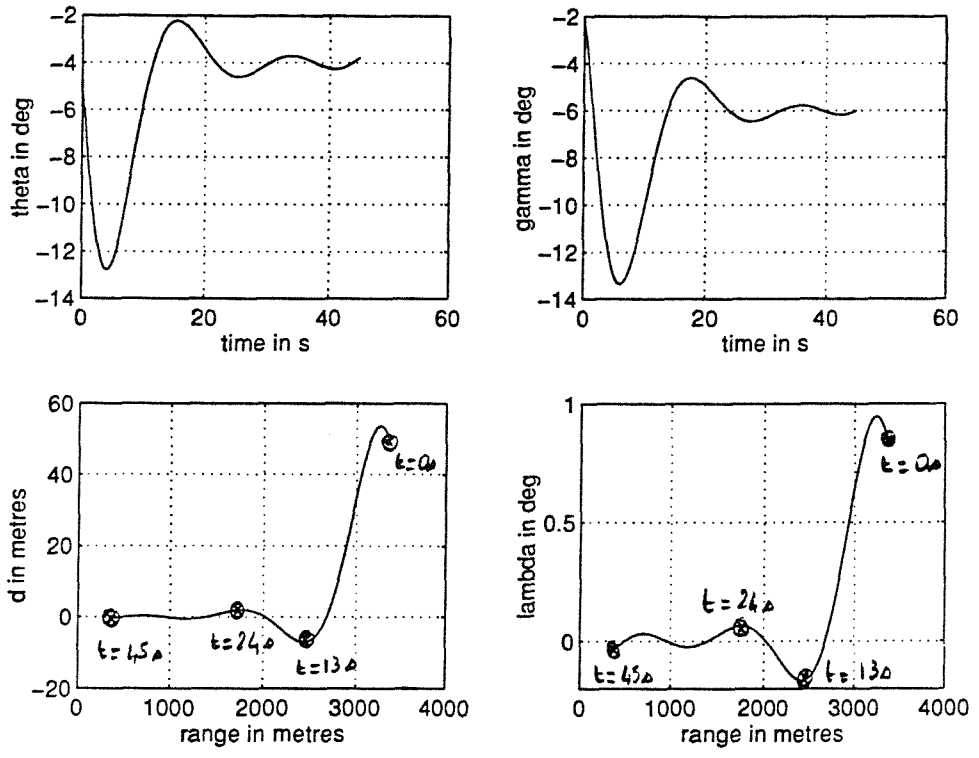

$\theta(0) = -3°$

$\gamma(0) = -2°$

$d(0) = +50$ m

Figure 4.18

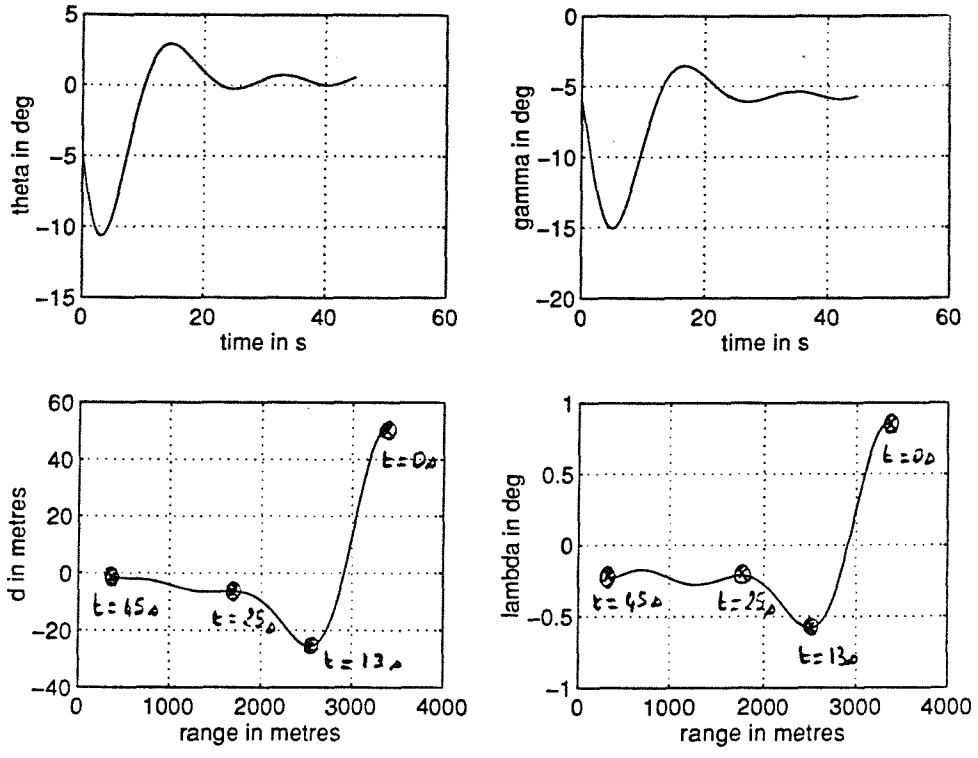

$\theta(0) = -3°$

$\gamma(0) = -6°$

$d(0) = +50$ m

Figure 4.19

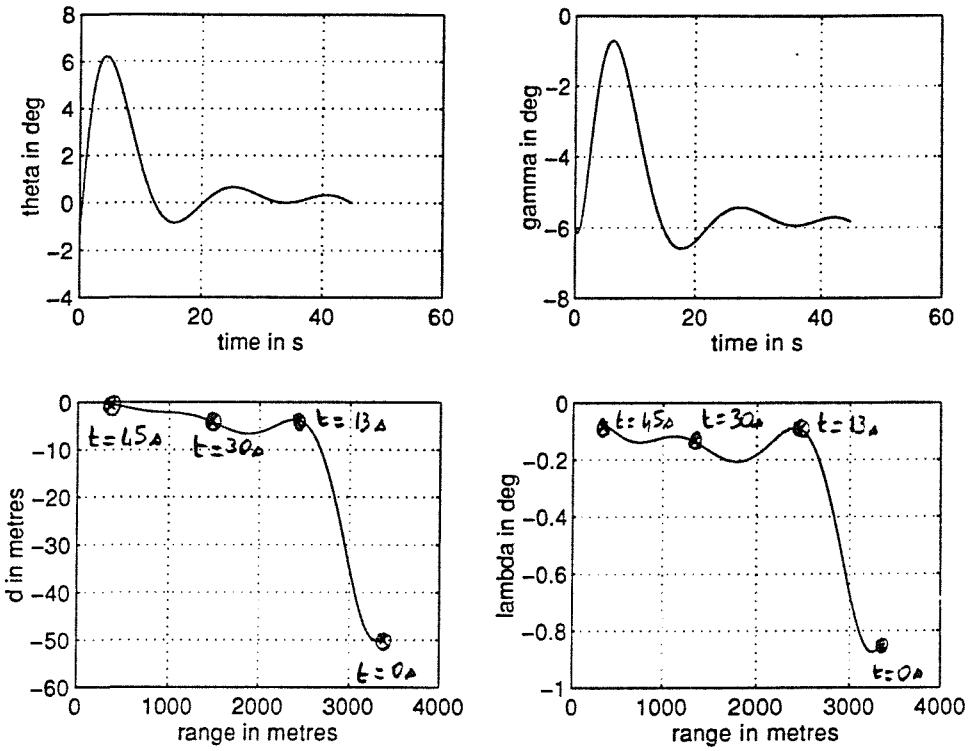

$\theta(0) = -3°$

$\gamma(0) = -6°$

$d(0) = -50$ m

Figure 4.20

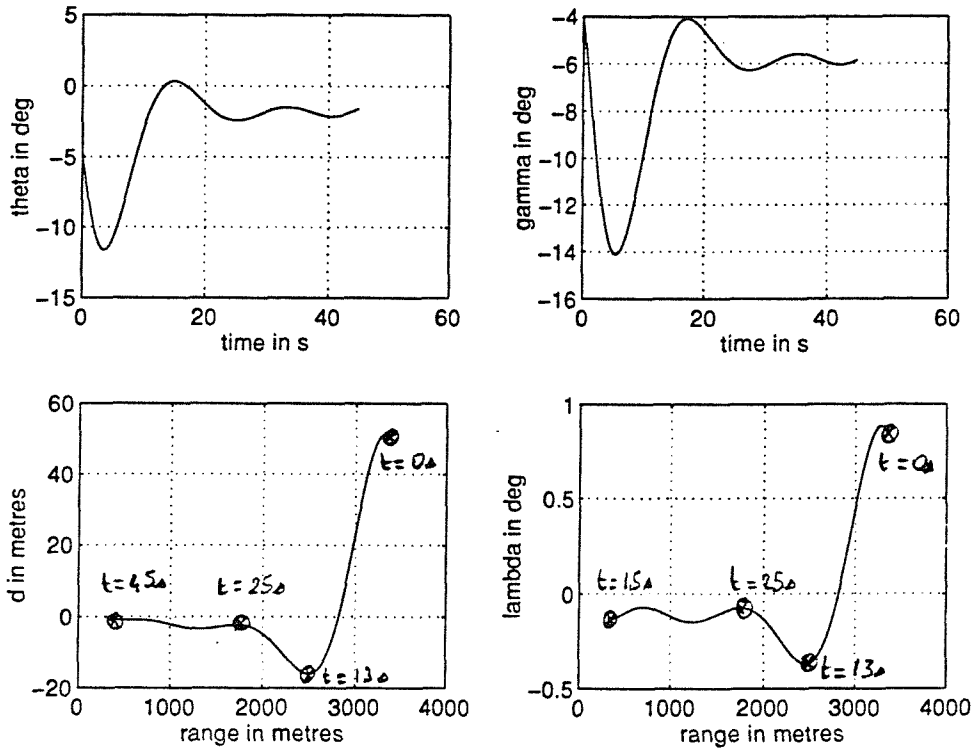

$\theta(0) = -3°$

$\gamma(0) = -4°$

$d(0) = +50$ m

Figure 4.21

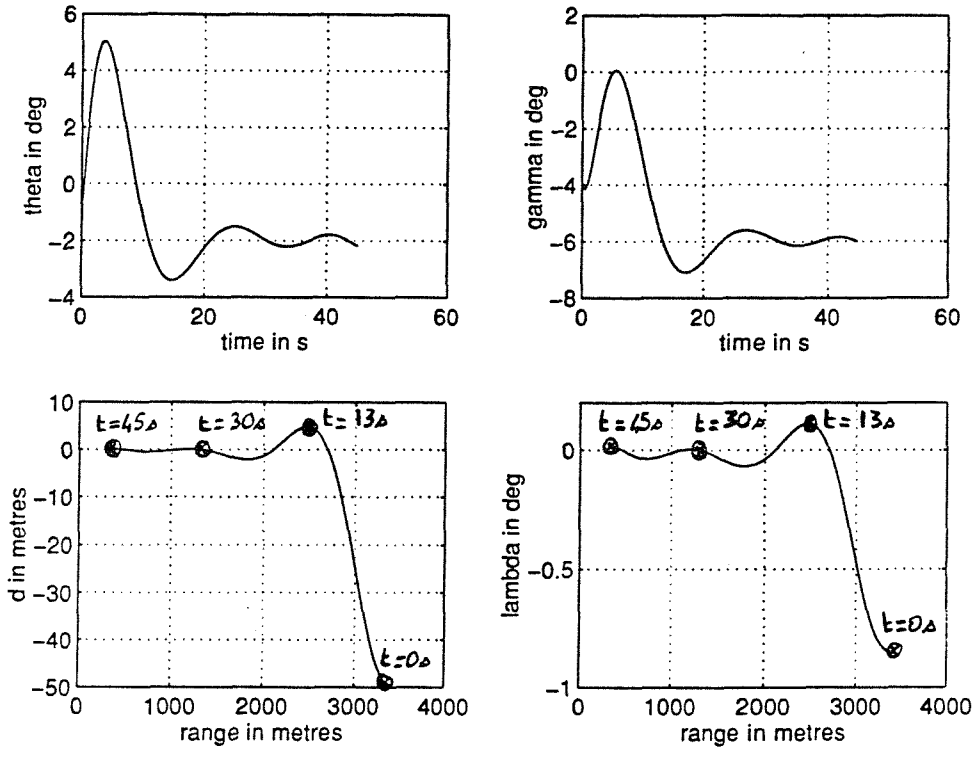

$\theta(0) = -3°$

$\gamma(0) = -4°$

$d(0) = -50$ m

Figure 4.22

Although small steady-state errors can be seen, the dynamics responses of the aircraft were all satisfactory. However, large and unacceptable variations in pitch attitude and in flight path angle occurred for a number of particular entry conditions like those expressed for Figures 4.18, 4.19 and 4.20. Note that in the case of Figure 4.18 the initial flight path angle was only -2°, whereas in Figure 4.19 it was at the nominal value. However, although the aircraft was above the glide path by 50 metres, the pitch attitude was not correct in either case, which is the cause of the large adjustment in pitch attitude. When θ(0) was selected as -6° to correspond with the required flight descent path angle then such large variations did not occur.

4.2.c.(ii) Sensor noise

This section describes the performances of the MLS Glide-Path-Coupled-Control system in the presence of sensor noise.

Noise on the output signal was regarded as a random signal, represented by a Gaussian distribution. It was generated from a linear first order filter, whose transfer function, $G_i(s)$, was defined as :

$$G_i(s) = \frac{1}{1 + T_f s} \tag{4.30}$$

where

- $T_f = 0.025$ s, is the filter time constant. (4.31)

The choice of T_f was made to ensure that the noise spectrum was configured to below 40 rad/s.

40 rad/s represented a frequency one order greater than the bandwidth of the coupled system.

A block diagram showing such a noise signal is shown in Figure 4.23 :

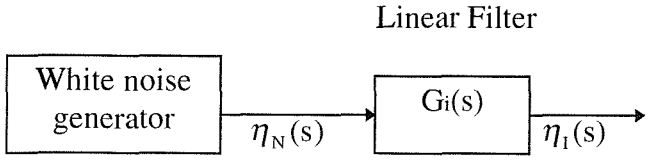

Figure 4.23

The system responses in presence of sensor noise are given in Figure 4.24 for the particular entry conditions expressed in Table 4.4.

FIGURE	$\gamma(0)$ Degrees	θ Degrees	d(0) Metres
4.24	-6	-3	-50

Table 4.4

After 45 s, the displacement from the glide path angle was zero, which was very satisfactory. However, because large variations were occurring, the addition of a filter was necessary.

A second order filter was used, with a transfer function, $G_F(s)$, as follows :

$$G_F(s) = \frac{1}{T^2.s^2 + 2.\xi.T.s + 1} \tag{4.32}$$

where

- $T = 0.25$ s (4.33)

- and $\xi = 0.7$ (4.34)

Note that the noise spectrum was now configured to below 4 rad/s.

Figure 4.25 shows the corresponding responses, which are much less oscillatory.

Notice that all the responses are given over a 15 s interval time, which explains why the path displacement is not zero at the end of the simulation.

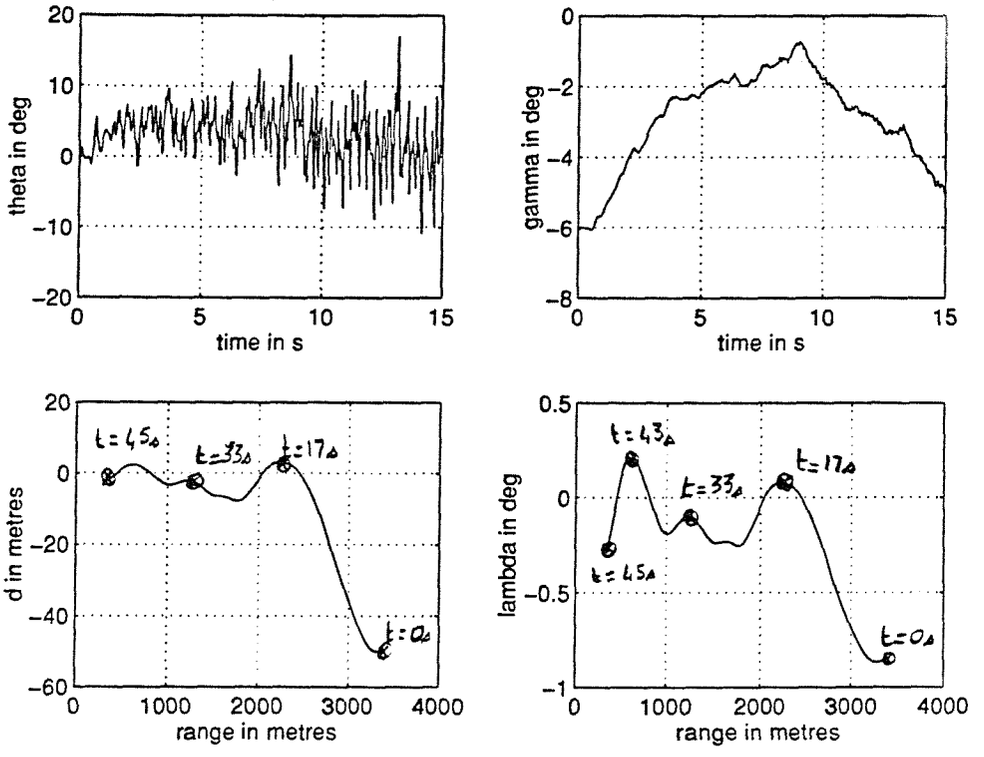

$\theta(0) = -3°$

$\gamma(0) = -6°$

$d(0) = -50$ m

Figure 4.24

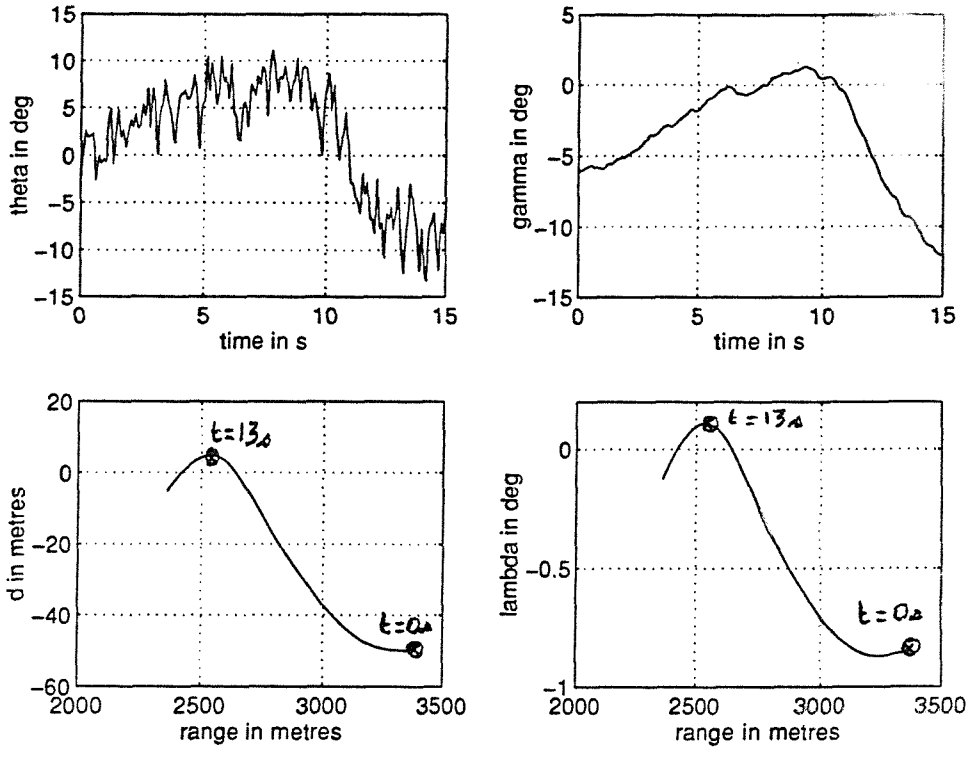

$\theta(0) = -3°$

$\gamma(0) = -6°$

$d(0) = -50$ m

Figure 4.25

4.2.d Use of the GPS

The purpose of this section is to present the results of the performances of a GPS-coupled-glide-path control system. As with MLS, the approaches were curved and the sensitivity of the receiver, K_{GP}, was considered to be equal to 1V/°. However, there were two major differences :

- the GPS receiver did not always provide permanent information. If the aircraft was flying in an area where only four satellites were in view, the act of banking, for example, could induce the loss of a satellite signal and during a period of about 2 seconds, the aircraft would then receive no update information from that GPS receiver.
- by having to use the C/A code instead of the P code, the GPS receiver displacement signal was in error by about 3 metres.

Figures 4.26, 4.27 and 4.28 present the responses obtained from the GPS glide-path-coupled control system for the entry conditions indicated in Table 4.5 when considering only for 2 seconds the loss of a satellite signal, at t = 15s. The time chosen for the loss of the satellite signal was arbitrary, but was selected to correspond approximately with the time at which the beam error was at its greatest value after the initial beam displacement. (see figure 4.26)

At t = 17s, the value from the receiver signal was assumed to be equal at that which obtained at t = 15s.

FIGURE	$\gamma(0)$ Degrees	$\theta(0)$ Degrees	d(0) Metres
4.26	- 6.0	-6.0	+50
4.27	-4.0	-6.0	+50
4.28	-2.0	-6.0	+50

Table 4.5

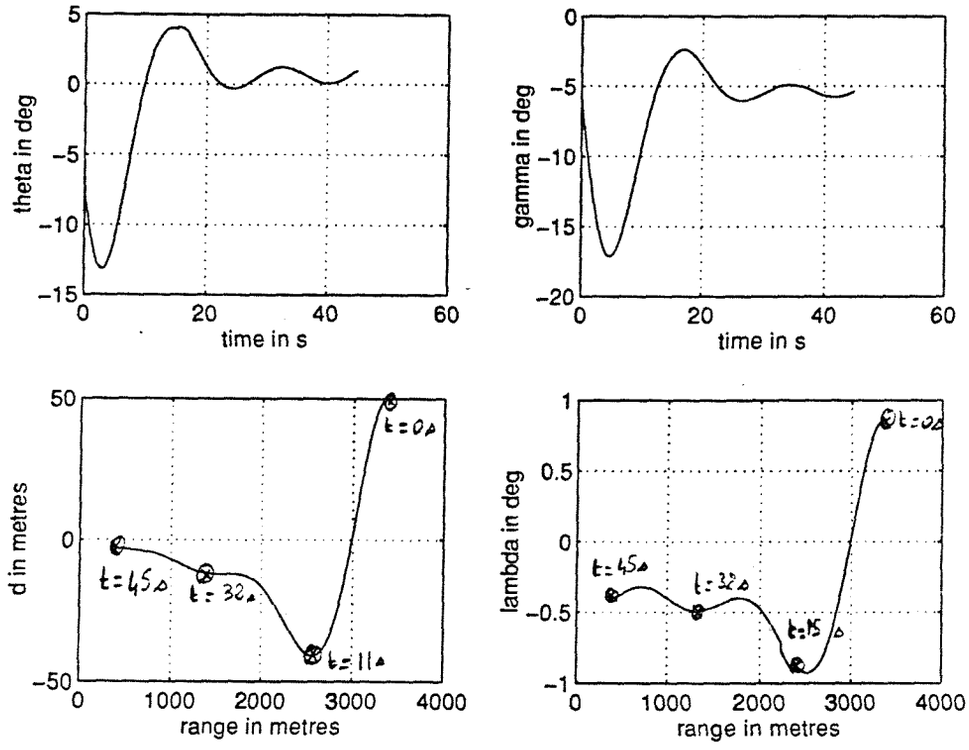

$\theta(0) = -6°$

$\gamma(0) = -6°$

$d(0) = 50$ m

Figure 4.26

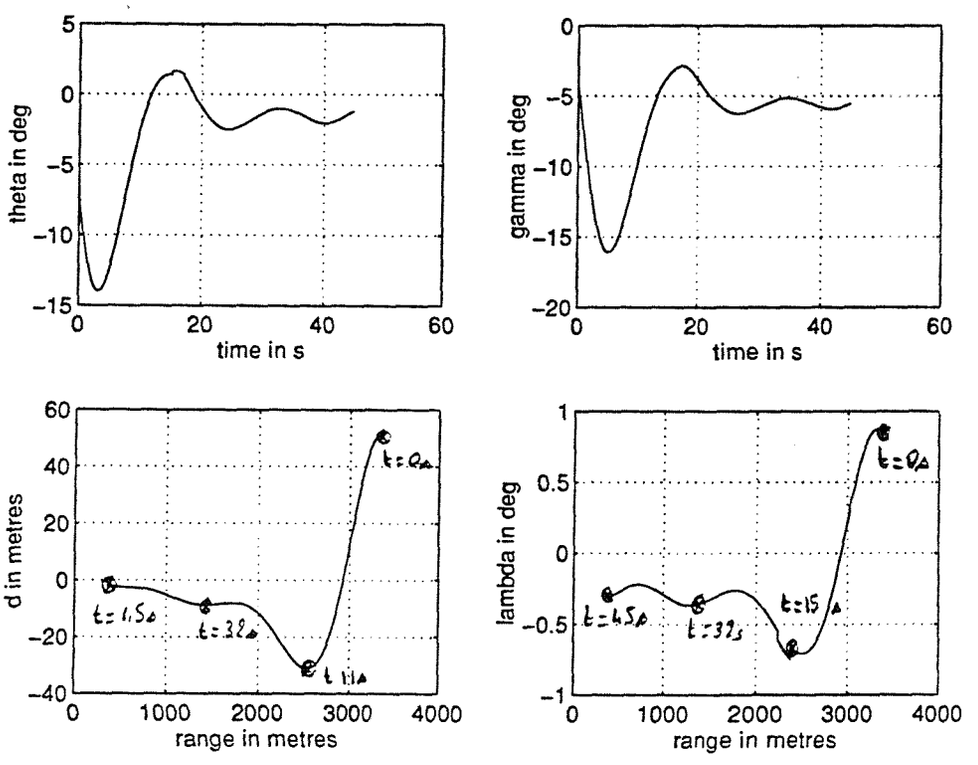

$\theta(0) = -6°$

$\gamma(0) = -4°$

$d(0) = 50$ m

Figure 4.27

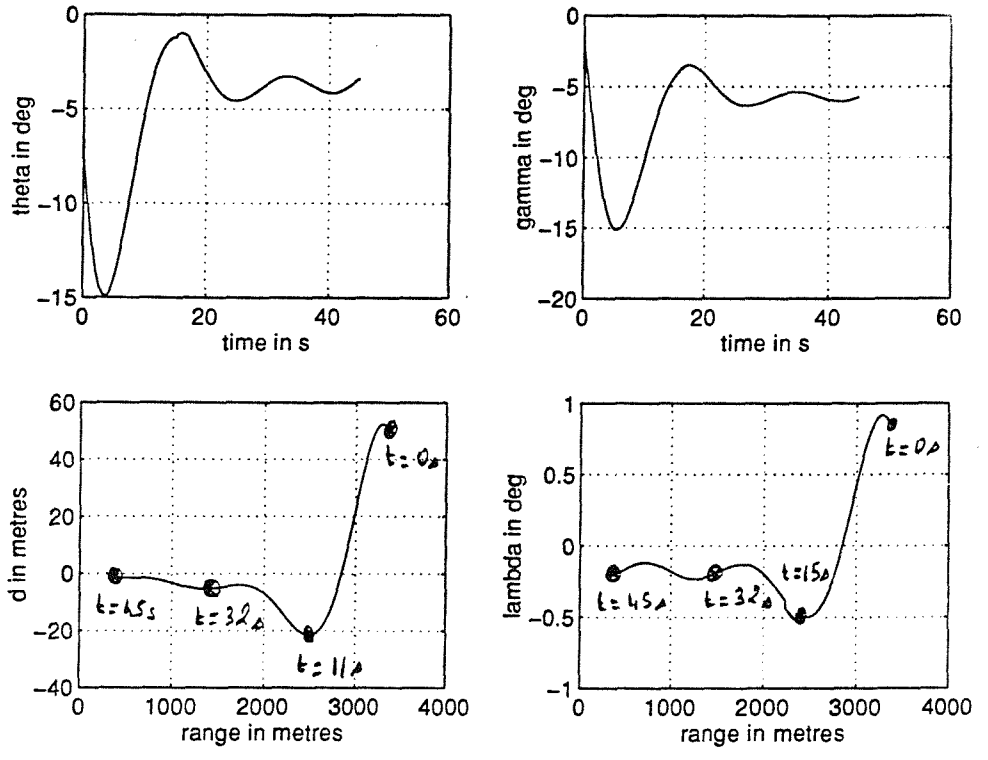

$\theta(0) = -6°$

$\gamma(0) = -2°$

$d(0) = 50$ m

Figure 4.28

The results obtained were all satisfactory and were very similar to those obtained from the MLS glide-path system. Note that the extreme entry conditions (parallel to the glide-path but above by 50 metres) caused large changes in the pitch attitude and flight path angle, which resulted in the aircraft being 40 metres below the glide slope at a distance of about 2500 metres from the runway threshold. Although not dangerous, such a response requires further design of the coupled control system to reduce the extent of the attitude changes and path deviation.

Figures 4.29, 4.30 and 4.31 present the responses obtained from studies relating to the existence of a random error of 3 metres from the GPS receiver. The entry conditions were those indicated in Table 4.5.

Note that, in every case, after 45s the flight path angle did not equal the reference angle of -6°, and the path displacement was about 20m. These results were unsatisfactory and the use of the GPS glide-path system as an automatic landing system would demand a complementary system to eliminate the error produced by the GPS receiver. It was indicated in section 2.4, that a suitable system would be the Differential Global Positioning System (DGPS).

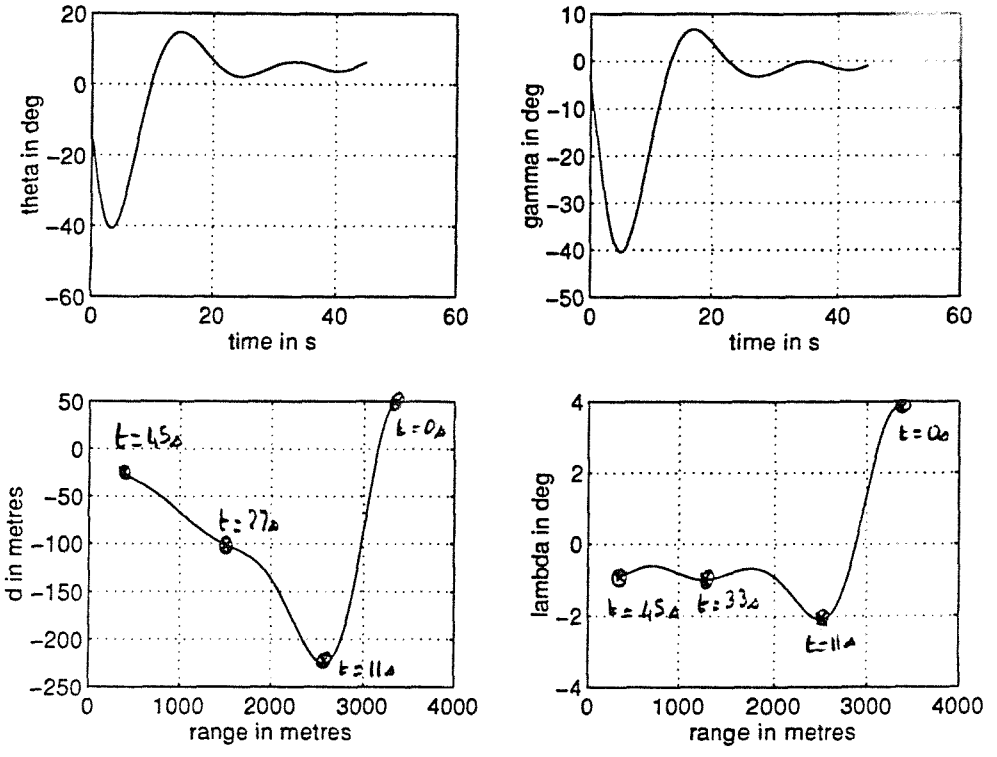

$\theta(0) = -6°$

$\gamma(0) = -6°$

$d(0) = 50$ m

Figure 4.29

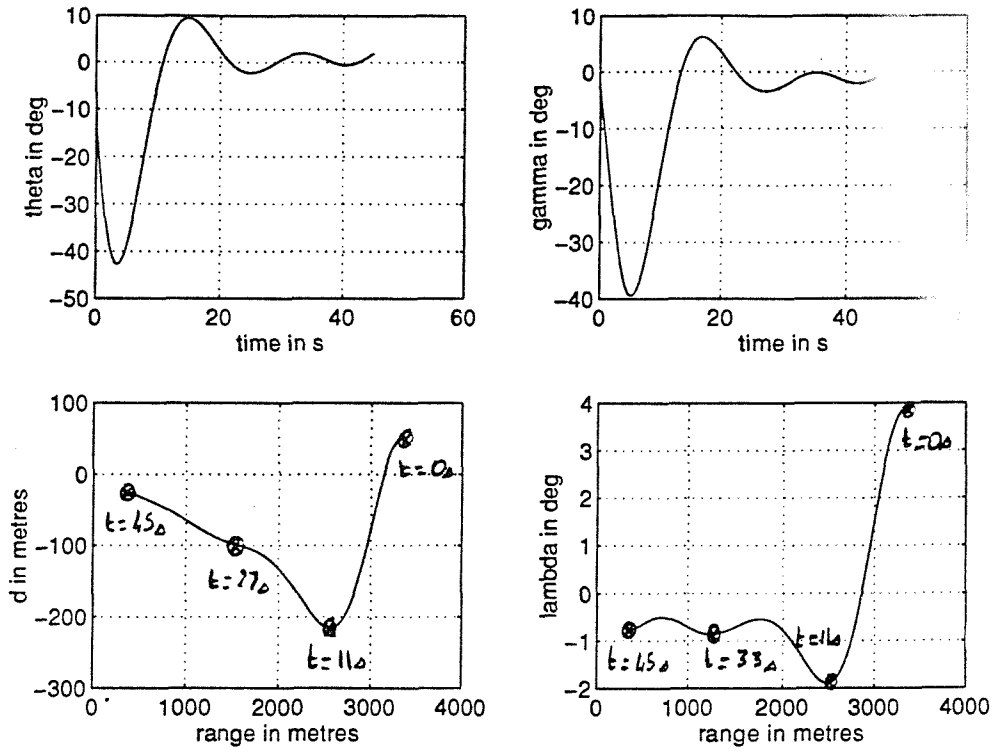

$\theta(0) = -6°$

$\gamma(0) = -4°$

$d(0) = 50$ m

Figure 4.30

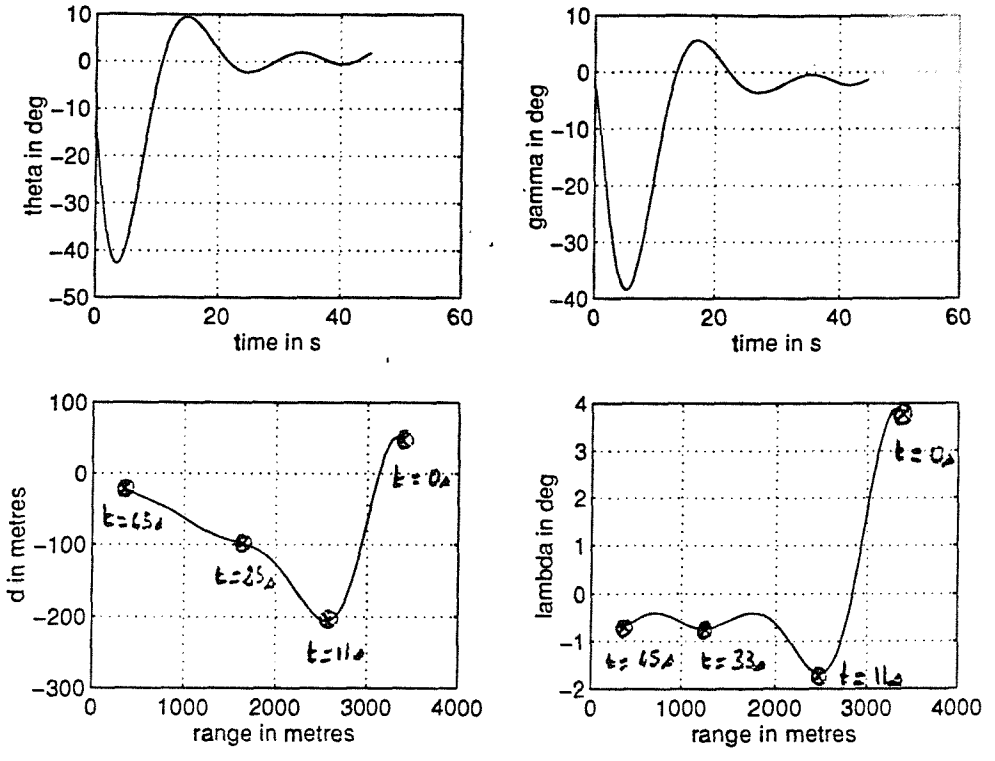

$\theta(0) = -6°$

$\gamma(0) = -2°$

$d(0) = 50$ m

Figure 4.31

4.2 Localiser-coupled control system

This system provides information about whether the aircraft is flying to the left or the right of the runway centre-line, which is approaching.

4.2.a Generalities

The output signal from the localiser receiver was proportional to the angular deviation, Γ, from the runway centre-line. The difference between the reference angular deviation, Γ_{ref}, and the angular deviation, Γ, was used as a command signal for the direction control system, which was designed to drive the aircraft back onto the centre-line.
In a similar relation to the glide-path coupled control system, the relationship between angular deviation and displacement can be shown to be :

$$\Gamma(t) = \frac{57.3}{R(t)} * d(t) \qquad (4.35)$$

where

- d is the displacement from the beam centre-line (See Figure 4.32).

Any aircraft turn was assumed to be coordinated with the angles involved being not greater than 15°. Hence, the following relationship can be established viz.

$$\dot{\psi} \cong \frac{g}{U_o}.\phi = r \qquad (4.36)$$

Note also that :

$$\dot{d} = \frac{U_o}{57.3} * \sin(\psi - \psi_{ref}) \cong \frac{U_o}{57.3} * (\psi - \psi_{ref}) \qquad (4.37)$$

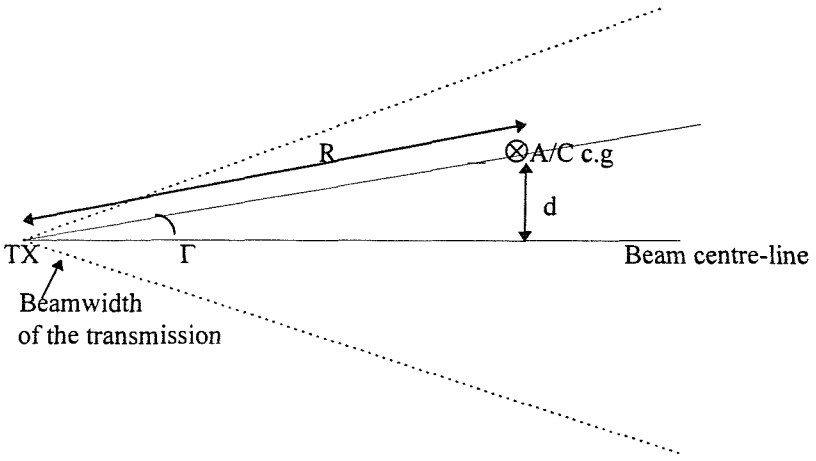

Figure 4.32

The transfer function, Gc(s), chosen for the localiser-coupled controller comprised :

- a proportional term

- and an integral term. The second term was added to ensure that this system provided the required response even in the presence of a severe cross wind component.

Therefore :

$$Gc(s) = \left(2 + \frac{.1}{s}\right) \tag{4.38}$$

A roll rate damper SAS was also used as an inner loop, in order to provide extra-stabilization.

Figure 4.33 shows the corresponding block diagram.

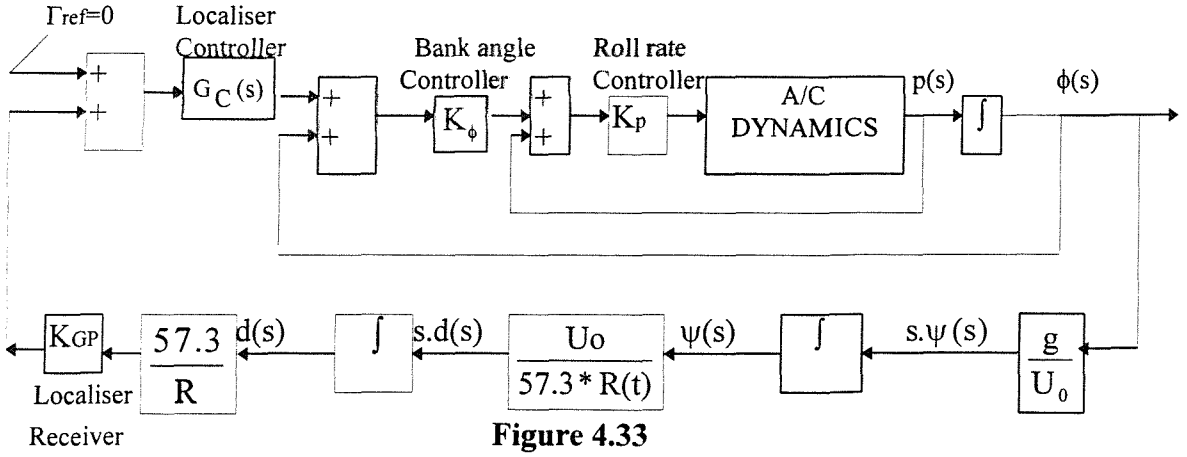

Figure 4.33

4.2.b Use of the ILS

The dynamics of the ILS localiser receiver were considered to be ins[illegible], even though it contained 90 Hz and 150 MHz filters to handle the localiser mo[illegible]ion signals. The transfer function was represented by the sensitivity viz.

$K_{GP} = 1$ V/° 9)

4.2.b.(i) Responses for different entry conditions

Figure 4.34 show the responses for sideslip, bank angle, roll and yaw rates, heading, displacement and angular deviation for the entry conditions indicated in Table 4.6.

FIGURE	$\beta(0)$ Degrees	$p(0)$ Degrees/s	$\phi(0)$ Degrees	$r(0)$ Degrees/s	$\psi(0)$ Degrees	$d(0)$ Feet
4.34	1	1	1	1	0	+10

Table 4.6

The changes in heading angle and angular deviation were small even though the aircraft deviated from the runway centre-line by a maximum of 1200 ft at 20 s after the start of the approach. All the corresponding rates and sideslip and bank angles were very small. The bank angle, ϕ, never exceeded 1.2° (at 1 second after entry) : this is better than the requirement, universally adopted, that the roll attitude should not deviate from the reference value by more than 2°.

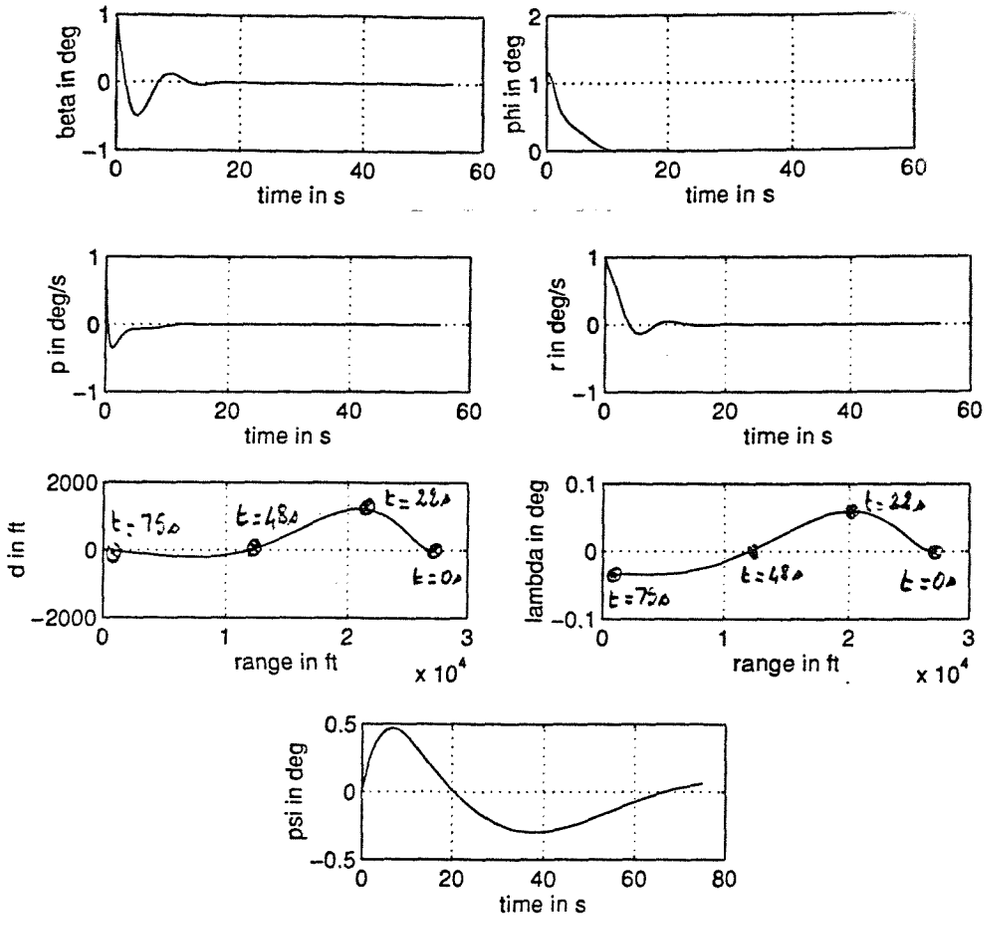

$\psi(0) = 0\ °$

$d(0) = 10\ ft$

Figure 4.34

4.2.b.(ii) Responses in presence of side gusts

This section describes the performance of the localiser coupled control system in the presence of a side gust. The consideration of such disturbances is very important in the case of an approach, because of the aircraft's low altitude and speed.

A sidegust, BCW, as shown in Figure 4.35, was introduced into the sideslip equation as an additional forcing term, Y_v.BCW.

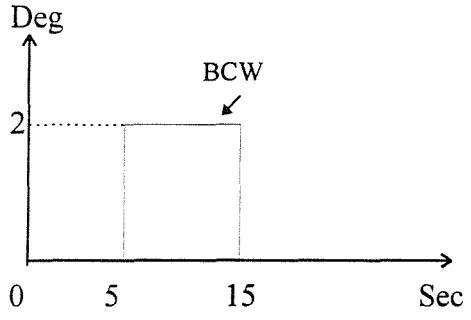

Figure 4.35

Figure 4.36 shows the corresponding responses for sideslip, heading, bank angle, roll and yaw rates, displacement and angular deviation from the localiser beam in response to this side gust.

Even though a maximum sideslip gust of 2° had been introduced, the corresponding maximum displacement from the runway centre-line was only 1000 ft some 5 seconds after the sidegust subsided and at a range of 20000 ft from the touchdown point. However, at the end of the approach, after 80 s, the offset from the runway centre-line was about 0 ft and there was an angular deviation of about 0.03°. Obviously, the localiser coupled system is extremely effective in maintaining the aircraft's lateral path.

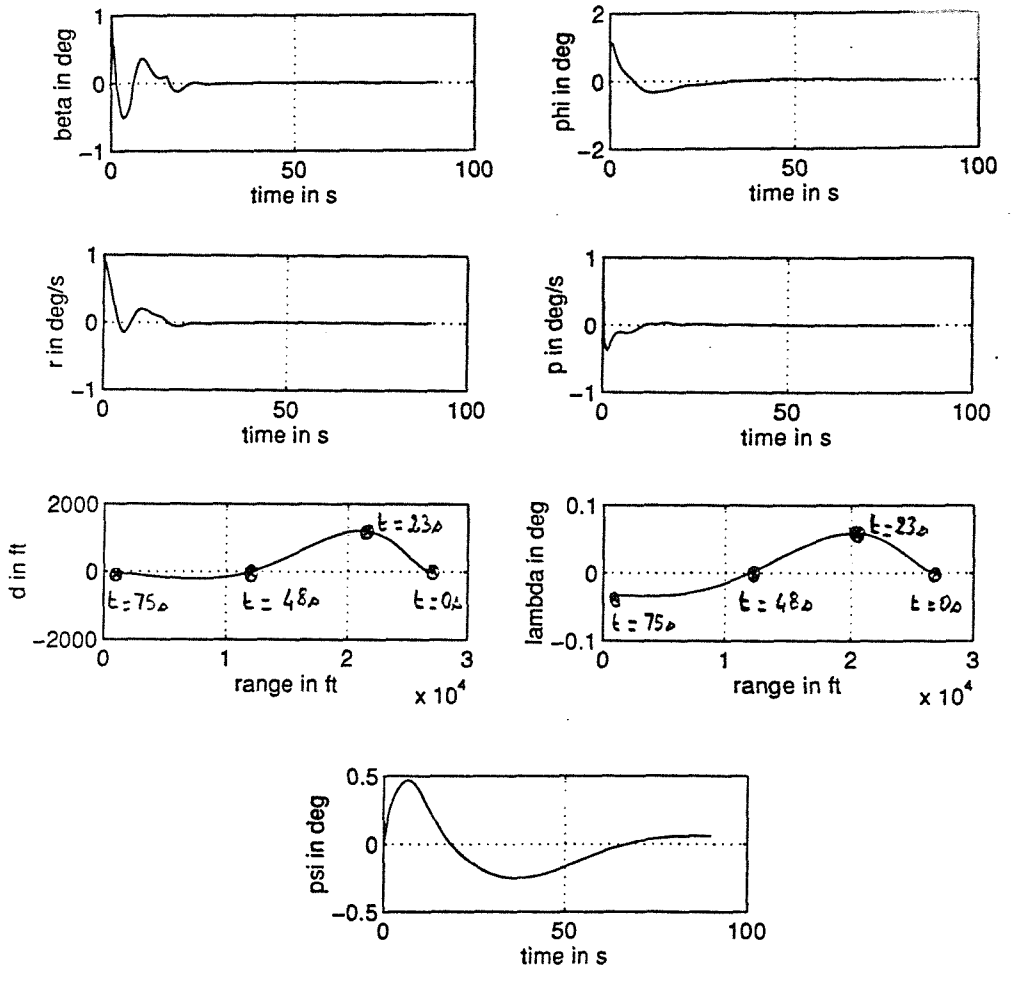

$\psi(0) = 0°$

$d(0) = 10$ ft

Figure 4.36

4.2.c Use of the MLS

As with the ILS, the dynamics of the MLS glide-path receiver were considered to be instantaneous. The receiver transfer function was simply represented by a sensitivity, K_{GP}, viz.

$K_{GP} = 1V/°$ 0)

4.2.c.(i) Responses for different entry conditions

Figures 4.37 , 4.38 and 4.39 show the responses for sideslip, bank angle, roll and yaw rates, heading, displacement and angular deviation for the entry conditions indicated in Table 4.7.

FIGURE	$\beta(0)$ Degrees	p(0) Degrees/s	$\phi(0)$ Degrees	r(0) Degrees/s	$\psi(0)$ Degrees	d(0) Feet
4.37	1	1	1	1	180	+17855
4.38	1	1	1	1	45	+4688.5
4.39	1	1	1	1	0	+1000

Table 4.7

The responses converged to zero or were close. But it can be seen that there were a number of large variations, particularly for the "extremes" entry conditions indicated in Figure 4.37, which did not correspond to acceptable flying qualities and a "capture logic" system was required therefore.

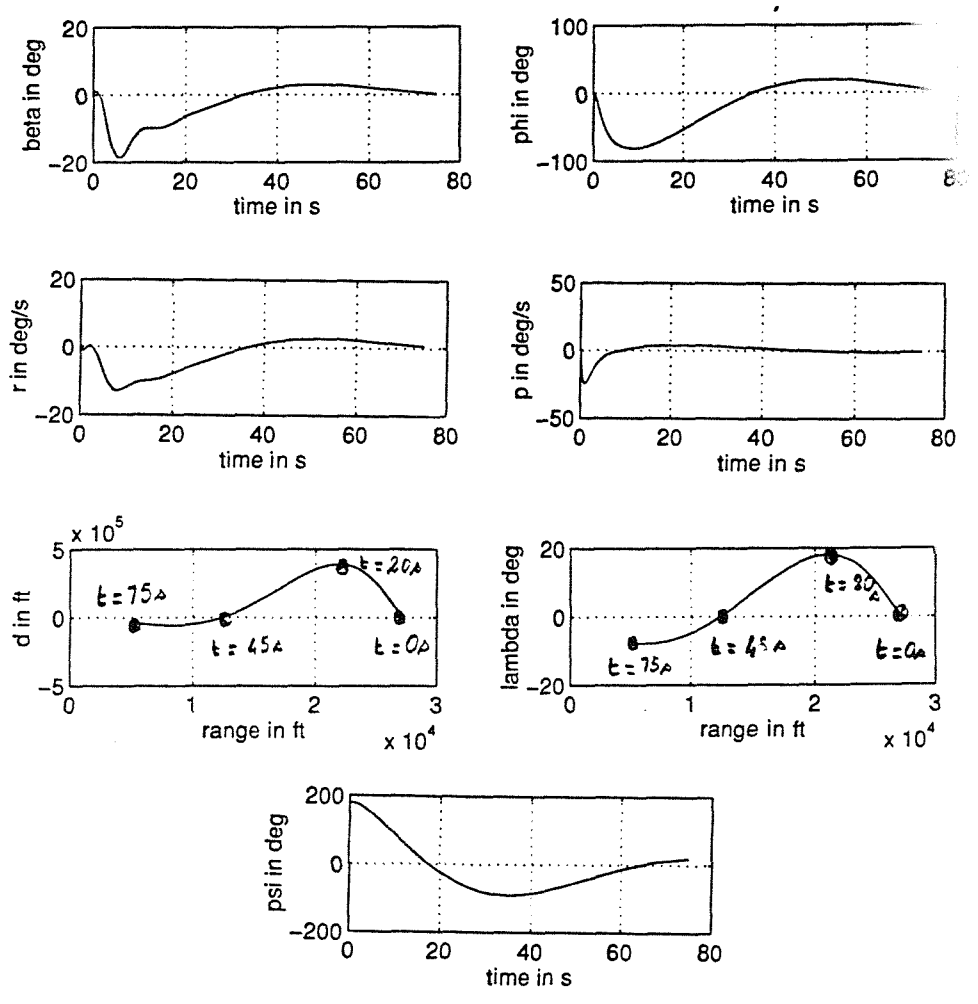

$\psi(0) = 180°$

$d(0) = 17855$ ft

Figure 4.37

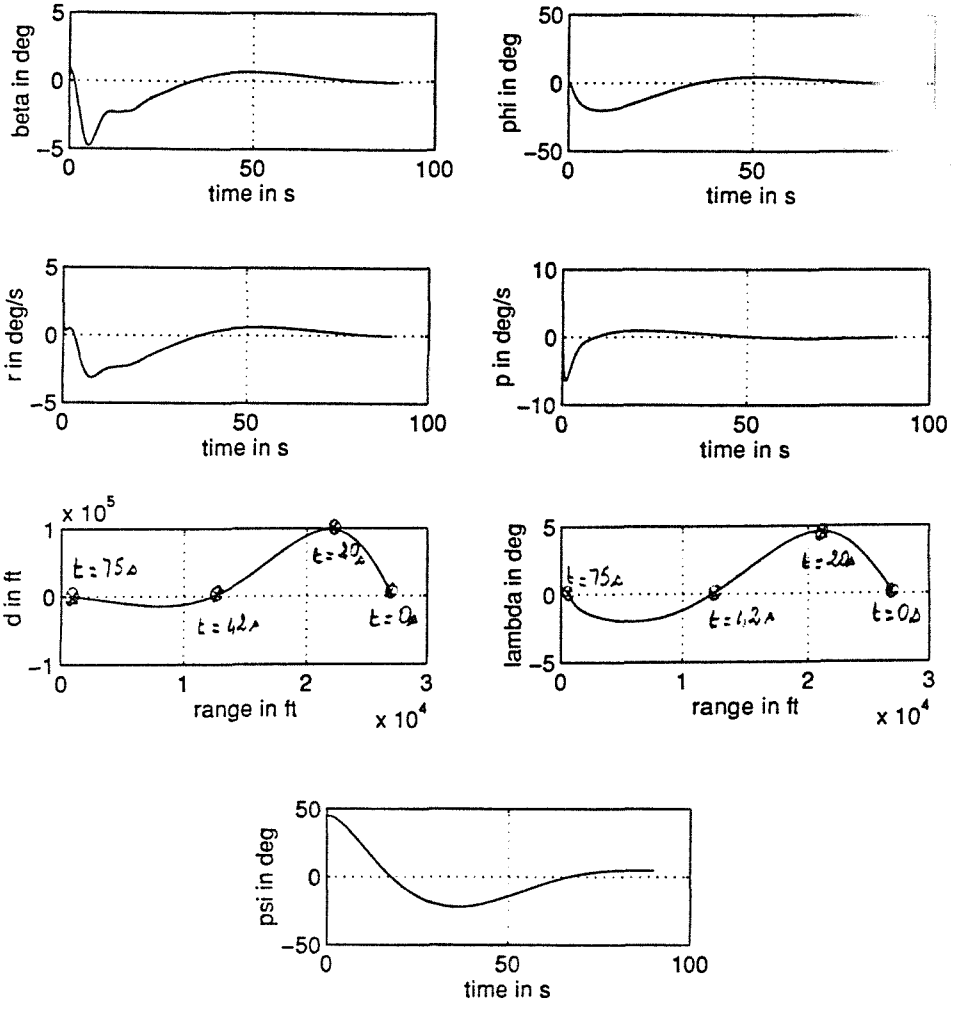

$\psi(0) = 45°$

$d(0) = 4688.5$ ft

Figure 4.38

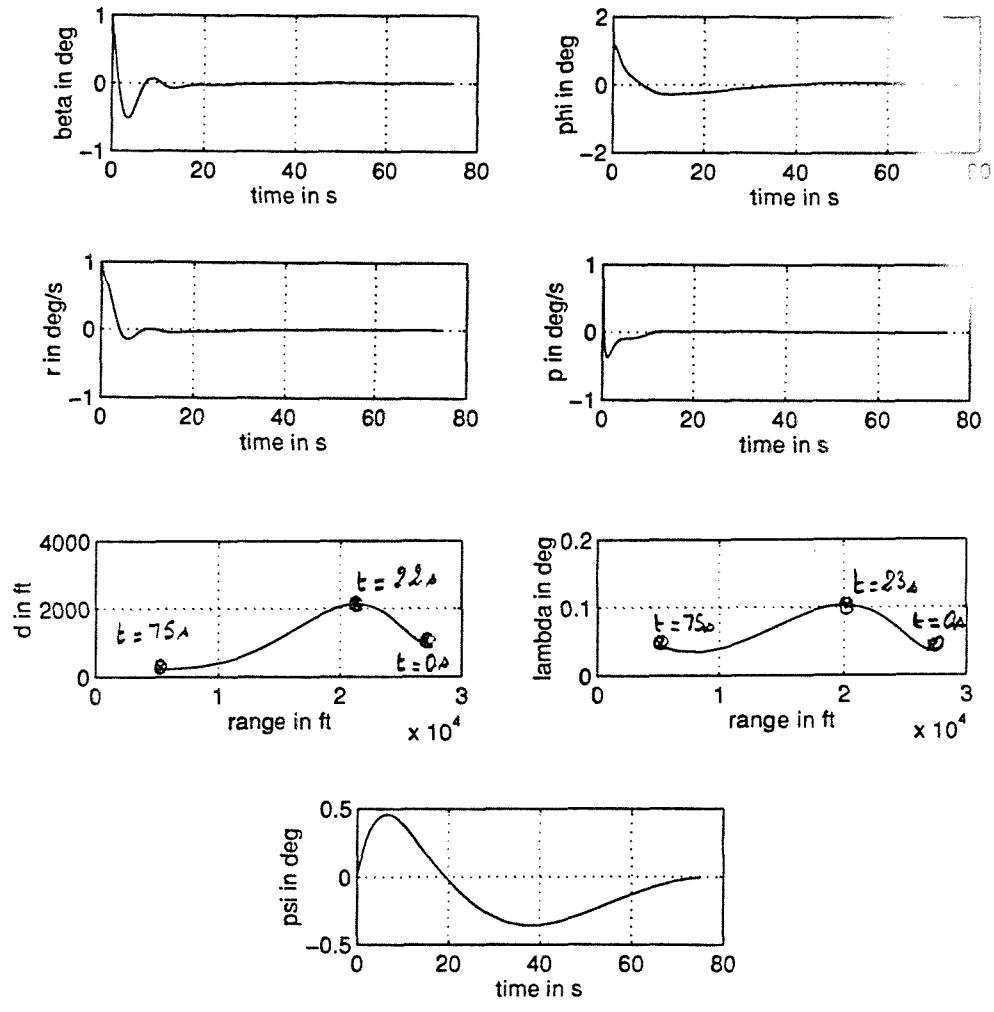

$\psi(0) = 0°$

$d(0) = 1000$ ft

Figure 4.39

4.2.c.(ii) Responses in presence of side gusts

This section describes the performances of the MLS localiser-coupled control system in the presence of a side gust. The side gust considered was identical to that used to test the ILS localiser-coupled control system and is shown in Figure 4.20.

Figures 4.40 , 4.41 and 4.42 show the corresponding responses for sideslip, heading angle, roll and yaw rates, displacement and angular deviation from the localiser beam with the entry conditions indicated in Table 4.6.

The responses have the same form as those which resulted without gust disturbances but these are larger variations in amplitude. However, the responses in Figures 4.41 and 4.42 still correspond to acceptable flying qualities. In the case of Figure 4.40, the need for appropriate capture logic system to prevent the system from manoeuvring the aircraft too vigorously is necessary.

4.2.c.(iii) Capture logic

The purpose of this section is to give the characteristics of the capture logic system used in the extreme case of an aircraft steered onto the runway centre-line via a MLS coupled system and whose initial position is opposite to the airport direction, ie. $\psi = 180°$. The limitations imposed by the system are as follows :

$$\phi_{limit} = \pm 25° \quad (4.41)$$

$$p_{limit} = 5°/s \quad (4.42)$$

$$r_{limit} = \pm 5°/s \quad (4.43)$$

When these conditions are respected the system responses provide acceptable flying qualities.

Figure 4.43 show the responses with a MLS coupled-system, an initial heading angle,$\psi(0)$, of 180° and an initial range of 17855ft.

Notice that the results were good for bank angle,ϕ, and roll rate, p, but were unsatisfactory for the yaw rate, r, and the heading angle, ψ. At 240 s, the roll rate was still 5°/s and although the heading went to zero the variations in amplitude were still strong.

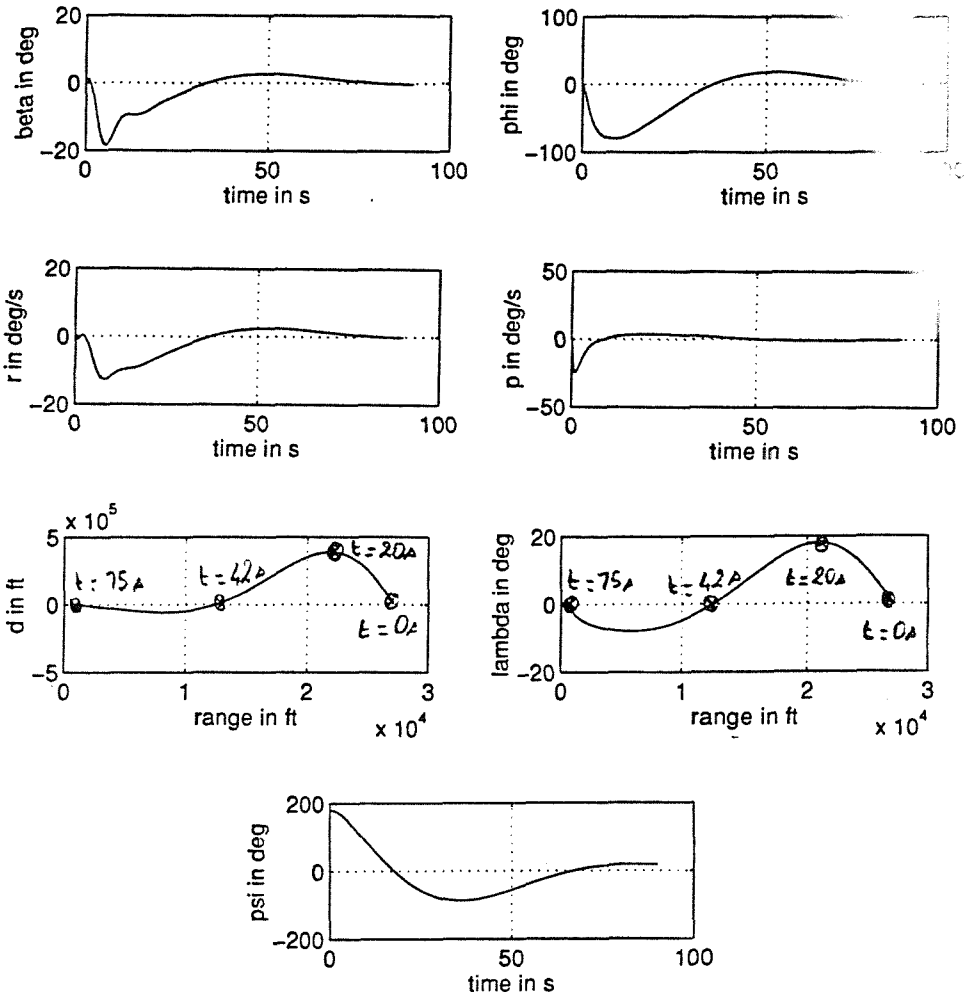

$\psi(0) = 180°$

$d(0) = 17855$ ft

Figure 4.40

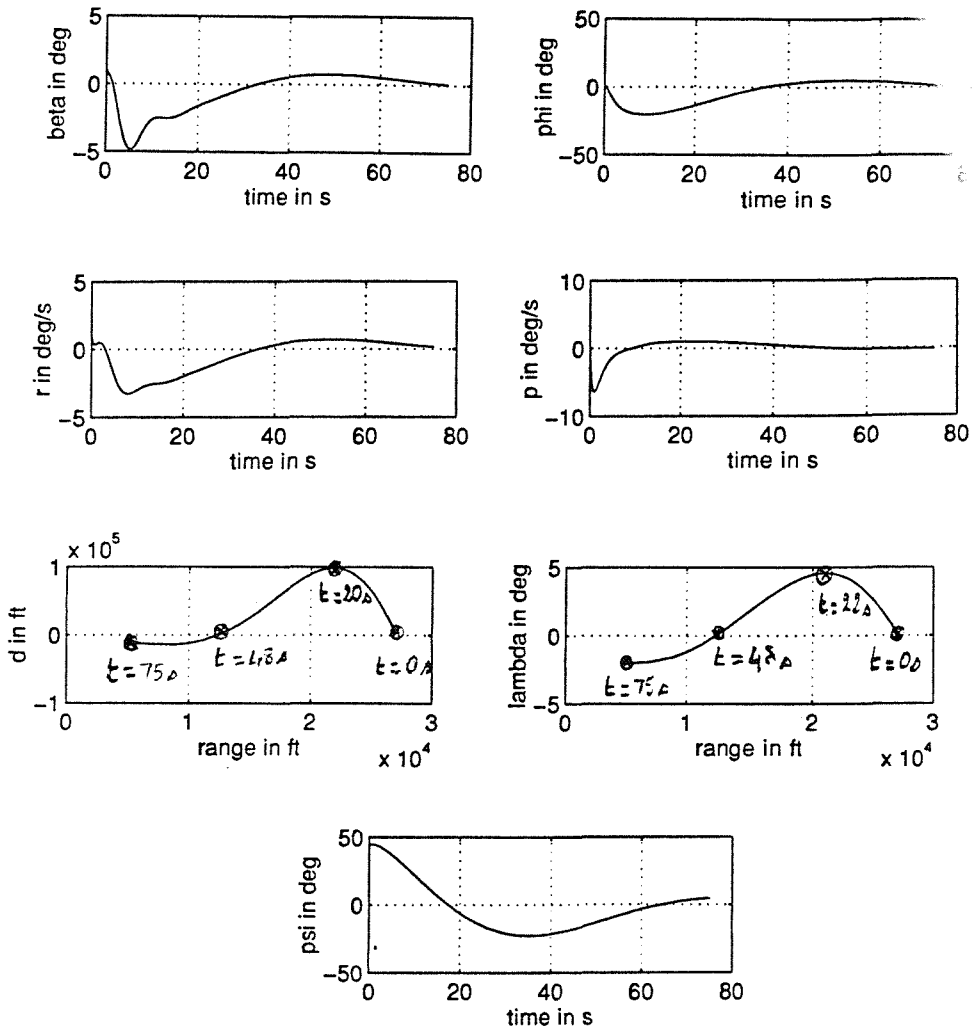

$\psi(0) = 45°$

$d(0) = 4688.5$ ft

Figure 4.41

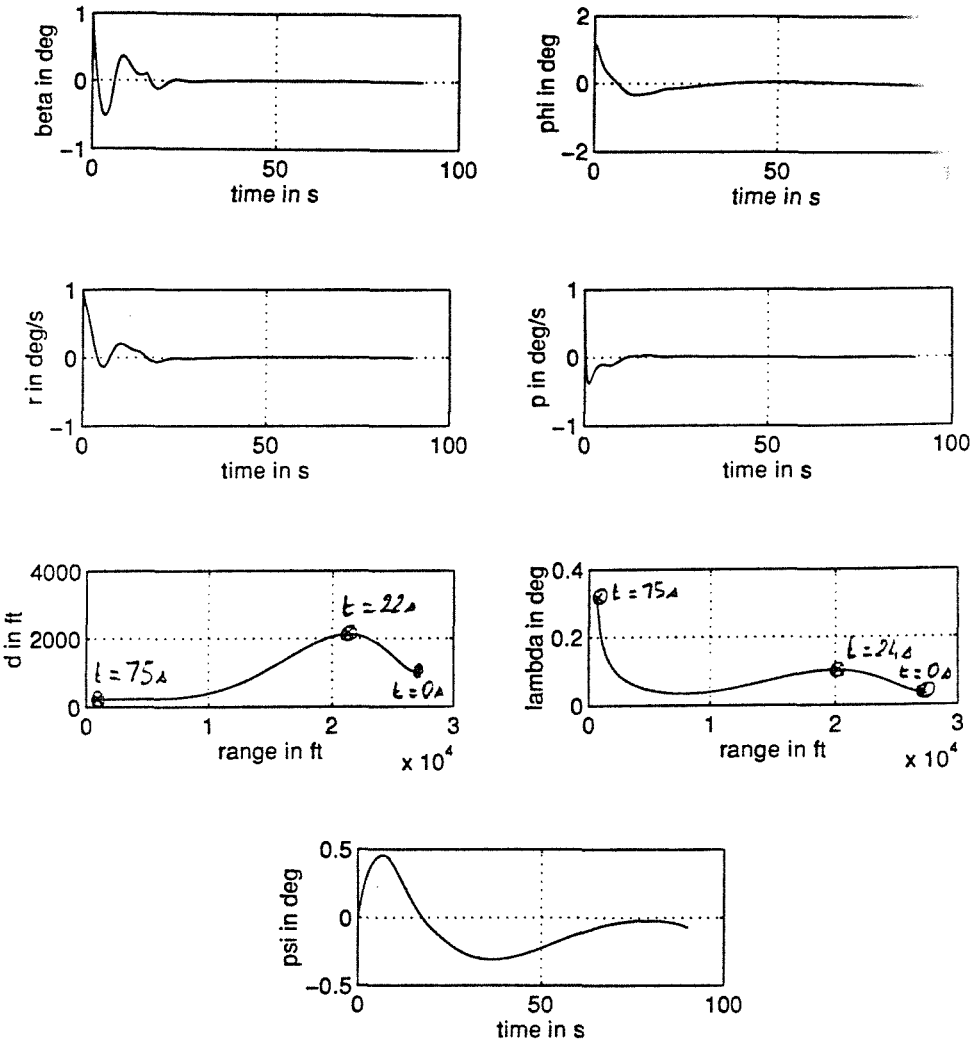

$\psi(0) = 0°$

$d(0) = 1000$ ft

Figure 4.42

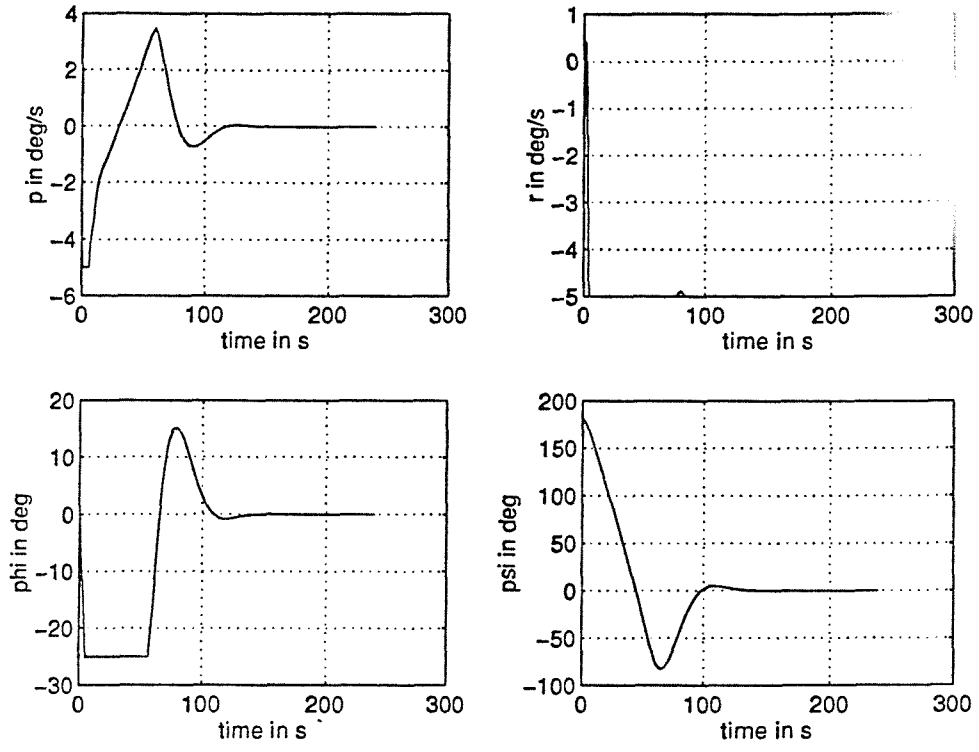

$\psi(0) = 180°$

$d(0) = 17855$ ft

Figure 4.43

An automatic landing with an MLS coupled-system and the entry conditions of Figure 4.37 or 4.40 is therefore impossible for a passenger aircraft like Boeing-747.

4.2.c.(iv) Sensor noise

This section describes the performances of the MLS localiser-coupled-control system in the presence of sensor noise. The simulation has been carried out in a similar way to that used with the MLS glide-path coupled control system, but with a change in the value of the filter time constant, T_f. For the localiser, T_f equalled :

$T_f = 0.741$ s, ie. (4.44)

$$G_i(s) = \frac{1}{1+0.741s} \tag{4.45}$$

The corresponding responses for the entry conditions indicated in Table 4.7 are shown in Figures 4.44, 4.45 and 4.46.

In the cases of Figures 4.44 and 4.45, the noise has an insignificant effect. For the entry conditions expressed by Figure 4.46, the results are more oscillatory and the steady-state error on lateral angular deviation, Γ, is more important. But these responses were still satisfactory and there was no need to add another filter as in was the case for the MLS glide-path system.

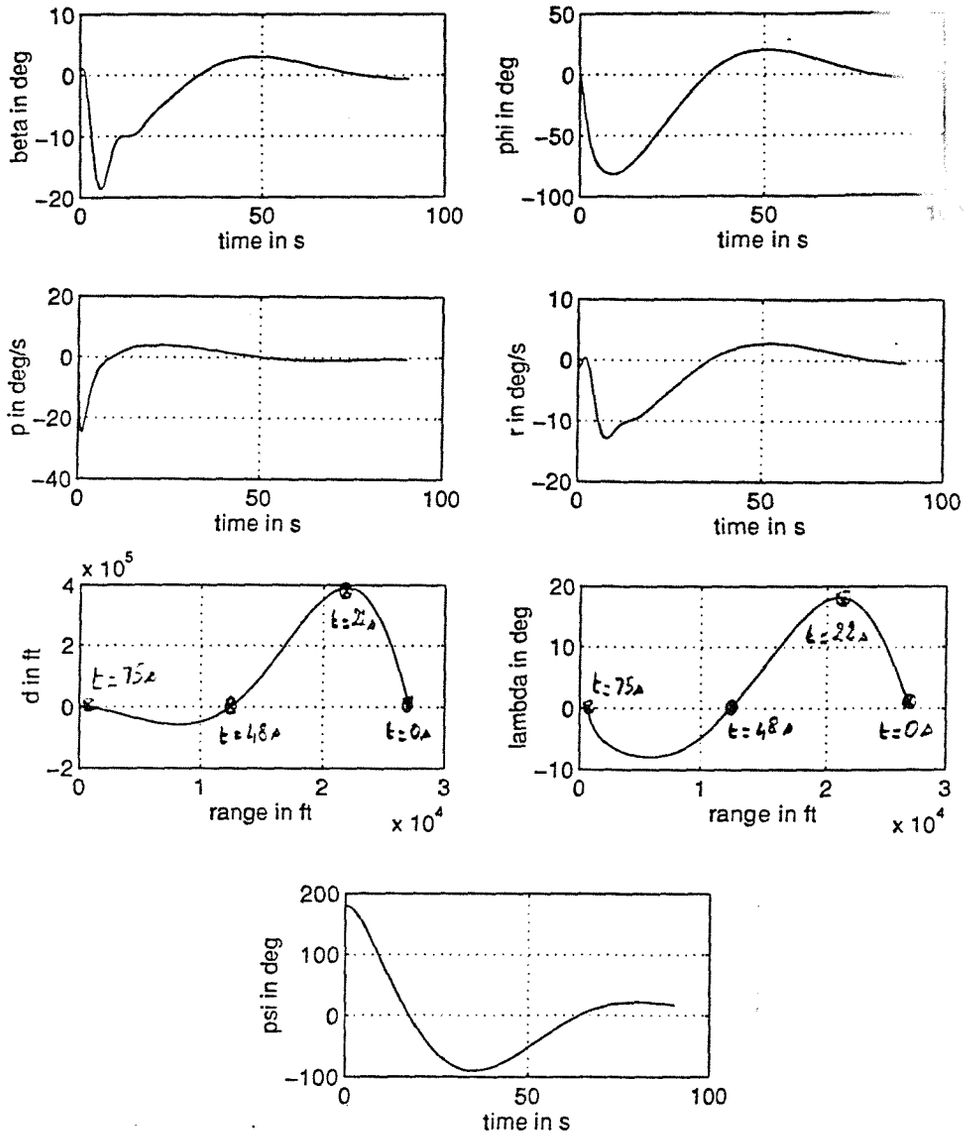

$\psi(0) = 180°$

$d(0) = 17855$ ft

Figure 4.44

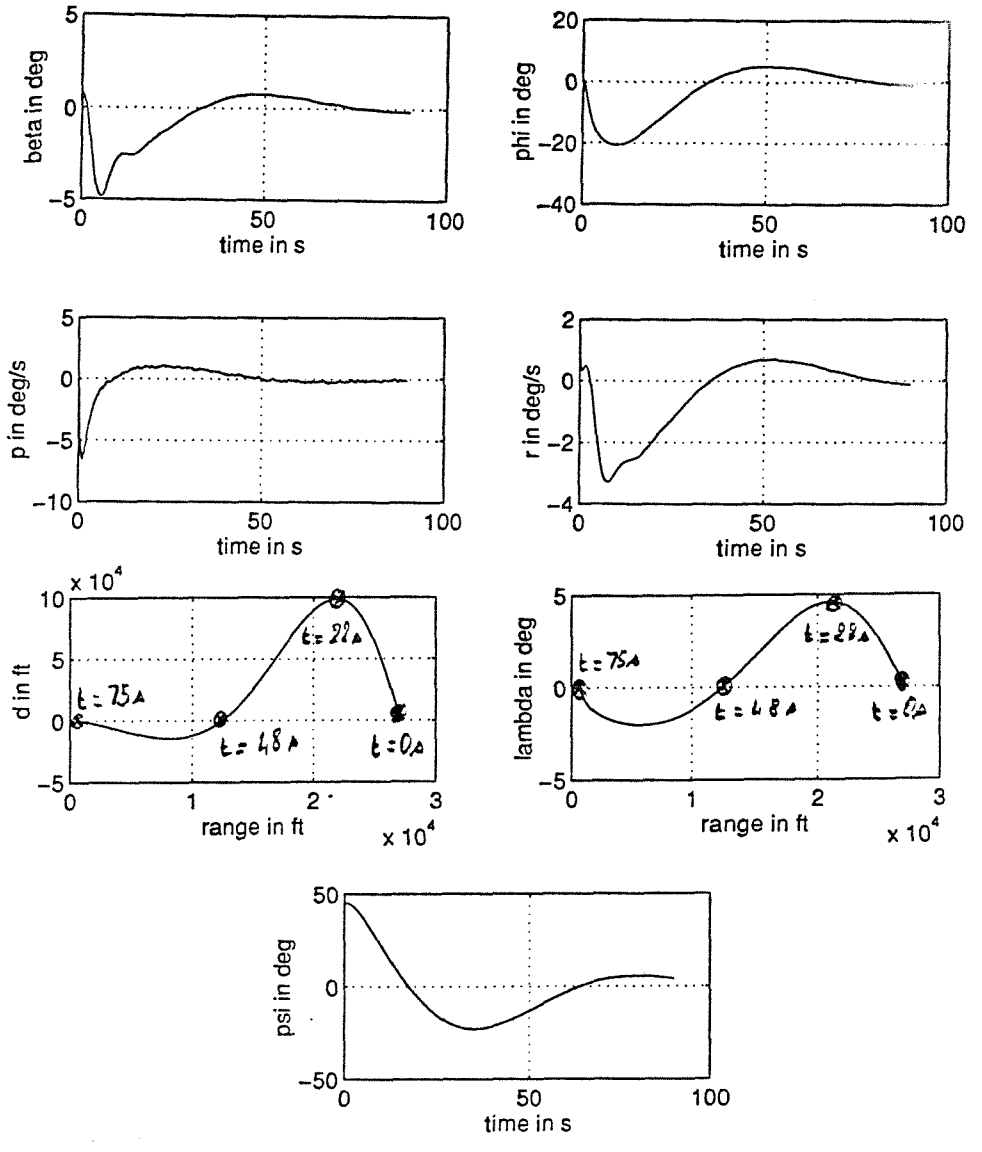

$\psi(0) = 45°$

$d(0) = 4688.5$ ft

Figure 4.45

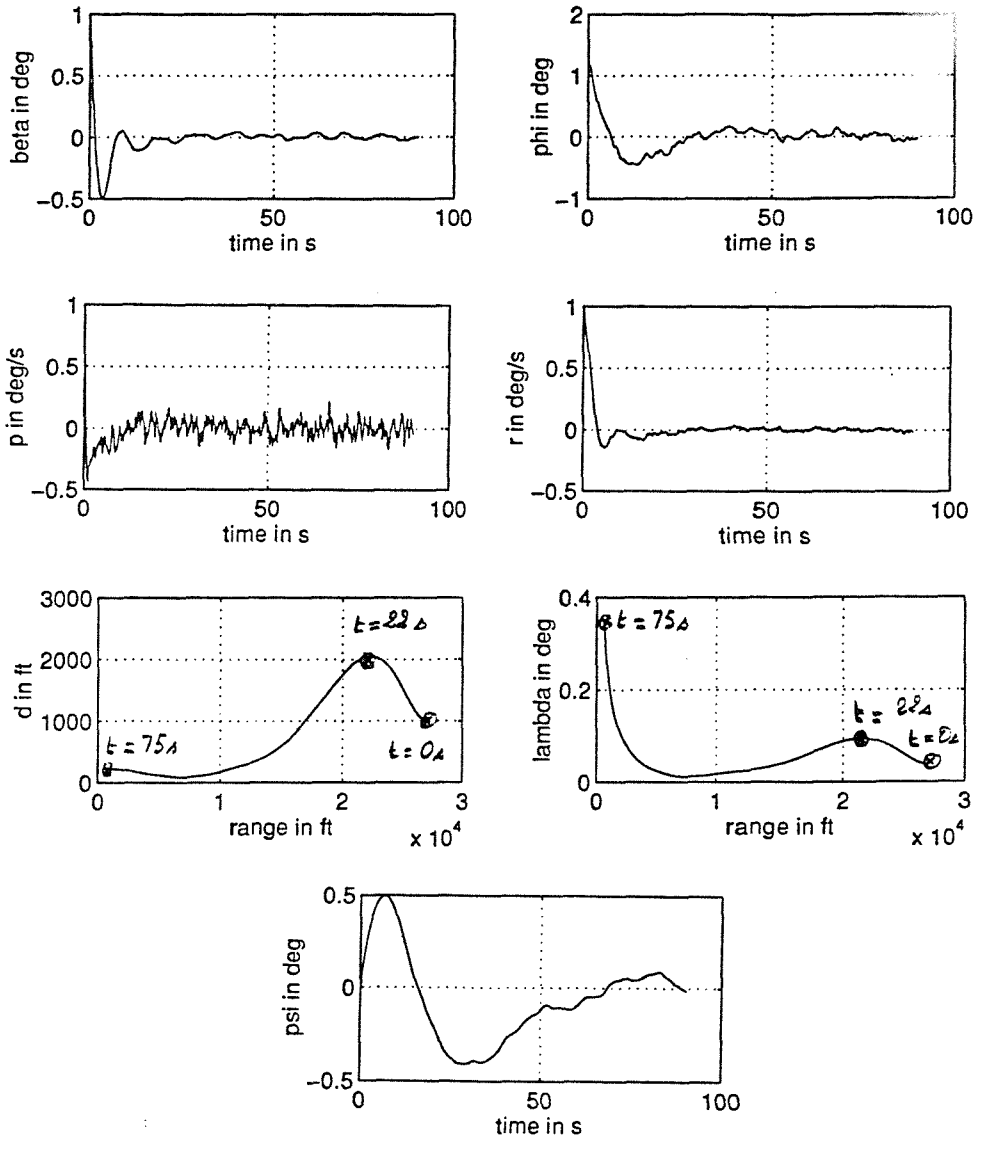

$\psi(0) = 0°$

$d(0) = 1000$ ft

Figure 4.46

4.3.d Use of the GPS

The tests carried out for the GPS localiser-coupled control system were the same as those carried out with the GPS glide-path system (See section 4.2.d). The sensitivity of the GPS receiver, K_{GP}, was taken to be 1V/°.

Figures 4.47, 4.48 and 4.49 show the results for the entry conditions given in Table 4.7 and when the signal from one satellite was missing for 2 seconds, 40s after the beginning of the approach.

Remarkably, it can be seen that the responses were satisfactory. A comparison with the MLS localiser system showed identical results except when the initial heading angle was 0°; in that case the angular deviation was a somewhat larger : being 0.3° instead of 0.05°.

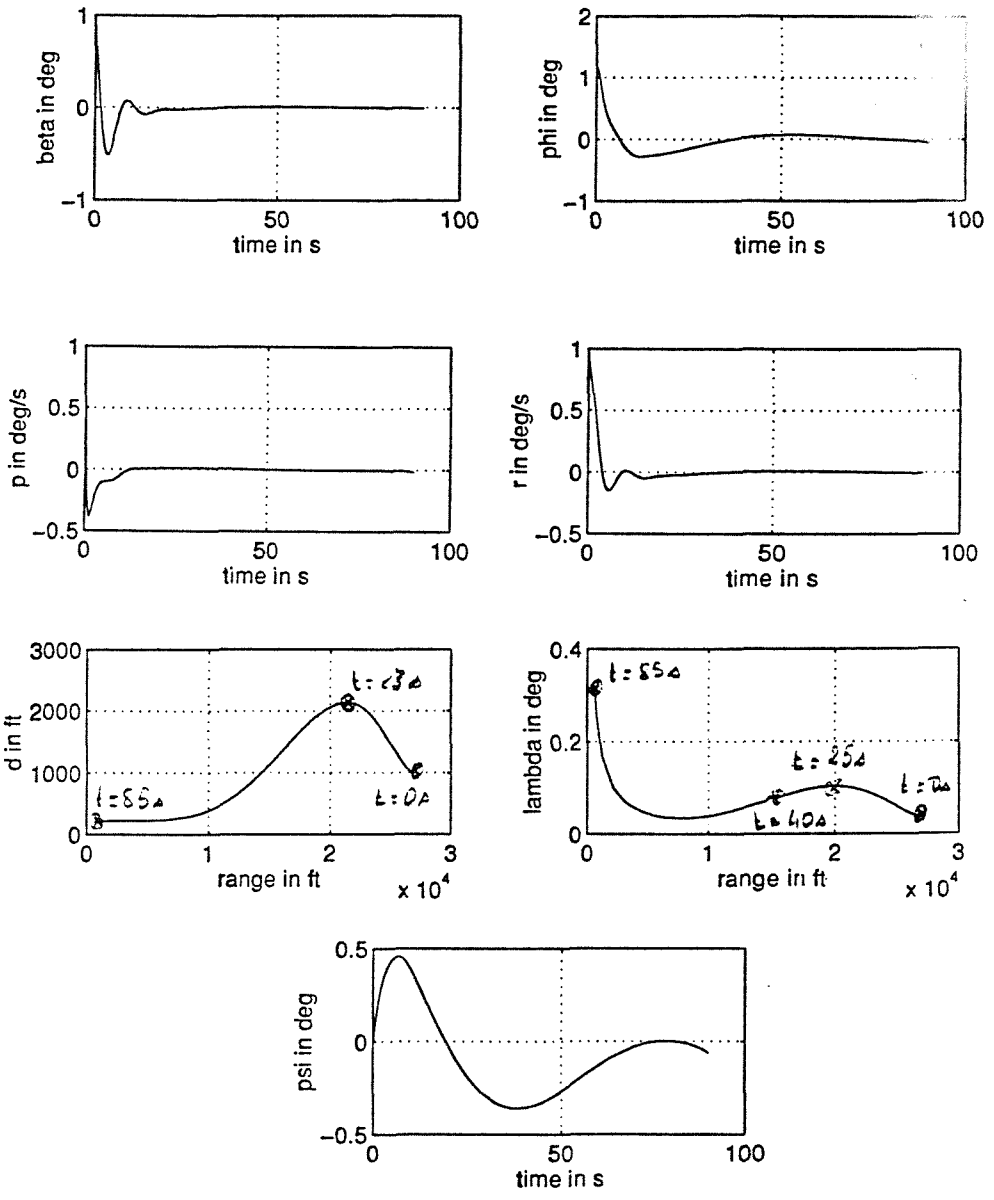

$\psi(0) = 0°$

$d(0) = 1000$ ft

Figure 4.47

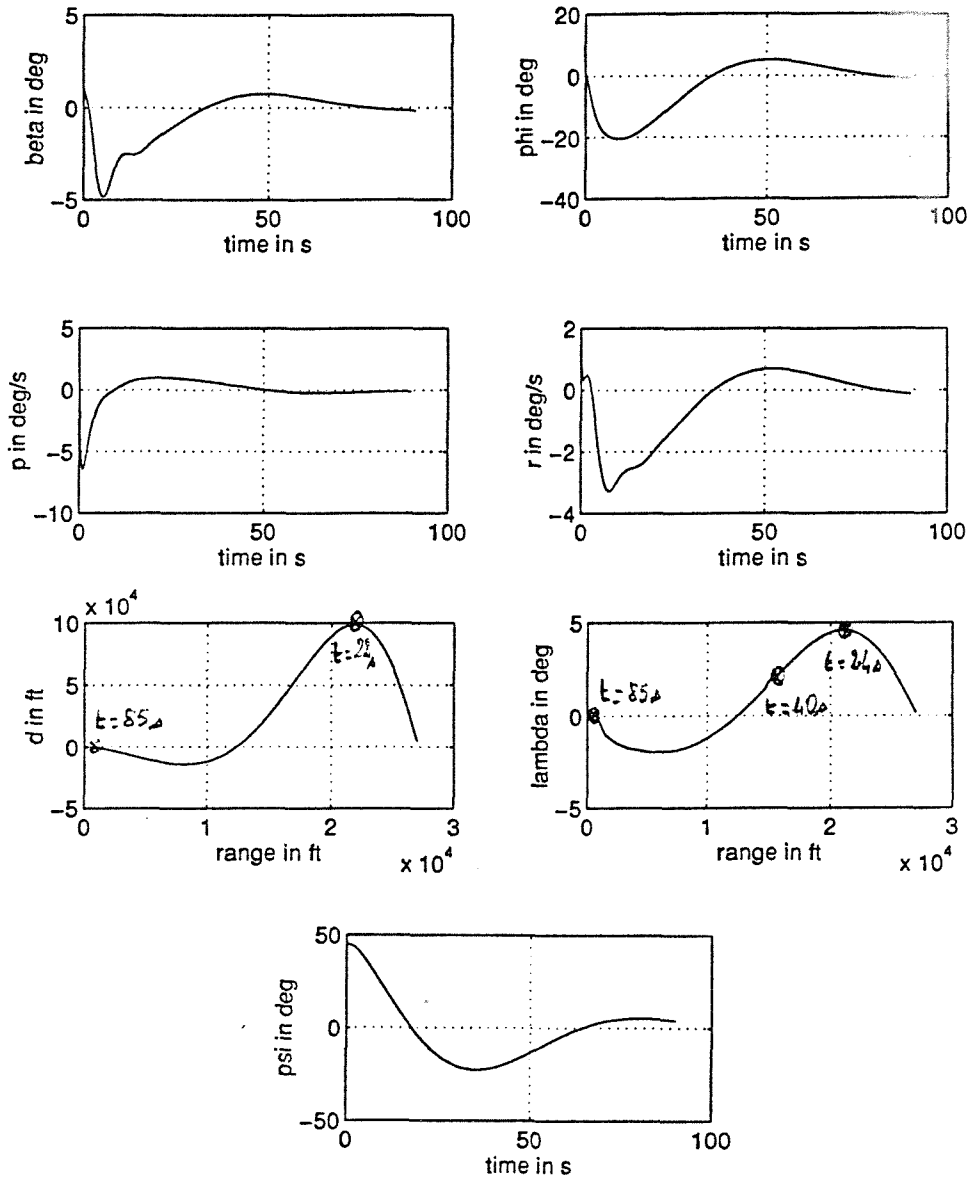

$$\psi(0) = 45°$$

$$d(0) = 4885 \text{ ft}$$

Figure 4.48

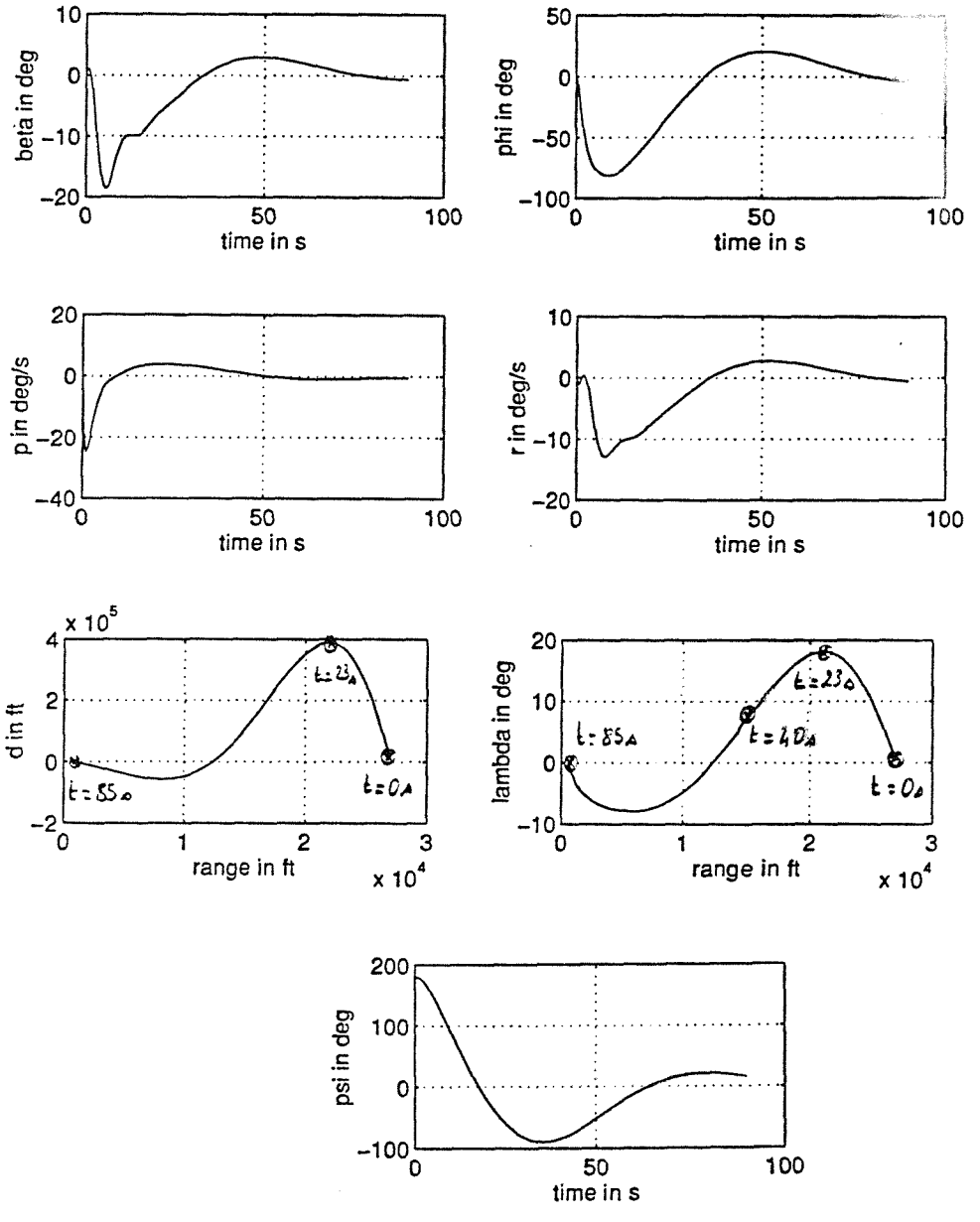

$$\psi(0) = 180°$$

$$d(0) = 17855 \text{ ft}$$

Figure 4.49

Figures 4.50, 4.51 and 4.52 show the responses obtained from the simulation after introducing a precision error of 3.0 metres to represent the lack of precision of the GPS receiver. The results obtained can be summarized as follows :

- when the initial heading was $\psi(0) = 180°$, the error introduced caused an angular deviation of -25° instead of -8° obtained when the error was absent;
- when the initial heading was, $\psi(0) = 45$ °, the steady-state path displacement error, was -20,000ft, the angular deviation became -25° from an error free value of -2° and the heading angle became 10° instead of 2°.
- when the initial heading was $\psi(0) = 0°$, none of the angles or rates corresponded to acceptable values.

As with the GPS glide-path coupled system, when a random error of 3.0 metres was introduced, the results were entirely unsatisfactory. The need for DGPS for use with the GPS localiser system was seen to be necessary to overcome the effect of the intrinsic GPS error.

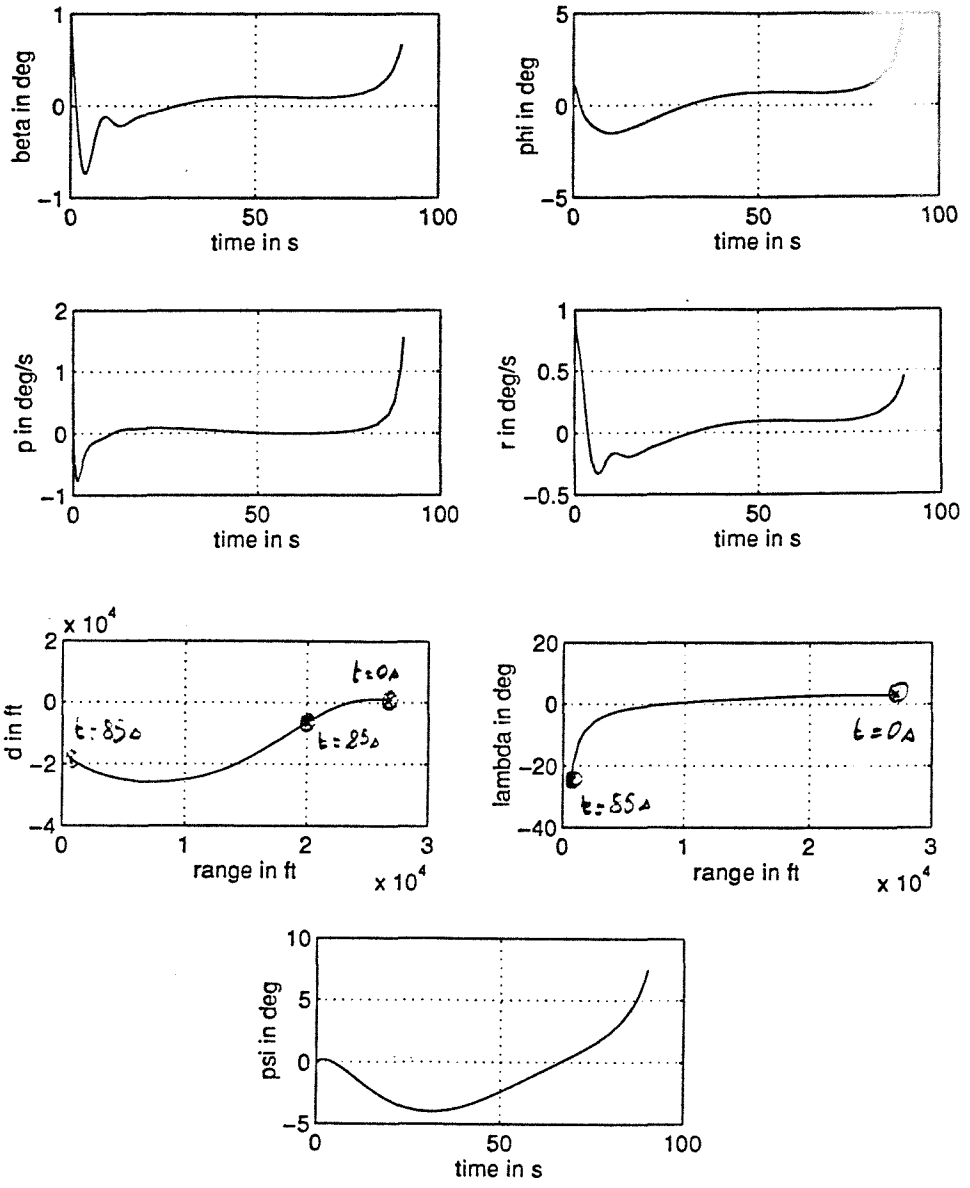

$$\psi(0) = 0°$$

$$d(0) = 1000 \text{ ft}$$

Figure 4.50

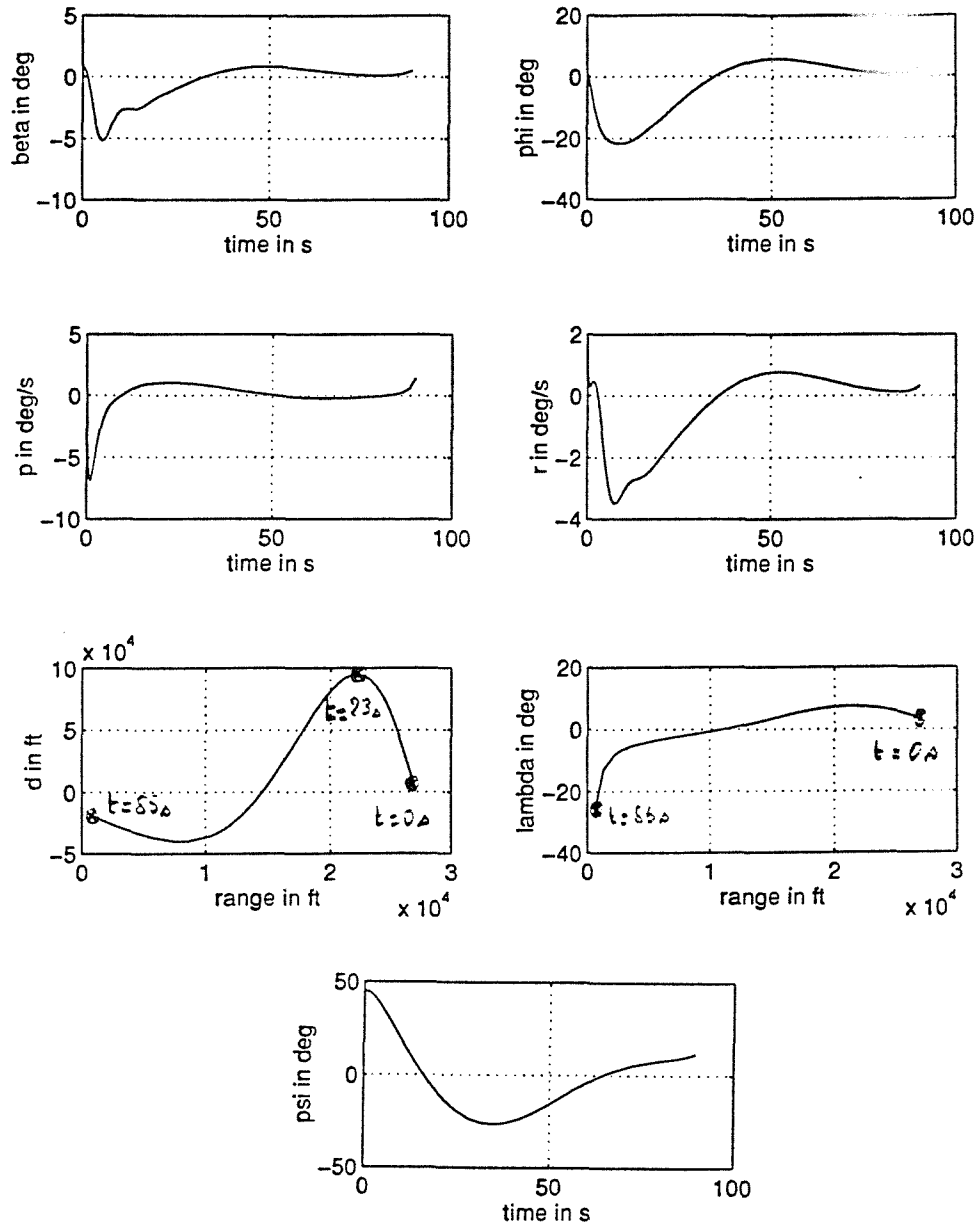

$\psi(0) = 45°$

$d(0) = 4885$ ft

Figure 4.51

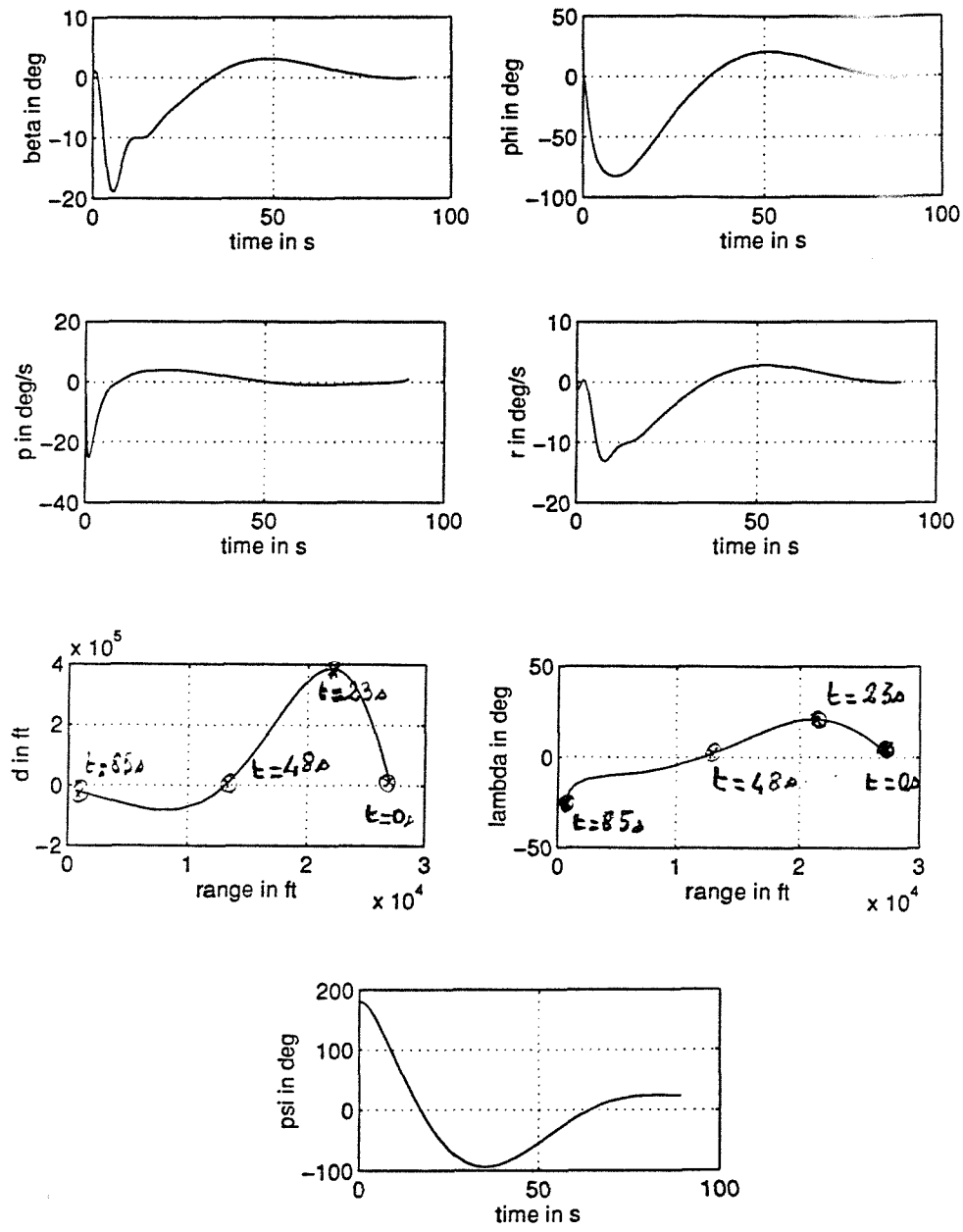

$$\psi(0) = 180°$$

$$d(0) = 17855 \text{ ft}$$

Figure 4.52

5.1 Discussion of results

The objective of the research which forms the basis of this thesis was to study, for a variety of entry conditions and disturbances, the dynamic performance of an automatic landing system used with a large, passenger aircraft, which employed as its path deviation sensor, an airborne receiver for the ILS, the MLS or the GPS.

To study the responses of the automatic landing system required first that a satisfactory simulation of the aircraft dynamics was available. The aircraft chosen was a Boeing 747-100 on approach. Since its flying qualities were marginal for automatic landing, it was necessary to design attitude control systems for both longitudinal and lateral motion. Two different control methods were used to obtain closed loop automatic flight control systems which provided the aircraft with greatly augmented damping, more rapid response and with no detectable coupling between longitudinal and lateral motion. A speed control system was also designed to provide, via engine thrust, accurate control of the aircraft's speed during descent.

All the results obtained from the ILS-coupled systems designed for this study were found to be satisfactory for whatever entry and atmospheric conditions obtained. All the deviations of motion variables and path displacements were sufficiently smooth and small to provide acceptable landing performance.

Using MLS as the path sensor also produced good results, particularly for curved approaches which could not be handled by the ILS. However, in one pathological case, in which the entry conditions were such that the automatic landing was initiated when the aircraft was pointing away (at 180°) from the prescribed runway, the automatic landing could not be achieved, although the lateral control produced a path timing the aircraft on to the correct azimuth trajectory, the resulting amplitude variations in the bank angle were unacceptable for passenger aircraft.

When GPS was employed it was found that the basic GPS signal was inadequate to produce acceptable automatic landing. Although the aircraft could respond accurately to commands, the presence of a displacement error of 3.0 metres in the GPS signal meant

that the resulting response from the GPS coupled system was unsatisfactory. The system could cope with the loss of one satellite signal; tests were carried out in which, as a result of antenna blanking during a banking manoeuvre, a satellite signal was lost for 2 seconds. The results proved that the automatic landing system could still produce acceptable performance in this situation. However, it is necessary to overcome the serious operational difficulty relating to the intrinsic displacement error in the GPS signal (using the C/A code). The solution to this problem appears to be the use of an additional ground station, located at an accurately-defined point near the airport, which can provide signal error correction. Such a system (Grossin, 1994) is referred to as the Differential Global Positioning System (DGPS). Trials using such a system have been carried out successfully in Germany and the USA.

Curved approaches using MLS have been assessed in NASA trials using 50 pilots (Summers and Feather, 1992). The results obtained confirm the conclusion arrived at in this thesis that curved MLS approaches for automatic landing for a large passenger aircraft is operationally acceptable, but the complexity of the curved approach and the length of the final straight segment are critical parameters for success.

Both MLS and DGPS should be regarded as components of FANS, which will be implemented world wide by the end of the century. However, ILS will probably still remain in operation at some airports with its use for automatic approaches and landings being carried out in conjunction with DGPS and, possibly in Europe, MLS. At present Multi-Mode Receivers (MMR), which include ILS, MLS, and GPS channels, have been produced, by, among others, GEC-Marconi, Honeywell and Sextant Avionique, and these permit aircraft equipped with them to use any of the systems as path sensors. No operational automatic landing trials have yet been completed, although several experimental studies have been carried out in France, Germany, United Kingdom and the USA.

5.2 Recommendations for further work

Further work should be carried out on the design of the automatic landing system to produce smaller attitude changes and path displacements for the entry conditions adopted for this study. A more careful assessment of the parameters used for the capture logic system should be undertaken with particular emphasis on the effect on path deviations and landing delay of limiting aircraft motion variables.

The GPS-coupled system should be investigated to examine the influence dynamic receiver errors. In this work the error assumed was a stationary one, but the measured GPS position can change, because of satellite movement, even when there is no change in the aircraft's position, and also as a result of the effects of acceleration on the crystal oscillations used in the GPS receiver as a clock. These dynamic errors will effect DGPS coupled systems too.

In this work masking was taken to result in a loss of signal of 2.0 s, but GPS receivers differ in the time they need to re-lock and also in the accuracy achieved for the first position measurement made after masking is removed. Some receivers can take as long as 15.0-60.0s to lock on and the error of the measurement after first locking on can be as great as 80 metres. It would be absolutely necessary to examine the effects of such locking delays and errors in any further work relating to a DGPS coupled system.

Finally, it has been shown in this work how serious are the effects of simple stationary errors on the performance which can be achieved with GPS based systems. A study should be carried out to establish the performance which could be achieved using the P code of the GPS. It is most important that any future work should base any studies on a hybrid positioning system in which additional position information is provided by a robust, autonomous sensor.

- A -

C.ALARI; Instruments de radionavigation.
Enac, 4eme edition, 1987.

- C -

CAA; Microwave Landing System.
Civil Aviation Authority, 1988.

O.CAREL; Les systemes de navigation par satellites et l'aviation civile : point et perspectives.
Nouvelle Revue d'Aeronautique et d'Astronautique, no 3, 1993.

C.R CHALK, T.P.NEAL, T.M.HARRIS, et al; Background information and user guide for MIL-F-8785 flying qualities of piloted airplanes.
AFFDL-TR-69-72, 1969

M.COMBES; Avionique de la navigation aerienne.
Cepadues Editions, 1993.

J.B.CROLL; Flight evaluation of Curved Path MLS Precision Approaches in a Falcon 20 aircraft.
National Research Council Canada, June 1995.

- D -

D.DAOUST; Air et Cosmos / Aviation International
no 1565, 10 mai 1996.

R.DORF and R. BISHOP; Modern Control Systems;
Addison-Wesley, 1995.

C.S.DRAPER; Control, navigation and guidance.
IEEE Control Systems Magazine, 1981

- G -

J.GROSSIN; L'aviation civile et les satellites de navigation : le point de vue d'un avionneur.

Nouvelle Revue d'Aeronautique et d'Astronautique, 1994.

- K -

M.KAYTON; Navigation -Land, Sea, Air and Space-

IEEE Presss, 1989.

M.KAYTON and W.R FREID; Avionics Navigation Systems.

New York : Wiley, 1969.

R.J.KELLY, Time Reference MLS Multipath Control Techniques.

Journal of The Institute of Navigation, Vol.23 No1, Spring 1976.

S.KINGSLEY and S.QUEGAN; Understanding Radar Systems.

Mc Graw-Hill, 1992.

- M -

MAHAPATRA and POULOSE; Accurate ILS and MLS.

IEEE Conference Code 12685, 1989.

D.McLEAN; Automatic Flight Control Systems.

Prentice Hall, 1990.

McRUER and GRAHAM; Eighty years of flight control : triumphs and pitfalls of the systems approach.

Journal Guid.Cont, 1981.

- N -

NFL I-3350/72; Nachrichte fur Luftfahrer fur den Allwetterflugbetreib nach betriebsstufe Burdensanstadt fur Flugsicherung, 1972.

- S -

L.G.SUMMERS and J.B.FEATHER; Evaluation of MLS Approaches in a wide-body transport simulator.

NASA, June 1992.

K.STEIN; MLS Development Progresses.

Avionics, August 1993.